

American University in Cairo

## AUC Knowledge Fountain

---

Theses and Dissertations

---

6-1-2017

### Effect of Graphene addition on the mechanical and tribological behavior of nanostructured AA2124 /Graphene self-lubricating metal matrix composite

Ahmed Hazem EL Ghazaly

Follow this and additional works at: <https://fount.aucegypt.edu/etds>

---

#### Recommended Citation

##### APA Citation

EL Ghazaly, A. (2017). *Effect of Graphene addition on the mechanical and tribological behavior of nanostructured AA2124 /Graphene self-lubricating metal matrix composite* [Master's thesis, the American University in Cairo]. AUC Knowledge Fountain.

<https://fount.aucegypt.edu/etds/659>

##### MLA Citation

EL Ghazaly, Ahmed Hazem. *Effect of Graphene addition on the mechanical and tribological behavior of nanostructured AA2124 /Graphene self-lubricating metal matrix composite*. 2017. American University in Cairo, Master's thesis. *AUC Knowledge Fountain*.

<https://fount.aucegypt.edu/etds/659>

This Thesis is brought to you for free and open access by AUC Knowledge Fountain. It has been accepted for inclusion in Theses and Dissertations by an authorized administrator of AUC Knowledge Fountain. For more information, please contact [mark.muehlhaeusler@aucegypt.edu](mailto:mark.muehlhaeusler@aucegypt.edu).



**The American University in Cairo**

Effect of Graphene Addition on the Mechanical and Tribological Behavior of  
Nanostructured AA2124 /Graphene Self-Lubricating Metal Matrix  
Composite

By  
**Ahmed Hazem EL Ghazaly**

A thesis submitted in partial fulfillment of the requirements for the degree  
Of  
**Master of Science in Nanotechnology**

Under the supervision of  
**Dr. Hanadi Salem**

Professor, Department of Mechanical Engineering

The American University in Cairo

**Spring 2017**

The American University in Cairo

**Effect of Graphene Addition on the Mechanical and Tribological  
Behavior of Nanostructured AA2124/Graphene Self-Lubricating Metal  
Matrix Composite**

A Thesis Submitted by Ahmed Hazem El Ghazaly

To The Nanotechnology Program

February /2017

In partial fulfillment of the requirements for the degree of Masters of Science in

Nanotechnology

Has been approved by

**Prof. Dr.Hanadi Salem**

Affiliation: Associate Chairperson  
Materials & Manufacturing Area Coordinator  
Mechanical Engineering Department  
The American University in Cairo

Thesis Committee Chair / Adviser \_\_\_\_\_

**Prof. Dr. Amal Esawi**

Affiliation Professor, Mechanical engineering department  
Associate Dean of graduate studies  
The American University in Cairo

Thesis Committee Reader / examiner \_\_\_\_\_

**Prof. Dr. Ahmed Abd E-Moneim Abd El-Hamid**

Affiliation: Professor Materials Science and Engineering Department  
School of Innovative Engineering Design  
Egypt-Japan University of Science and Technology

Thesis Committee Reader / examiner \_\_\_\_\_

Department Chair/ Date Dean Date

Program Director

## **ABSTRACT**

In the current research, the mechanical and tribological behavior, and structural evolution of AA2124-3 and 5-wt.% graphene (G) composites prepared by a combination of ball milling and hot extrusion were investigated. Mixing followed by energy ball milling of the powders was conducted under argon atmosphere. Hot extrusion of the green compacts was carried out at 0.46 and 0.68 of the alloy melting temperature. Properties such as macro and micro-hardness, nanohardness, tensile and lattice strain were characterized. Wear rates, coefficient of friction (COF) were characterized using dry pin-on-disc test under loads of 50, 100N and 150N. Nanoscratch testing were employed to investigate the self-lubricating tribological behavior. X-ray diffraction, optical and scanning electron microscopy were used to determine the influence of the G-content on the crystallite size variation and the lattice strain for the ball milled powders compared to the hot extruded rods. Density measurements and optical microscopy (OM) were employed to investigate the consolidation degree and porosity variation as a function of increasing G- of the G and Al-matrices for the variable conditions. Bulk texture variation was analyzed to evaluate the influence of the extrusion temperature.

AA 2124-3 wt.% G composites displayed the highest tensile properties, highest hardness and lowest wear rates and COF, as well as lowest scratch width and depth compared to the 5 wt.%G and the plain alloy. The uniform distribution of the G-particles within the Al-matrices for the 3wt.% containing composites hindered grain coarsening by the induced lattice strain compared to that of 5 wt% G ones. Moreover, addition of 3 wt.% G smeared thin uniform tribofilm on the surfaces of the worn composite rods. The formed layer reduced friction and wear. Increasing the G content up to 5 wt.% resulted in segregation and clustering of the G-particles within the Al-matrices, which caused microploughing and sever plastic deformation wear mechanism and excessive delamination.

Lower consolidation temperatures of 300°C produced composites with lower wear rates due to the excessive strain hardening effect. Extrusion at 300°C produced a continuous G-encapsulating layer around the Al-matrix compared to an interrupted G-layer for the 450°C extrusions. The G-layer morphology influenced the dominating mechanism of the composite during deformation. Texture analysis of the AA2124-3 wt.%G extruded at low and high temperatures proved that both the Cu-and Shear are the dominating texture components, while increased texture intensities from 1.2-to-1.76 occurred with increasing the extrusion temperature.

## **Acknowledgment**

I would like to thank the mentor and the advisor of this research, Prof. Dr Hanadi Salem, who supported this work from day one till its end. She provided me with the science, the technical support, the personal advice, and all kinds of support needed for a researcher and student and a son.

I would like to show gratitude for the director of Youssef Jameel Science and Technology Research Center members (YJSTRC) Prof. Dr. Ehab Abd el Rahman and the technical team Ahmed Nour, Ahmed El Beltagy and Saleh for providing me with facilities, financial and technical supports throughout this research. I am deeply appreciative to my colleagues from the American University in Cairo, Mohamed Shokier, Dina Fouad, Ehab Salama, Irene Fahmy, Sandy El Mogazy, Ahmed Fathy, Nouran Ashraf, and Basamat Shaheen and from the staff, Mr. Zakarya Taha, Eng. Khaled, Hussien, Saeed, Magdy and Eng. Mohamed Bakr. I am thankful for the lab assistants that maintained the suitable lab atmosphere for producing this work, their work had an impact on producing results of high accuracy and reliability. Additionally, I would like to acknowledge Dr Ahmed Salah from university of Wollongong for conducting the macrotecture tests.

It is indispensable to mention the personal and mental support of the family members during the whole period of the research Salma Mohamed, Shaymaa, Moataz and Radwa and my mother Laila, who provided me with care and continuous encouragement. I never would have been able to attain my aim without her

## **DEDICATION**

To My Mother...

To Amira ....

## NOMENCLATURE

<b>Item</b>	<b>Description</b>
G	Graphene
GS	Graphene sheet
XRD	X-Ray Diffraction
FESEM	Field Emission Scanning Electron Microscopy
MA	Mechanical Alloying
HVN	Hardness Vickers
OM	Optical Microscopy
XPS	X-ray photoelectron spectroscopy
YS	Yield Strength
UTS	Ultimate Tensile Strength
MMC	Metal Matrix Composite
HIC	Hot Isostatic Compaction
BPR	Ball-to-Powder weight Ratio
PCA	Process Control Agent
PF	Pole figure
ODF	Orientation Distribution Function
$\theta$	Diffraction angle
K	Scherrer constant 0.91
D	Grain size
$\Lambda$	Wave length
$\epsilon$	Lattice strain
D	Interplanar distance



FWHM	Diffraction peak width at half maximum intensity
CNTs	Carbon nano tubes
BM	Ball Mill

## List of Figures

Figure 2-1 High energy planetary ball mill.....	25
Figure 2-2 Graph represents the coefficient of friction of a) A wear test under dry nitrogen and humid air for graphite deposited on steel and b) Behavior of graphene in dry and humid environment versus number of cycles at 1N load. ....	41
Figure 2-3 crystal orientations in sheet (a) and bar (b), presented with respect to Miller indices .....	42
Figure 2-4 Schematic showing construction of a (100) pole figure .....	43
Figure 3-1 bar chart shows the influence of G on the mechanical properties of Aluminum .....	52
Figure 3-2 Al-0.3wt.%G fracture surface.....	52
Figure 4-1 SEM images for As-received (a, b) AA2124 Powder (c, d) Graphene particles, at low and high magnifications, respectively and (e) Raman spectroscopy pattern for G.....	56
Figure 4-2A model represent the compaction and extrusion die.....	58
Figure 4-3 Tensile Specimen .....	59
Figure 4-4 Wear test machine.....	61
Figure 4-5 Panalytical MRD XRD machine components 1. Goniometer stage -2. Linear detector 3- solar slits, Cu-Ni filter and optics 4- Cu-Alpha .....	64
Figure 5-1 FESEM micrographs for (a) mixed Al/G powders, arrow points at G particle (b) milled Al/G powders and (c) graphene layers stacked on and in between Al-particles pointed at by black arrows]...	67
Figure 5-2FESEM micrographs for the AA2124 milled powders (a, b) 0 wt.%G, (c, d) 3wt% G and (e, f) 5 wt.% G at low and high magnifications, respectively .....	67
Figure 5-3 Relative density (RD%) variation as a function of increasing G-content .....	68
Figure 5-4Vickers micro-and macro-hardness variation as a function of G-content for the hot extruded BM powders at 300C .....	70
Figure 5-5FESEM images showing Fractography of the tensile tested AA2124 extruded rods at 300°C (a, b) 0 wt.%G, (c, d) 3 wt.%G and (e) 5 wt.%G.....	72
Figure 5-6 Optical Microscope images for AA2124 Composites (a, b) 0wt.%G, (c, d). 3Wt.%G and (e, f) 5Wt.%G on the sections cut longitudinal and transverse to the extrusion direction, respectively. Blue arrows point at extrusion direction, while arrows pint at microcracks.....	73
Figure 5-7Wear rate for monolithic AA2124 and the composite as function of load and graphene contents. ....	74
Figure 5-8 SEM images for the worn surfaces of the AA2124 matrices containing (a, b) 0 wt.%G, (c, d) 3wt.%G and (e, f) 5wt% G under 100N load. Representative debris are shown at the bottom right corner of each condition ..	76
Figure 5-9 (a) Load vs displacement AA2124 alloy as a function of graphene content (b) Hardness and Young’s modulus.....	77
Figure 5-10 Diagrams for representative behavior for the AA2124 hot extruded BM powders (a) scratch depth profile Vs. scratch distance and the (b) variation of scratch depth and width as a function of increasing G-content.....	78
Figure 5-11 SEM images for scratch surfaces of (a, d) plain AA2124, (b, e) 3wt.%G and (b,e) 5wt.%G.....	80
Figure 5-12Relative density (RD%) variation as a function of increasing G-content .....	82

Figure 5-13 Vickers micro-and macro-hardness variation as a function of G-content for the hot extruded BM powders .....	84
Figure 5-19 shows pin-on-disc results displayed for the hot extruded milled powders of AA2124 (a) wear rate, (b) Coefficient of friction (COF) as a function of G-content at 100 N load dry sliding tests [64] .....	93
Figure 5-22 Nano-hardness test results: (a) Load-displacement and (b) Young's Modulus for AA2124 hot extrudates as a function of increasing G-content.....	97
Figure 5-23 shows the Orientation Distribution Function (ODF) for the AA2124-3wt.%G longitudinal cross sections hot extruded at (a) 300° C and (b) 400 °C taken at 0, 45 and 90° Euler angles. ....	112

## List of Tables

Table 2-1 Different reinforcements of MMCs .....	35
Table 2-2 G and CNT properties .....	39
Table 2-3 Major texture components .....	44
Table 4-1 Aluminum alloy 2124 chemical composition .....	55
Table 5-1 Tensile Properties of the AA2124 rods with and without G-Additions .....	71
Table 5-2 represents the Micro -Macro hardness as function of G content . ....	84
Table 5-3. Average values for tensile properties of extrudates as a function of increasing G content. ....	86
Table 5-4. Effects of reinforcement type and processing technique on the Mechanical properties of Aluminum alloys.....	108
Table 5-3. Tribological properties of Aluminum alloys-carbon composite .....	86

## Table of Contents

Chapter 1 Introduction*	15
chapter 2 Theoretical Background	18
2.1 Metal Matrix Composites and Nanocomposite	18
2.2 Reinforcements selection criteria	19
2.3 MMCs Fabrication	20
2.3.1 Gas phase processes	20
2.3.2 Liquid phase processes	21
2.3.3 Solid phase Process: Powder Metallurgy	21
2.4 Advantages and Disadvantages of Powder Metallurgy	22
2.5 Mechanical Alloying/Milling	23
2.5.1 Milling process parameters	24
2.5.2 The type of mill	24
2.5.3 Grinding Medium	25
2.5.4 Milling speed (RPM)	25
2.5.5 Milling time	25
2.5.6 Ball-to-powder weight ratio	26
2.5.7 Milling atmosphere	26
2.5.8 Process controlling agent	26
2.5.9 The contamination in milling process	27
2.6 Powder Consolidation	27
2.6.1 Cold Compaction	27
2.7 Sintering of Powders	28
2.8 Hot Isostatic Pressing	28
2.9 Hot compaction	28
2.10 Powder Rolling	29
2.11 Hot extrusion:	29
2.12 Spark plasma sintering	29

2.13	Wear .....	30
2.14	General types of wear mechanisms.....	31
2.14.1	Adhesion:.....	31
2.14.2	Abrasion: .....	31
2.14.3	Delamination: .....	31
2.14.4	Oxidative: .....	32
2.15	Wear Characterization .....	33
2.16	MMC Applications .....	34
2.17	Al-based MMC for Mechanical and Tribological application.....	35
2.17.1	Effects of Graphite.....	36
2.17.2	Effect of Carbon Nanotubes .....	37
2.17.3	Effect of Graphene.....	38
2.17.4	Graphite Vs Graphene .....	40
2.18	Bulk Crystallographic Texture.....	41
2.18.1.	Grain Orientation .....	42
2.18.2.	Pole Figures.....	42
2.18.3.	Orientation Distribution Function (ODF) .....	43
2.18.4.	Texture components and Fibers .....	44
Chapter 3.	Literature Review.....	45
3.1.	Nanotechnology in Wear application.....	45
3.2.	Metal-Graphene Nanocomposite .....	49
3.3.	Wear mechanism in Al- CNTs and Al-G.....	53
Chapter 4	MATERIALS AND EXPERIMENTAL PROCEDURES .....	55
4.1.	Materials .....	55
4.2.	Processing of AA2124/Graphene Nanocomposite .....	56
4.2.1.	Handling and Mixing of the As Received Powders (AA2124+Graphene) .....	56
4.2.2.	Dispersion of Graphene via Mechanical Milling .....	57
4.2.3.	Powder Consolidation.....	57
4.3.	As-Extruded Consolidated Rods.....	58
4.3.1.	Physical Properties: Density .....	58

4.3.2.	Mechanical Properties: .....	58
4.3.3.	Hardness: .....	59
4.3.4.	Tensile Testing .....	59
4.3.5.	Tribological Behavior .....	60
4.3.6	Nanoscratch Test .....	61
4.3.7.	Structural Characterization .....	61
4.3.8	Raman Spectroscopy .....	62
4.3.9.	X-ray Diffractometry .....	62
4.3.10.	Bulk Texture Analysis .....	63
4.3.11.	Optical Microscopy (OM).....	64
4.3.12.	Scanning Electron Microscope (SEM) .....	64
Chapter 5. RESULTS AND DISCUSSION*.....		66
5.1	Mixed and Milled Powders .....	66
5.2	Hot Extruded Bulk AA2124-G Nanocomposites at 300 °C .....	68
5.2.1	Relative density .....	68
5.2.2	Mechanical Properties .....	69
5.2.3	Structural Evolution.....	72
5.2.4	Tribological Properties .....	73
5.2.5	Nanohardness and Nano scratch Behavior .....	76
5.2.6	Conclusion.....	80
5.3	Hot Extruded Bulk AA2124-G Nanocomposites at 450 °C .....	81
5.3.1	Relative density .....	81
5.3.2	Hardness .....	82
5.3.3	Tensile Properties .....	84
5.3.4	XRD analysis.....	89
5.3.5	Tribological Properties .....	92
5.3.6.	Nanohardness and Nanoscratch Behavior .....	96
5.3.6.2.	Conclusions:.....	100

5.4. Influence of Extrusion Temperature on the Behavior of AA2124-3wt.G Composite: A comparative Study: .....	101
5.4.1. Physical and Structural Behavior .....	103
5.4.1.1. Microstructure .....	103
5.4.2. Mechanical and Tribological Behavior: .....	104
5.4.2.1. Mechanical Properties .....	104
5.4.2.2. Tribological Properties.....	109
5.4.2.3. Texture analysis .....	112
Chapter 6. Conclusions .....	115
Chapter 7. Future work .....	117

## Chapter 1. INTRODUCTION\*

Powder Metallurgy (PM) is the science of fabricating powdered metals into bulk materials in different shapes and sizes [1]. PM are fabricated through various manufacturing methods, which influences the produced properties of the final product. Alloy metal powders are produced through numerous techniques such as electrolysis, mechanical alloying (MA), gas atomization, and chemical methods including reduction of oxides [2]. The selection of any of these procedures depend on parameters among which is the chemical and physical properties of the powders or the rate of production. Gas atomization is the preferable method for producing metallic powders at a wide range of rates and sizes. The rates range from 1 to 105 tons per year of powders, while the sizes range from 10 to 1000  $\mu\text{m}$  for powders and from 0.5 to 500  $\mu\text{m}$  for atomized metallic powders [3].

Nanostructured materials have proven their superiority over micro structured materials. nanostructured materials are characterized to be of average grain sizes equal to or less than 100nm and their dimensions can be 1D, 2D, or 3D [4]. Nanomaterials with a single or 2D are mainly used for coatings or in electrical applications. On the other hand, the 3D nanomaterials are such as nanoparticles are used either to produce bulk nanostructured monolithic bulk products, or nanodispersions for strengthening of micron or nanostructured metallic matrices producing nanocomposites [5]. Addition of nanoscale reinforcement to metal matrices results in the enhancement of the mechanical properties and hence would be suitable for applications with higher performance and higher reliability.

Graphene, the first truly two-dimensional crystalline material recently identified and analyzed, is a single atomic layer of carbon where  $\text{sp}^2$  hybridized carbon atoms are arranged in a hexagonal lattice structure [6]. Since its isolation in 2004, it has been studied for several applications due to



its unique physical properties, which attracted the attention for areas related to electronics [7]. One promising field in the application of nanoscale materials such as graphene is their extraordinary strength and light weight, which made them suitable reinforcement candidate for ultrahigh strength nanocomposites [8]. Considered to be the thinnest and strongest material discovered, graphene addition to the various matrices is expected to improve the composites performance and reliability due to the enhanced mechanical properties and hence cost effectiveness compared to other conventionally reinforced composites. Due to the ease of fabrication and the promising results, graphene has been widely investigated as reinforcement in polymer matrix composites [9]. Only few researches investigated the effect of graphene in metal matrix composites due to difficulty in dispersion within the metallic matrices.

Like graphite, graphene also exhibits self-lubricating properties when added to metal matrices for tribological applications. However, contrary to the behavior of graphite, graphene is able to provide solid lubrication and notably reduces wear regardless of the environment in which the composite operates [10].

In addition to the self-lubricating function of graphene to minimize abrasive wear [11] an increase in tensile strength of metal-graphene composites is observed compared to that of monolithic materials. Three main mechanisms are believed to contribute to the increased strength of the fabricated composites depending on the size and morphology of the graphene phase introduced [12]. The strengthening mechanisms are namely; Orowan strengthening; Hall-Petch strengthening; and thermal coefficient mismatch.

Despite the numerous advantages of using graphene as fillers in composites for wear resistant applications, many challenges are still frequently encountered by metal/graphene fabricators. Generally, research efforts directed towards the use of higher graphene contents have

often led to a decline in mechanical properties due to non-uniform distribution of G within the various ', increased clumping [11] , and extensive carbide formation [13, 14] Hot extrusion, hot rolling [15], friction stir processing [16], and wet mixing techniques [17] are techniques used for the fabrication of the composites containing graphene. However, the use of powder metallurgy while overcoming its drawbacks, is still favorable since it remains a less expensive alternative for the fabrication of aluminum-G composites and thus has higher industrial prospects [new source: Liu et al. Graphene oxide and graphene nanosheet reinforced aluminum matrix composites: Powder synthesis and prepared composite characteristics.

Accordingly, the aim of this work is to investigate the influence of adding graphene up to 5 weight % to AA2124 matrices via combination of ball milling and hot extrusion on the mechanical and tribological properties of the resulting composites. Mechanical properties such as hardness on the macro, micro and nanoscale as well tensile strength, and toughness are evaluated. The tribological performance of the composites produced including their wear rates, and nanoscratch resistance under dry sliding conditions are investigated. Moreover, the influence of graphene content on the structural stability of the Al-matrices against coarsening that is associated with sintering is evaluated.

\*This chapter was written based on the following publication "El-Ghazaly, A., Geraldine Anis, and Hanadi G. Salem. "Effect of graphene addition on the mechanical and tribological behavior of nanostructured AA2124 self-lubricating metal matrix composite." Composites Part A: Applied Science and Manufacturing 95 (2017): 325-336".

## Chapter 2 THEORETICAL BACKGROUND

### 2.1 Metal Matrix Composites and Nanocomposite

Composites being composed of two or more distinct materials, offer several new possibilities in the field of material science [18]. A composite produces a tailored- material with specific characteristics significantly different from its individual components. The two prime components of most composites are “matrices” and “reinforcements”. The matrix encompasses the reinforcement material, which inherently reinforces the matrix by imparting its distinctive physical and/or mechanical properties [19]. This synergy, as elaborated, results in remarkable material property combinations highly desirable to designers and innovators worldwide.

There are three main types of composites: Metal Matrix Composites (MMCs), Polymer Matrix Composites (PMCs), and Ceramic Matrix Composites (CMCs) [20]. Such identification depends on the type of matrix material by being either a metal, polymer, or ceramic. Additionally, different composite microstructures form according to the reinforcing constituent shape (flakes, whiskers, sheets, fibers, particulate or dispersions), size, and distribution within the matrix and/or its orientation [21]. Such parameters are key performers in composite materials and various alterations play an immense role in the final composite outcome. Achieving an optimum mixture of both the matrix and reinforcement has been the focus of many researchers and material scientists over the past decades.

MMCs in particular, during the past few decades have witnessed immense efforts towards the synthesis of metal composites of properties significantly superior to its alloy rivals [22, 23] Achievement of enhanced mechanical properties such as high specific strength and Young's modulus and wear resistance [24] can be done based on the selected reinforcement and matrix. For

instance, several types of particulate ceramic reinforcements have been composited in alumina matrices demonstrating enhanced composite properties [25] Addition of high strength refractory material to a ductile metal matrix produces a material possessing intermediate properties of the two. Other examples lead to reduction in material density translating into a structure of higher specific strength to serve markets such as the automotive and aerospace industries [25] .

The challenge to keep up with the perpetual demand has extended research on MMCs to rather more progressive systems that is metal matrix nanocomposites (MMNCs) and functional ones such as self-lubricating, self-healing, and self-cleaning composites [26]. Taking the radical concept of composite creation, that reinforcement particle size plays a major role in the final resultant properties of composites, researchers have used nano-size particles and have made it possible to achieve the future generation of MMCs. The MMNCs overcome the shortcomings of MMCs, having high strength as well as fracture toughness, strongly influenced the properties of MMCs [27]

With all the aforementioned advancements in the field of MMCs, it is vital to optimize the design of such promising class of materials. After all, the main goal of MMC materials is to combine the desired attributes of both the metal and the reinforcement. For that reason, thorough understanding of selection criteria as well as synthesis techniques have to be established.

## 2.2 Reinforcements selection criteria

Inherent from its designation, reinforcements prime role are to reinforce encompassing materials and thus it becomes of dramatic importance to make judicious decisions while selecting to ensure that mechanical properties of composites will not otherwise decrease [18] .First and foremost, they have to be compatible with the matrices materials. For example, a small difference

in the thermal coefficient of expansion between the two constituents is highly recommended to avoid high-accumulated strains [18]. Furthermore, different mechanical testing are required to ensure a successful fabrication process as well as service performance, such as tensile strength, modulus of elasticity, chemical stability at high temperatures [18]. Certainly, such properties coupled with the appropriate choice of reinforcement type and morphology -as discussed in the previous section- would ensure an efficacious outcome

### 2.3 MMCs Fabrication

Over the last three decades, unprecedented progress has been achieved in the development of processing techniques for particulate reinforced MMCs. The fabrication process generally employs two steps- production of the composite followed by transformation into a useful end product [22]. Although, the operational steps are similar in the different processes, different properties are resulted from the output MMC. This makes the synthesis method highly crucial to choose- as it plays a major role in the mechanical properties of the MMCs. There are three main categories of classified in accordance to the temperature of the metal matrix whilst processing; (a) Gas Phase processes, (b) Liquid Phase processes, (c) Solid Phases Processes.

#### 2.3.1 Gas phase processes

Sputtering deposition and plasma spraying and are considered the primary form of gas phase processing. Using this processing technique, either laminated nanocomposites or matrix coated fibers with tailored chemical structure can be produced. Sputtering deposition technique has been used successfully for synthesizing metal to metal layered system.

### 2.3.2 Liquid phase processes

Molten liquid metal is the state at which this phase processing occurs- various proprietary techniques to incorporate and mix the ceramic particulates within the matrix are applied. Then, the final casting of the MMC to produce the outcome follows this step. The main limitation of such technique is that most molten alloys do not wet the ceramic particulates, which necessitates the addition of either wetting agents to the melt or coating of the particulates prior to mixing. Several attempts to solve such predicament proved successfully.

In all the processes mentioned above, a strong bond between the metallic matrix and the reinforcement material is achieved by the usage of high processing temperatures (T more than about 900 °C for the Al-Al<sub>2</sub>O<sub>3</sub> system) and alloying the matrix with an element which can interact with the reinforcement in order to produce a new phase.

### 2.3.3 Solid phase Process: Powder Metallurgy

Solid State processing is considerably the best, compared to its rivals, to produces MMCs of highest mechanical properties. The achievement of superior homogenous mechanical properties is easily obtainable by Powder Metallurgy- the most commonly used solid-state fabrication method. Defined as the production of valuable composites from metal powders without melting; it overcomes the difficulty in the liquid phase processing [12]. Blending of the constituent matrix and reinforcement powders into the mold of desired shape precede consolidation. Cold pressing to form a compact followed by sintering and hot isostatic pressing comprise the consolidation process. This is to develop solid-state diffusion and highly dense uniform structure. Subsequently, the resultant consolidated composites is extruded via secondary approaches: extrusion, forging, rolling. Such homogeneity in reinforcement distribution achieved by PM techniques not only

ensures greater mechanical and structural properties but also the reproducibility of these properties. From the discussion above, it is inferred that achieving a homogenous mixture whilst blending is of crucial importance to ensure a proper mixture and effectual outcome.

## 2.4 Advantages and Disadvantages of Powder Metallurgy

Powder Metallurgy (PM) is an advanced technique of producing finalized parts from particulate matter. In other words, consolidating metallic and/or nonmetallic powders to produce the final product with superior properties than Industrial Metallurgy (IM).

### **Advantages:**

- 1) PM is a clean process which is associated with minimal scrap. This is due to the absence of the machining process which is the process that wastes material the most.
- 2) PM finished products are well known for their superior surface finish.
- 3) PM is advantageous in producing an assembled part at once, while in IM this same part is produced by the assembling of separate parts, where each part is produced separately.
- 4) PM is known for its high rates of production when compared with IM. This can be concluded from the previous advantages mentioned above. The absence of the machining process and the ability to produce a combined part at once are two main reasons for the high production rates of PM.
- 5) PM gives the accessibility to producing hard tools that are used for cutting, an example of these tools is the diamond impregnated tools.
- 6) PM products usually achieve a relative density of 95% which makes the mechanical properties comparable with cast and wrought materials. In special cases, the relative

density can reach 99.9% by liquid phase sintering. This is when the properties are much more superior to the cast and wrought materials.

**Disadvantages:**

- 1) The main drawback of PM is the limitation of the size and the shape of the part:
  - a. The shape can pose as a problem because PM requires that a shape can be easily shaped and ejected from a die, this can be problematic when a shape has complex edges and designs.
  - b. The size is limited by the capacity and the stroke of the applied pressure.
- 2) The initial costs of the PM are very high and capital intensive because a big initial investment needs to be made to buy the required dies.

## 2.5 Mechanical Alloying/Milling

Mechanical Alloying (MA), also known as Mechanical Milling (MM), is a common method for producing homogenous materials starting from blended powders. This method is favorable since it is a dry powder mixing in a high-energy ball mill [28]. Also, it is preferred sometimes over liquid phase dispersion. MA is mainly associated with the production of homogenous alloys from different powder materials, while MM is associated with pure or plain materials or pre-alloyed powders and as a result, MM requires less milling durations compared to MA.

The usage of MM to synthesize nanostructured materials is of interest to many researchers and developers. The powders experience rough collision between themselves and the balls in



the mill, which result in cold welding, strain hardening followed by fracturing, and re-welding of the powders, which facilitates grain refinement to the nanoscale level [28].

The high energy experienced by powders results in intense plastic deformation, which increases the dislocation density. Furthermore, the dislocation density reaches the threshold level where the nanosized sub grains start forming and when followed by subsequent deformation; the grains undergo more refinement [20]. Therefore, the process of MM is a process of severe plastic deformation of powders [24].

Nevertheless, the common use of MM, there exists no guide for the process that one can follow to reach the desired results. The process remains complex with all the factors that affect the final results. Although, the MM technique has been widely adopted by several researches, no standard guide of operation could be followed. The complexity arises from the fact that many interrelated parameters affect the process and the final product [24].

### 2.5.1 Milling process parameters

The milled powders would be of a quality and a quantity which are based on the milling process itself which is coordinated by several parameters. These parameters identify later the mechanical and physical properties of the bulk product produced. The following section explains the milling parameters in detail.

### 2.5.2 The type of mill

Spex shaker mill, planetary ball mill Figure 2-1 High energy planetary ball mill, attritor ball mill, and commercial mill are unlike types mills that carry the same process. However, the type of mill is selected based on the factors included in the experiment. These factors are such as the milling temperature, milling speed, degree of contaminations, and the amount of powders produced. These factors in specific, more, or less are controlled to guarantee the output.



Figure 2-1 High energy planetary ball mill

### 2.5.3 Grinding Medium

It is essential to count for the materials of the milling jars with respect to the milled powders. For example, powders of high hardness cannot be milled in soft jars that will erode and result in more contaminations. The jars are usually produced from hard material. Finally, the shape of the jar Figure 2-2 is another essential factor to avoid dead zones that may cause powders to accumula

### 2.5.4 Milling speed (RPM)

The speed of milling in RPM is directly proportional to the kinetic energy enforced on the powders and the milling temperature. The high speeds result in hitting the balls towards the walls without affecting the powders and the elevated temperatures promote the cold welding of particles which result in coarsening [28].

### 2.5.5 Milling time

Milling time is an essential factor that affects the final product and must be controlled since the amount of milling energy is directly proportional to milling time. For instance, to avoid explosion

of the zirconium magnesium powder. There is a specific time of milling that cannot be exceeded [28].

#### 2.5.6 Ball-to-powder weight ratio

The ball-to-powder ratio (BPR), also known as charge ratio (CR), is crucial when considering the results of milled powders. Researchers have been using various ratios that range from 1:1 to 1000:1, however, high BPR must be associated with reduced milling time and usually results in the erosion of the balls [28].

#### 2.5.7 Milling atmosphere

To avoid contaminations and/or oxidation of the milled powders, milling is carried out under vacuum or an inert atmosphere of Argon, Helium, or rarely Nitrogen [28].

#### 2.5.8 Process controlling agent

The process control agent (PCA) maintains the fracture of powders and therefore the size refining instead of the cold welding of particles. PCA works also on reducing the heat produced and the sticking of powders to the walls. On the other hand, PCA can react with the powders which is one of its drawbacks [28].

Methanol, Hexane, Ethanol, and Stearic acid are the known PCAs and their quantity is a crucial factor that affects the shape, purity, and size of the milled powders. Research has proven that the grain size is indirectly proportional to the PCA and most of the time PCA is added in the amount of 1-5% of the total powder [27].

The milling process has several disadvantages that will be discussed below [13]:

## 2.5.9 The contamination in milling process

Since the milling is a process that consists of collision between the balls, powders and the vial, the balls and vial experience wear which imposes contaminations on the milled powders. Such contaminations are unavoidable but they can be reduced to a minimum [21]. The contaminations are a function of milling time and these factors:

- a) Unique material of the powders and jars
- b) The pure milling atmosphere
- c) Maintaining the minimum milling time possible
- d) The process control agent
- e) Continuous self-coating of the balls as well as with the milled powders

## 2.6 Powder Consolidation

### 2.1.1 Cold Compaction

The process of cold compaction is basically the pressing of the powders in a metallic die that has almost the shape of the desired final product. The powders are compacted using a hydraulic press that imposes high pressure resulting in the cold welding of the particles at the surfaces [2]. The types of cold compaction are [29]:

- 1) Uniaxial compaction (one direction)
- 2) Uniaxial compaction (two directions)
- 3) Isostatic compaction (all directions)

The uniaxial pressing consists of a top punch that presses in the axial direction, while the two direction pressing consists of two punches that press towards each other to gain a homogenous

structure. Finally, the isotactic compaction presses in multiple directions to attain the best structure with the best density.

## 2.7 Sintering of Powders

The Sintering of powders is basically the transfer of material between compacted powders under high temperatures to achieve the final bulk product. The temperature is a function of the material itself and depends on the mix of the material [29]. The process affects the following factors:

- 1) Sintering time
- 2) Sintering temperature
- 3) Composition of the mix of powder
- 4) Material's density
- 5) Particles' shape and geometry

## 2.8 Hot Isostatic Pressing

This process differs from sintering that it needs hot gases as nitrogen or argon as well as very high pressure. The pressure is applied from the axial direction and the process can be used to compact powders of metallic, ceramic, or composite base. The advantages of HIP over cold compaction and pressing is:

- 1) The final product can reach a relative density of 100%
- 2) Higher tolerances can be achieved
- 3) Associated with the least pores and defects

## 2.9 Hot compaction

When cold compaction does not reach the best relative density the alternative is the hot compaction where the powders experience heat while being compacted to enhance the pressing. The heat usually softens the particles and this results in the better density [30,43]

## 2.10 Powder Rolling

Powders of metallic base can be rolled into strips that will be green compacts ready for consolidation to form the solid bulk state [30]. The advantages of the powder rolling are to avoid conventional processes as melting, hot forging, ingot casting, and hot rolling.

## 2.11 Hot extrusion:

Hot extrusion is another process for consolidating powders by directing the part towards a die orifice to reduce the cross-sectional area based on the desired reduction ratio. This ratio defines the properties of the material after processing and they vary according to the material itself. The temperature of the process is calculated based on the recrystallization temperature of the material. The process has an annihilation effect on the present cracks in the material and also produces better densification in less time [39,41].

Hot extrusion has been associated lately to consolidating nano-powders of MMCs and CMCs and above all the consolidation of aluminum based MMCs and this is due to the uniform distribution of the matrix [39].

## 2.12 Spark plasma sintering

Another method of consolidation powders is by the use of electric current and this dates to old days [32], later they reached the most common device which is the spark plasma sintering (SPS). SPS sinters materials by the use of pressure and electric current. The SPS process is explained where there is: a uniaxial press with a cooling system and it performs as electrodes, a reaction chamber, a pulsed direct current generator, and systems of regulating pressure and position. The SPS reduces the consolidation time from hours to minutes while the temperature is also reduced [32]. SPS is an encouraging consolidation technique that is being used in all advanced research.

### 2.13 Wear

In all mechanical applications, there exists solid parts that move in respect to one another. In order to maintain any movement, it is a must that two or more parts come in contact while preserving the relative motion. This motion must create friction forces and eventually lead to wear of the surfaces in contact, preferably the surface of the less-hard material. This phenomenon is known as “tribology”. Tribology has numerous factors that control it as the material itself, the motion, and whatever is between the two surfaces. However, it requires a high level of prudence to examine these factors causing wear and erosion.

Wear is simply defined as the damage of surface and/or the loss of material from the surface in contact to the moving object. This relative movement that creates wear is a common occurrence that could be found in cylinders moving in and out their chambers, car brakes plates, or even more other daily applications. Among the wear controlling factors there is the way of stacking the materials or surfaces and the kind of relative motion. “Rubbing” and “Grinding” are two common terms correlated with wear and tribology. Grinding can be referred to as the power created between the contacting surfaces while it acts tangential to the surface and has a course which is inverse to the drive's heading. Friction is rather the force created between the contacting surfaces while it also acts tangential to the surface but with a course opposite to the primary motion.

Wear is categorized according to several among which are the characteristics of the wear scar, the mechanism of material removal, and the conditions of wear. Each category of wear has some terms associated to it as for example, pitting, spalling, scratching, crazing, fretting, gouging, and scuffing are common terms of the first category. The second category is rather attributed to abrasion, delamination, oxidation, and adhesion. While as the third category is associated with

terms as rolling wear, high temperature metallic wear, metal-to-metal sliding wear, lubricated or unlubricated wear, rolling wear, high stress sliding wear, and sliding wear.

## 2.14 General types of wear mechanisms

### 2.14.1 Adhesion:

As two different surfaces have direct contact between one another, they tend to adhere at localized sites. If the surfaces develop motion relative to one another, adhesion wear takes place as a result of one material detaching material from the other surface at this specific localized site. [29]

### 2.14.2 Abrasion:

Abrasive wear is related to hard particles that exist between the interacting surfaces. Such particles can be either of a different material than the two surfaces and in that case is suspended between the surfaces or can be a hard particle of one of the surfaces. In both cases there still exists two kinds of abrasion. First, the two-body abrasions which occurs when wear is facilitated by protuberances on a surface or hard particles set to the surface. Secondly, three-body abrasion which takes place when the hard particles are not part of either surfaces and are unattached to any of them. A perfect example of abrasive wear is the micro-cutting of small sized chips by a hard cutting tool. [29]

### 2.14.3 Delamination:

Delamination is simply the elimination of large flakes of material from one of the rubbing surfaces. As a result of continuous sliding, rolling, or impacting, the surfaces in contact undergo cyclic stress which facilitates cracks. As the cyclic stress increases, the cracks propagate and they overlap with the surface and themselves. This is how a larger flake is removed from the rubbing surface. People refer to delamination as “fatigue wear” [29].



#### 2.14.4 Oxidative:

When two surfaces rub against each other but under light loads and in a dry condition the metallic wear scars are characterized by a smooth glassy appearance. This is when the wear rate is relatively low and when also the fine metallic oxides particles appear. The glassy appearance mentioned above is a result of the oxide layer formed on the surfaces of the wear scars. Henceforth, wear takes place either in the changed layer or at the interface between the layer and the parent material. Still between surfaces the oxides breed on the uncovered areas of the surface to be later detached by the asperity meeting. This process is named oxidation to refer to the chemical reaction that fluctuate the composition of the surface. However, this process is not concerned only with oxygen effects but it is widely mutual in engineering applications. It can also be referred to either as chemical wear or corrosive wear [29].

## 2.15 Wear Characterization

The tribological behavior is a major function of the service environment where the factors and parameters manipulating the wear will differ according to this environment. At this stage, it is important to identify and characterize wear mechanism to reduce failures and to recommend solutions for preventing wear [30].

The optimum method for characterizing wear is the classification of wear into general mechanisms and then study each one of them in depth or operational classifications. The mechanism of abrasive wear is when the material surfaces is exposed to wear by the abrasive particles or debris. Adhesive wear is when two solid surfaces are tend to adhere at localized sites. in contact and therefore they are exposed to wear, [30].

The operational classifications for the different types of nonabrasive wear is related to the elements in contact in the tribosystem itself:

- 1- Type of motion: rolling (with /without slip), sliding (High or low speed, fretting) or impact.
- 2- Lubrication: type and rate of lubrication.
- 3- Load: Variable or constant.
- 4- Contact geometry: whether the contact of the rubbing surfaces is over an area, point or line.
- 5- Environment: temperature, abrasive particles and humidity.
- 6- Materials: rubbing surfaces or of similar or dissimilar materials and/or harnesses.

In some cases, the sub categories strongly affect the abrasive wear behavior and they are number of abrasive bodies, relative hardness of the abrasive particles to the surface hardness, dry or wet abrasion and the level of stress applied [30].

Several types of the mechanisms can coexist in a tribosystem, which develops new complex wear condition. However, there must be a dominating mechanism that controls the process and this may change with the change of the parameters or the working conditions. As a result, materials often experience transitions of wear mechanisms with the alternation of parameters of which are velocity, load, and or friction [30].

## 2.16 MMC Applications

The advanced materials of high performance are of a great demand in several industries that acquire high technology as the aerospace industry, automotive industry, sports industry, and many other high-tech industries. MMCs grants scientists the luxury of tailoring new MMCs with the needed properties that would serve the proposed design of a certain application. For instance, the coefficient of friction (COF), coefficient of thermal expansion (CTE), damping capacity, specific strength, specific stiffness, thermal expansion, energy absorption, and thermal conductivity are some of many other factors that can be tailored in a MMC [21]. This is achieved by the addition of various reinforcements in different sizes, contents, and shapes to reach the desired properties.

Researchers have been focusing on developing metal matrix nanocomposites (MMNCs) to achieve advanced materials' properties as self-lubricating properties, self-cleaning properties, and self-healing properties. The nano reinforcements is one of the solid candidates as well as the shape memory alloy fibers, hollow balloons, and other types of reinforcements that open doors of novel MMCs [31]. Especially the idea of reinforcing MMCs with nano particles is of great success as the nanoscale has positive impacts on the overall properties of MMCs. These nano particles have been fabricated with reduced sizes up to 100nm which enhances the properties of MMCs even further. MMNCs have enhanced properties such as strength, fracture toughness and machinability

when compared to conventional MMCs. List the various properties that can be achieved by employing advanced MMC and MMNC [2].

Table 2-1 Different reinforcements of MMCs [19]

<b>Property</b>	<b>MMCs Materials reinforced with</b>
Wear resistance	Silicon carbide and alumina
Light weight	Low density ceramics, fly ash ecosphere
Self-cleaning	Biomimetic and hydrophobic filler coatings
Self-lubricating	G, graphite, Molybdenum sulfide
Thermal conductivity	Diamond, high conductive carbon or cubic boron nitride
Low cost	MMC with waste sand as fillers

### 2.17 Al-based MMC for Mechanical and Tribological application

The innovation in high strength, high elastic modulus and wear resistance materials is derived by the limitations of some mechanical designs and the new ambitious designs. Such designs are fully dependent on the evolution of new materials that could serve the purpose of its application. Mechanical behaviors of aluminum alloys matrices have been comprehensively studied. The studies showed that the diversity in the in the mechanical properties came from the variety in type, size and shapes of reinforcements than can be added to the matrices. Since the MMC, especially aluminum alloy, is being introduced to the industry in various amounts. For instance, the field of the aerospace, the Hubble space telescope antenna is made of AA6061 reinforced with phosphorus and graphite. The antenna should sustain compression strength, high thermal resistivity and good electric

conductivity for signal transportation. Moreover, the rib truss and frame members made of AA reinforced with boron which combines the low density and high strength behavior. The using of Al based MMC components in space shuttles saves more than 130 Kg of the total weight which consume a large amount of energy [32].

Aluminum alloys are boosted and modified frequently to advance their wear resistance. Aluminum alloys of different series such as 2xxx, 5xxx, and 6xxx are considered as alloys that perfectly fit the industrial needs and are used as reliant substitutions to cast irons. Additives to the aluminum alloys tend to develop casting and machining properties, corrosion characteristics, and wear resistance. Research was directed towards the investigation of the wear properties of these alloys yet, the majority of studies focused on dry sliding conditions [33].

Carbon based materials such as graphite served as an appropriate self-lubricant which has good dispersion inside aluminum matrices. During the past decade studies illustrated the behavior of graphite as reinforcing material under wear application.

#### 2.17.1 Effects of Graphite

Graphite is the most mutual reinforcement that serves as a solid lubricant in its composites and hence, it transforms the whole composite to a self-lubricating composite [34, 7]Composites that are reinforced with graphite show improved wear resistance and tribological properties which make their use in demand in most industrial applications where the wear is an issue. The wear rate is reduced significantly in the graphite reinforced composites as the damage accumulation is decreased due to the presence of graphite.

MMCs reinforced with graphite serve perfectly the aerospace and automotive industries due to their advanced tribological properties. Among various matrices of MMCs, aluminum is

extensively used due to its high strength to weight ratio, reasonable corrosion resistance, and its advanced tribological properties.

The wear mechanisms occurring in aluminum composites reinforced with graphite are the explanation of the theory of the advanced tribological properties. Aluminum exhibits a low yield strength and is prone to deformation during sliding of surfaces while the graphite reduces the deformation of the surface by forming a graphite solid lubricating layer after a brief running time. The COF decreases as well in MMCs reinforced with graphite as a result of the formed carbon based layer on the surfaces which act as a self-lubricant. This layer reduces the direct contact between the surfaces in contact which sums up the enhancement of the wear resistance of the composite [35]. The solid lubricating film decreases the cold welding which occurs between the rubbing surfaces as it prevents the transfer of atoms from the less hard to the harder material by the reduced direct contacts between the surfaces. Regardless to the fanciful tribological properties of the MMCs reinforced with graphite, their mechanical properties remain moderate.

#### 2.17.2 Effect of Carbon Nanotubes

Carbon nanotubes (CNT) is one of the solid candidates for self-lubrication that is widely used in modern composites due to its improved electrical, mechanical, and optical properties besides the superior tribological properties [36]. This makes MMCs reinforced with CNTs a reliable material in many industrial applications in terms of mechanical properties and wear resistance. It is claimed that multi walled carbon nanotubes (MWCNT) will be vigorously used in materials for industrial applications due to their reasonable costs. This directed the research towards the reinforcement of MMCs with MWCNTs through various methods of fabrication. Studies have proven that the same reason for the enhancement of the tribological properties is due to the self-lubricating properties of CNTs in general. It has been proved that the durable interfacial bonding

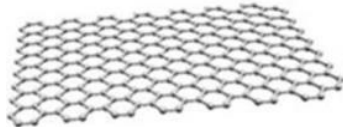
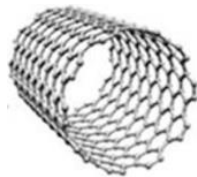
between MWCNTs and an epoxy matrix makes the outer shells of the carbon nanotubes rest embedded in the matrix [37]. This is not the case in MMCs as the carbon nanotubes will be bonded with the matrix by a weak Van der Waals force but this is beneficial as these weak bonds allow the sliding of surfaces easily with a lowered coefficient of friction. As explained previously, the CNTs act as spacers between the rubbing surfaces and thus, increase wear resistance [28]. The factors controlling the process of enhancement of tribological properties are amounts and sizes of the reinforcements, as well as the special distribution of the reinforcements in the matrices.

### 2.17.3 Effect of Graphene

The two-dimensional structure of G gives it even more advanced tribological properties than other carbon based reinforcements. It also experiences advanced electrical, optical, and mechanical properties which introduce its usage to solid or colloidal liquid lubricants. Its tribological properties are credited to its extremely high strength, chemical inertness, and the easiness of shear on its surface of densely packed atoms. G is ultrathin even if it is on multilayers and this makes it suitable for microelectromechanical systems (MEMS) and nanoelectromechanical systems (NEMS) to be reducing frictions and improving wear resistance. Lee et al. [34] tested the mechanical strength of G and concluded that it is one of the strongest materials in the creation which is why the G inhibits advanced tribological properties. They made use of free standing G membranes to test their breaking strength by atomic force microscopy (AFM) probe. Their results showed a 1TPa Young's modulus for the defect-free G sheets. The tip radius is the controlling factor of the breaking force rather than the radius of the membrane. While the grain boundaries have no effect on the strength of G [38], other defects as oxidation negatively affect the mechanical properties of G and make it experience a dramatic decrease in strength and stiffness. However, for the enhancement of tribological properties, the extremely high strength of G is a must.

Moreover, G is impermeable to liquids and gases which does not allow the passage of oxygen which is an advantage for decreasing the corrosion of surfaces [39]. In addition, water has been proved to improve the friction occurring on surfaces of G which controls the effects of capillary forces in humidity. Singh et al. [40] validated the alteration of the wetting angle as a function of the surface beneath the layer of G. Unfortunately, the effect of the substrate is only valid for low numbers of G layers and is insufficient for multi layers. G has a low surface energy and has a two-dimensional structure which makes it perfect for the replacing of thin lubricating films. To conclude, G has unique properties which are mentioned above and that is why they experience the unusually enhanced tribological properties. The table 2.2 introduces the main physical and mechanical differences between G and CNTs.

Table 2-2 G and CNTs properties. [38, 41, 42]

Property	Graphene (G)	Carbon Nanotubes (CNT)
Structure	<p><b>A</b></p>  <p><b>graphene</b> Sheet</p>	 <p><b>SWCNT</b> Tube</p>
Chemical Structure and Types	Single sheet with an approximate thickness 1 atomic layer and multi sheet.	Single walled with an average internal diameter 2nm, and Multi walled tubes with internal diameters between 4 -20nm.
Synthesis Methodologies	<p>CVD Epitaxial growth Chemically Mechanical cleavage Organic method</p>	<p>CVD Arc discharge Laser ablation Hydrothermal</p>
Density	0.8 gm/cm <sup>3</sup>	2.2 gm/cm <sup>3</sup>



Young's Modulus	1TP	1TP in axial direction
Average tensile strength	105 GPa	130 GPa
Average thermal conductivity	5400 (W/mK)	3500 (W/mK)

#### 2.17.4 Graphite Vs Graphene

The tribological properties of G were tested at the nano and micro scales to propose it as a solid lubricant. Also, macro scale tests were carried on G and the results were as predicted which allows the usage of G as a lubricant on the macro scale as well. However, G at the macro scale must be studied and compared with the behavior of bulk graphite. Micro scaled graphite had been tested and used in the industrial applications since 40 years ago [42]. Bulk graphite has its optimum performance in humid environments while it does not serve as expected in inert, vacuum, or dry environments [44]. This is due to the intercalation of water molecules between graphite sheets which results in easy shearing of graphite and hence, the friction is reduced. Research on graphite flakes in tribological conditions had proved that graphite forms scrolls at the rubbing interfaces [45]. Such scrolls are beneficial in reducing the surface energy and friction [46,47]. To compare, the recent research mixed 5% wt. ethanol with graphite powders which is much higher than the percentage of G in ethanol but this was done to reach similar deposition procedure as the one stated below in "G as a solid lubricant". The tests were carried under the same conditions of humid air and dry nitrogen to be comparable with G results. Graphite failed to show tribological enhancements when tested in dry nitrogen, the friction and wear were increased. It is of importance to determine the behavior of G in dry conditions. In this work, G showed reduced wear rates regardless to the working environment. Figure 2-2 explains the advanced behavior of G when

introduced as a solid lubricant in wet and dry conditions. These results were only associated with G and not with polycrystalline graphite [43]. It was required to test the stability of the coefficient of friction of G and therefore, it was tested on steel surfaces with the change of relative humidity by filling the chamber where the test takes place with nitrogen to demonstrate a dry conditions and then open the chamber to achieve humid conditions. The results were always showing improved coefficient of friction and reduced wear. The behavior of G on the macro scale is explained in the next chapter

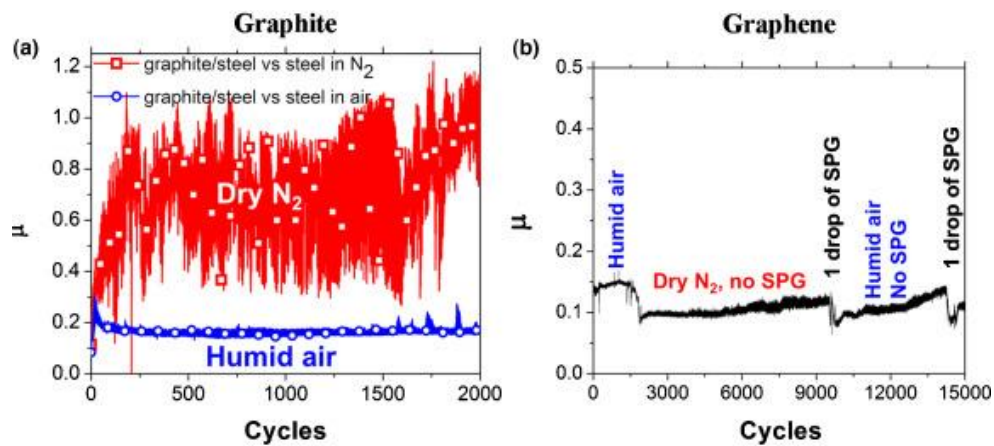


Figure 2-2 Graph represents the coefficient of friction of a) A wear test under dry nitrogen and humid air for graphite deposited on steel and b) Behavior of graphene in dry and humid environment versus number of cycles at 1N load. [43]

### 2.18 Bulk Crystallographic Texture

Mechanical, thermal and magnetic properties of metallic materials are directly dependent on the crystal (grain) orientation. When a material has a preferred grains orientation then this material has a crystallographic texture.

### 2.18.1. Grain Orientation

Before introducing the concept of pole figure (PF) and orientation distribution function (ODF), it is crucial to introduce the grain orientation. The grain orientation is presented with respect to a three-dimension coordinate system. For instance, in sheets and plates this coordinate system is the rolling (RD), normal (ND) and transverse (TD) directions. On the other hand, the miller indices  $\{hkl\}\langle uvw \rangle$  represents crystal orientation, as shown in Figure 4-5 a, the (001) is parallel to the rolling plane and  $[1\bar{1}0]$  is parallel to the rolling direction. When then crystallographic is equivalent such as the asymmetric products (wires and bars), one miller indices will be enough to define the crystal orientation. Fig (4-5 b) show an extruded bar its crystallographic direction is parallel to  $[111]$

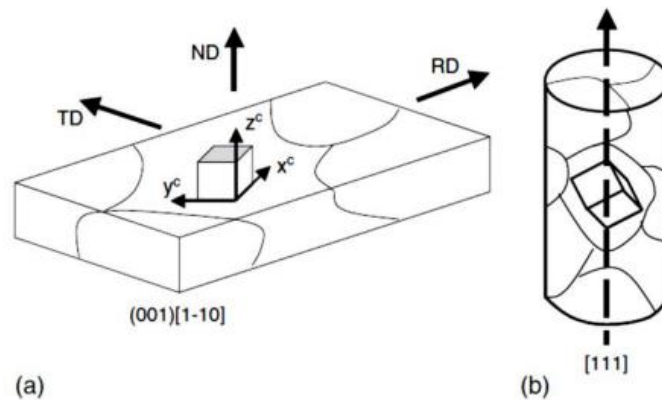


Figure 2-3 crystal orientations in sheet (a) and bar (b), presented with respect to Miller indices [44]

### 2.18.2. Pole Figures

Pole figures are a 2D stereographical projections in which the variation in pole intensities and locations are relative to the crystallographic planes and plotted with respect to the geometry of the

specimen. For instance, as shown in Figure (4-6 a) a plot of PF (100) is illustrated, however, Figure (4-6 b) shows the (100) poles of a single crystal. Figure (4-6 c,d) represent the polycrystalline materials without and with texture. A counter maps (Figure 4-6 e) is usually used to plot the textured polycrystalline specimen.

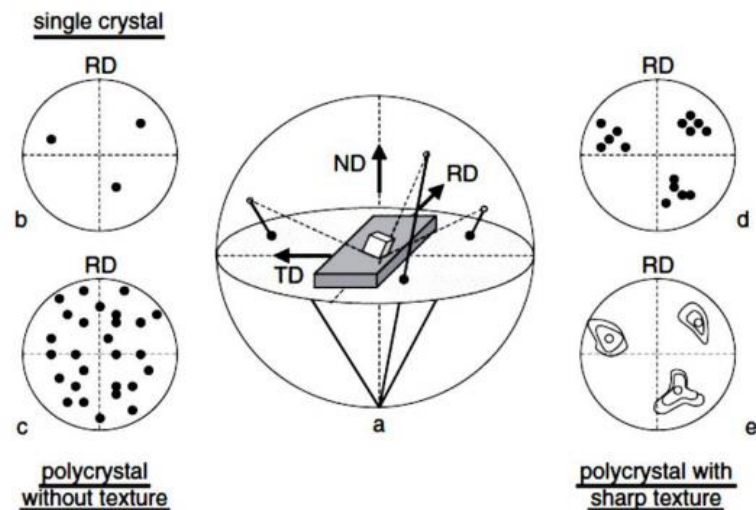


Figure 2-4 Schematic showing construction of a (100) pole figure [44]

### 2.18.3. Orientation Distribution Function (ODF)

The OFD method has been developed since the PF has some limitations. While converting PF from three dimensions' space to two dimensions' circle various orientations are missed. The ODFs helps to introduce a complete texture for any specimen. The ODF is an expansion which represent the volume fraction of grain orientation in all possible intervals. The integral values of ODF is equal to a constant and if this be applied on any textured specimen the ODF will have a maxima and minima integral values which represents in graphically. The ODFs maps represents the crystals

orientation with respect to Euler angles. The Euler angles are ( $\phi, \psi$ , and  $\theta$ ) which are between the crystal axes and the specimen deformed axes (RD, ND and TD).

#### 2.18.4. Texture components and Fibers

For the explanation of pole figures, it is essential to introduce the locations of some important ideal orientations in pole figure form. Table 2-3 Major Texture Components in FCC structure which presents a series of (200) pole figures, showing the ideal positions of a few important texture components that are belongs to materials have FCC and BCC unit cells. The B {110} <112> and S {123} <634> components, are generally found in the deformed texture of FCC materials. Cube {100} <001> component is a sign for the dynamic recrystallized in the FCC materials.

Table 2-3 Major Texture Components in FCC structure [44]

Component, Symbol	{hkl}	<uvw>	$\phi_1$	$\Phi$	$\phi_2$
Copper, C	112	111	90	35	45
S	123	634	59	37	63
Goss, G	011	100	0	45	90
Brass, B	011	211	35	45	90
Dillamore, D	4,4,11	11,11,8	90	27	45
Cube	001	100	0	0	0

## Chapter 3. LITERATURE REVIEW

### 3.1. Nanotechnology in Wear application

Progressive developments in nanotechnology over the past years enabled several appealing advancements in metal matrix nanocomposites. Along with structural applications, the use of MMCs has been extended to functional devices such as self-healing and self-lubricating ones. Depending on the final desired outcome, different reinforcements are used. Amongst the numerous reinforcements, the evolving materials, carbonous materials, are of profound interest. Owing to their lubricious nature, materials such Carbon nanotubes (CNTs), graphite, and graphene have enticed researchers to investigate the possibility of creating a synergy between metals and carbon-based reinforcements to produce materials with superior mechanical and tribological properties [27] [37].

Recently considerable amount of research has been made to study the influence ceramic and carbonous reinforcements embedment into metal matrices would have on their tribological properties. The study basically focuses on the investigation of wear and friction performance of the tailored composites. When two surfaces in contact are imposed to external load and are allowed to move against each other, atoms of the softer materials are taken off and tend to position themselves on the asperities of the rather harder one [10]. Consequently, cold welding takes place and fracture may occur at the conjunct points and eventual shear. Avoiding friction and deterioration of mechanical parts subjected to wear, has been the main drive behind the intricate desire to synthesize such self-lubricating materials. Conventionally, liquid or solid lubricants are applied on mechanical systems undergoing sliding and eventually resulting into wear of their surfaces as a result of their contact. The application decreases the coefficient of friction and wear

rate. However, undesirable performance of liquid and grease lubricant types has been noticed when imposed to rough environments of high heat and speeds [45]. Likewise, poor adhesion of solid coatings on to material surfaces as well as the limited lifetime has enticed the need for self-lubricating composite materials.

In general, reinforcements tend to reduce the coefficient of friction and increase wear resistance of MMCs, which improves their tribological characteristics compared to its individual rivals. They play a role in bearing loads contact surfaces are exposed to and thus protect them from deteriorating during sliding [13]. However, in some cases, the hard-ceramic particles would poorly adhere to the composite and gets trapped in between the sliding parts; acting as a foreign additional abrasive which in turn increases the wear rate instead of the opposite. In comparison, graphite particles or carbon fibers are embedded within the metal matrix and form a lubricant film between the interacting surfaces which hinders cold welding of atoms during atoms and the subsequent harmful wear and fractures .Additionally, they acquire exceptional high thermal conductivity, low coefficient of thermal expansion, and high damping capacity .In this regard, compared to ceramic enforced metal composites, solid carbon-based lubricants tend to be more effective reinforcing fillers in self-lubricating composites [11].

During the past years, researchers have been using graphite in the micron size as reinforcements in MMCs to attain enhanced tribological properties [8]. However, the content of graphite is directly proportional to the enhancement of tribological properties to a certain limit where the content will not further enhance the properties. The reasons behind this limit is the softness of graphite, its chemical inertness and, its agglomeration issue that all contribute to reduce the mechanical strength of the MMC. Therefore, it is preferable to use nanosized particles in order to avoid the drawbacks mentioned above while maintaining the enhanced tribological properties.

The nanocomposites have shown smooth and clean fine grooves while the micro composites deteriorate and their surfaces wear more than the nanocomposites [46]Recent research work has been focusing on the use of nanosized graphite particles instead of the nanoscale ones in order to counteract their drawbacks Moreover, more focus is being made on the employment of carbon nanosolid lubricating fillers such as CNTs and graphene [38]

Principally, the reinforcement size immensely influences the mechanical properties such as strength and fracture of the MMCs. Traditionally, metals are reinforced by graphite in the micron size to form the self-lubricating composite but it has been evident that larger size reinforcements has an undesirable effect on strength and ductility. It is thus expected to overcome some of these limitations by using filler particles in the nano range. While nano carbon nanotubes and graphene are both strong candidates, dispersion of graphene in any matrix is relatively easier than its relatively expensive rival, CNTs. Dispersion of graphene is easier within the metallic matrices compared to CNTs for the following features: its 2D structure that has a high deflection capacity, its high aspect ratio that allows it to cooperate from two sides, and finally it has a unique surface texture that interlocks perfectly with the matrix. Graphene is also less favorable to rotate and hinder atomic diffusion at elevated temperatures [38] .

It exhibits better properties such thermal conductivity, electrical conductivity, mechanical strength making it highly recommended substitution to CNTs [47].In this manner, an excellent combination of having a low coefficient of friction and high mechanical properties is achievable which led to their increased industrial uptake in applications where tribological attributes are of prevailing significance [1].

It has been verified by Huang et al. that during sliding, the nano-sized particles are able to fill most of the asperities of the surface forming a solid thick adherent layer between the composite



and interacting surface. In the case of the micron-sized particles, relative to their larger size, it becomes more difficult to penetrate the narrow grooves leading to a less efficient lubricating film [48].

As this is a fairly novel material, few studies have been performed in attempt to investigate the tribological properties of graphene reinforced metal matrices. Rajkumar et al. [49] synthesized copper reinforced by nano-graphite particles with an average size of 35nm. Powder mixing followed by compaction and microwave sintering were employed as the composite fabrication technique. Furthermore, copper coated the graphite particles using the electroless-plating method. It is important to note that the graphite particles have not been exfoliated and cannot be considered as graphene platelets (few layers of graphene sheets) in this investigation. Generally, results have demonstrated that particles in the nano range decreases the coefficient of friction and wear rate of the composite in contrast to its micro size counterpart. A prime finding was that the amount of nanographite particles has a major role in the resultant wear properties of the composite; this decrease in the COF is associated with the increased availability and uniformity of the lubricant layer. This lubricant film, which is responsible for the reduction of the rate of deformation and wear, is uniformly formed with the volume percentage of graphite particle reaching 15 vol.%. Another phenomenon enhanced with such increase more porous cavities are filled leading to lower porosity and increased relative density. In divergence, when the volume fraction is increased to more than 15 vol.% , the nano particles agglomerate with no uniform spreading along the contact surfaces leading to an increased wear rate as well as reduced relative density of the copper composite [49].

Similarly, by increasing the sliding speed up to 1.77m/s, the COF decreases considerably as it facilitates the formation of a continuous lubricant film. Above speeds of 1.77m/s, the film peeks

off the contact surface resulting to an observant increase of the friction coefficient. Nevertheless, at higher amounts of graphite particles up to 20 vol.%, the COF was not greatly affected by higher speeds due to the continuous strongly adherent film formed. Another evident phenomenon was that with the increase in the applied normal load comes an increase of both the COF and wear rate [30]. As an explanation, Huang et al. [50] has suggested that the fine graphite particles would get squeezed out at high loads and thus deforms the lubricant layer formed hence leading to reduction in the wear and friction properties of the composite.

As a summary, the high hardness, the low porosities, the fine microstructure are the main benefits behind the addition of nano sized graphite in self-lubricating MMCs. The only obstacle in this innovation is the creation of a composite with homogenously distributed graphene/graphite sheets.

### 3.2. Metal-Graphene Nanocomposite

The fabrication of aluminum with graphene nano sheets (GNSs) is as similar the fabrication of aluminum with CNTs in terms of the homogenous dispersion of GNSs in the matrix while sustaining the structural integrity of the GNSs. The aggregated graphene has a similar behavior as the particulate graphene platelets. 2D graphene sheets are able to give super high surface areas but unfortunately, this surface area is lost when the graphene clusters [54,104]. This leads to a challenge of finding a method to fabricate MMCs reinforced with graphene that if fully dispersed in the matrix or even exfoliate single sheets of GNSs. The exfoliation of GNSs in polymer based composites has been researched aggressively and attained the needed results, while the same process in metal based composites still lacks the research and knowledge.

The difference between the surface energies of the carbon reinforcement and the metal matrix is what controls the exfoliation of the graphene in MMCS. The remarkable difference in the surface energies prevent the metal from wetting the graphene sheets and falling them separately. Researches tried several methods to fabricate the fully dispersed graphene reinforced MMC such as metal evaporation, electrochemical deposition, and hydrogen reduction metallic salts-graphite composite [105-107]. In all cases, the fully exfoliated graphite flakes in a MMC has not yet been achieved. The inconvenience in the fabrication of such composites makes it an obstacle for mass production. On the other hand, powder metallurgy (P/M) is considered as the optimum method for fabricating aluminum reinforced with CNTs and that is why it is also considered a fabrication method for aluminum reinforced with graphene nano sheets (GNSs) [51]. The hydroxyl and epoxy groups present in the Graphene Oxide (GO) nano sheets facilitates the dispersion in solvents and produce solutions which are more stable than graphene. This creates the favorability of GOs over GNSs [108]. Wang et al [31] testified a method for fabricating aluminum reinforced with GO by P/M techniques in four consecutive steps which are: (1) exfoliation of GO into single-layered or several-layered nano sheets through the sonication of GO in an aqueous dispersion like deionized water, (2) modifications of the surface of aluminum flakes surfaces by ball milling and then the introduction of a hydrophilic membrane as PVA on their surfaces, (3) addition of the powder slurry of the milled aluminum flakes in deionized water to aqueous solution in step 1 in order to confirm adsorption reduction of G oxide nano-sheets. The color of the mixed slurry alters from brown to transparent in the existence of stirring. The heating of the composite will decompose the hydrophilic membrane as well as it will reduce the G oxide nano-sheets to GNSs and this will be carried till powders of aluminum and GNS are achieved. (4) The compaction and the

consolidations the powders will be obtained by sintering in argon atmosphere and finally hot extrusion.

Bastwors et al. [10] exfoliated graphite to graphene through a solution of nitric acid and sodium chlorate. Sedimentation gave the intercalated graphite which was then exfoliated to monolayers or few-layers of graphene oxide through ultra-sonication. Later, A16061 powders were ball milled with graphene through different milling times and followed by synthesizing through hot compaction in semi-solid regime of the A16061. Literature also claims that the attachment of molecules or polymers to graphene sheets decrease the effect of aggregation [52]. Xu et al. [53] recommend a mixture of graphene oxide, a solvent, and an inorganic nano particle to obtain graphene as individual sheers in metal matrices. The inorganic nano particles rest between graphene sheets to impede the re-agglomeration of graphene. Later the solvent will evaporate and the dispersion of isolated graphene sheets would be attained to acquire graphitic stacks with inorganic nano particles between the interlayer spacing. Another composite of aluminum and 0.3 wt.% graphene is fabricated by the usage of a slurry based process which is followed by sintering and hot extrusion . Figure 3-1 shows the comparison between the normalized tensile strength and ductility of Al reinforced with GNS composites and the pure matrix. The composite experiences a tensile strength of 249MPa which is about 62% improvement when compared to a tensile strength of 154MPa attributed to the pure matrix. This explains the effect of GNSs on enhancing the mechanical properties of aluminum alloys and proposes GNSs to be used as a reinforcement in nano composites.

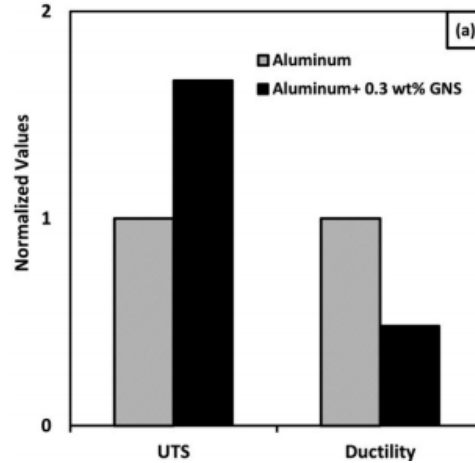


Figure 3-1 bar chart shows the influence of G on the mechanical properties of Aluminum [19]

Basically, the GNSs enhance the strength by dislocation strengthening and stress transfer while also considering the grain size refinement. Grain refinement is achieved by the GNSs impeding grain growth and by resisting the movement of dislocations during plastic deformation or thermal processing. This is a brief explanation for the increase in tensile strength in the presence of GNSs. Graphene could also bear high loads during plastic deformation or in general and this is another clarification to the enhanced tensile strength. Figure 3-2 shows the fracture surfaces.

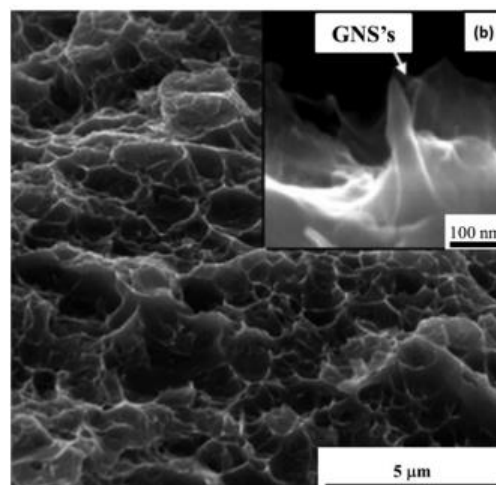


Figure 3-2 Al-0.3wt.%G fracture surface [19]

While the fracture strength of a single layered graphene is 125GPa, the theoretical fracture strength of an aluminum composite reinforced with graphene is 500MPa. The strength of aluminum with 0.3 wt.% G is experimented and tabulated as 250MPa. The loss of strength compared to the theoretical values is a factor some different parameters. The alignment of G with the direction of the tension (tensile test), microstructure, weak interfacial bonding, and the processing parameters are some of the parameters that lead to an inferior tested tensile strength [49]. Latief et al. [54]fabricated aluminum composites reinforced with graphene but in different percentages of exfoliated graphite nano-platelets particles through the employment of P/M to be able to examine the physical and mechanical properties of the produced nano composite

Bartolucci et al. [55] made a comparison between the mechanical properties of aluminum composites reinforced with multi walled nano tubes (MWNT) and aluminum composites reinforced with graphene nano-platelets. The hardness results of the 1.0 wt.% MWNT showed the highest hardness when compared to 0.1 wt.% GNP. The MMC reinforced with nano tubes exhibit the highest strength when compared to the MMC reinforced with graphene. The tensile strength of the extruded Al/MWNT composites is almost 12% higher than the pure aluminum while at the same time the strength of the Al/GNP is 18% less than the strength of the pure aluminum.

### 3.3. Wear mechanism in Al- CNTs and Al-G

Lee et al [8] showed the classical wear maps of composites with and without reinforcements in order to explain the effect of solid lubricants on the tribological properties of metallic matrices. The maps consist of wear tracks, wear rates of sintered composites, and cross sections at several speeds and loads. The map is divided into two parts which are the mild and severe wear and the

seizure follows them at the end. The beginning of the wear with the oxide layer being removed and the appearance of solid lubricant on the worn surface and this is dominant at low loads and speeds. When the loads increase, the wear is shifted towards abrasive and adhesion where the continuous oxide film is present and solid lubricant withdraws while imposing shear forces that results in body abrasion and the formation of cracks by the delamination, in the case the composites. The increase of solid lubricant has shown to delay the nucleation of the crack and its propagation which also shortens the phase of the severe wear in composites when compared to unreinforced metals [56]. The wear rate has been decreased in the composites because of the delamination and this relates also to the enhanced hardness and strength which are also related to the addition of solid lubricant. On the other hand, unreinforced metals exhibit adhesive wear as they are soft and are accompanied with a low yield stress and a large area of plastic deformation which is followed by the severe delamination and the micro ploughing that are not present in C-nano solid lubricant -reinforced MMNCs [8].

The addition of Carbon nano solid lubricant was predicted to affect the wear properties as changing the mechanism from the adhesive region to the abrasive region associated with nanoscale reinforced metals and this has a direct effect on the coefficient of friction and wear rate. [57]. The nano solid lubricant embedded gets out on the metallic surface and covers it in the form of a lubricate film that gets worn later during the sliding and therefore stops the delamination which enhances the wear resistance.

## Chapter 4. MATERIALS AND EXPERIMENTAL PROCEDURES

### 4.1. Materials

In this research work, powders of Aluminum Alloy 2124 (AA2124) are used as the matrix material. The chemical composition of the powders is listed in Table 4.1, where it was obtained from the Aluminum Powder Co. Ltd, UK. Figure 4.1 (a) shows the morphology of the as-received AA2124 powder particles. Nonuniform polycrystalline particles irregular in shape can be observed ranging between 5-to-75 $\mu\text{m}$ . The average particle size measured was 45 $\mu\text{m}$ , while two levels of structures were measured within the individual polycrystalline particles. An average grain size of 0.8 $\mu\text{m}$  (measured using SEM) and an internal crystallite size of around 87nm (measured using XRD). Figure 4.1(b) shows high magnification image for the polycrystalline particles, revealing the 0.8 $\mu\text{m}$  grains clearly on the surfaces of the particles.

SEM images (Figure 4.1 (c, d)) of the as received graphene sheets (GS), which was purchased from the SkySpring Company, USA. Figure 4-1 (c) shows clustered graphene monolayers with an average particle size of 15  $\mu\text{m}$ , Higher magnification imaging revealed multilayered G-platelets about 5-10nm thick (Figure 4-1 (d)). The purity of graphene is 99.5% and was extracted chemically from graphite. The Raman spectroscopy in (figure 4-1(e)) presents graphene pattern

Table 4-1 Aluminum alloy 2124 chemical composition

Elements	Al	Mn	Mg	Fe	Ti	Zn	Cu	Si
Weight percentage	Balance	0.1	1.5	<0.3	0.15	<0.25	3.9	<0.2



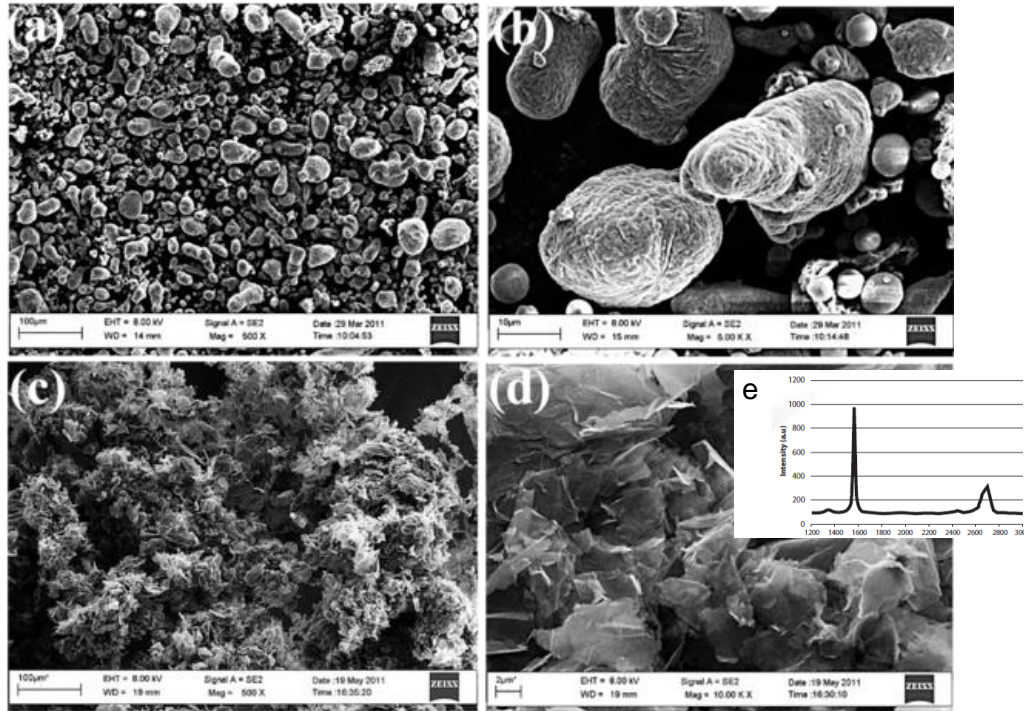


Figure 4-1 SEM images for As-received (a, b) AA2124 Powder (c, d) Graphene particles, at low and high magnifications, respectively and (e) Raman spectroscopy pattern for G [58]

## 4.2. Processing of AA2124/Graphene Nanocomposite

### 4.2.1. Handling and Mixing of the As Received Powders (AA2124+Graphene)

To ensure a controlled atmosphere for the experiment, all of the powders' handling and weighing processes were conducted in an argon filled atmosphere inside the LABCONCO glove box. Afterwards, the mixing process took place inside the off centered TURBULA T2F mixer. This was done to ensure the homogeneity of the dispersion of the filler powder inside the Aluminum Alloy matrix. The mixer is set to run at 96 rpms for 60 minutes.

#### 4.2.2. Dispersion of Graphene via Mechanical Milling

A Retsech planetary ball mill PM 400 was used for the high energy milling process. The milling process was operated in a discontinuous operation to eliminate the occurrence of overheating. The actual milling time was 2hrs. Additionally, the milling process was done under an argon atmosphere to minimize any oxidation from occurring. 125 ml stainless steel jars and stainless steel balls were used for the grinding process, where the ball to powder ratio was 15:1. The average diameter of the stainless-steel balls was 8-10 mm. Each jar was filled with powders, stainless steel balls, and some ethanol, with 14 grams, 210 grams, and 0.2 wt.%, respectively. The ethanol was added as a control agent to minimize the occurrence of cold welding between the powder particles. Moreover, the powders were emptied inside the argon filled glove box to avoid their reaction with oxygen due to their high reactive affinity. And to ensure the delivery of the required morphology and the dispersion of the graphene inside the powder matrices, an SEM analysis was conducted.

#### 4.2.3. Powder Consolidation

The consolidation process was divided into two processes before extrusion: the compaction and the sintering. The milled powders were first compacted under a pressure of 525 MPa inside a W302 heat treated steel die [Figure 4.1], for 60 minutes. The designated pressure was assigned after several trails that were based on the density of the green compact. The cold green compacts had a diameter of 20 mm and a height of 30 mm. In the sintering process, the green compacts were placed in an induction heating coil at a temperature of 300 °C and 450°C for 75 minutes. After both processes are done, the specimens are extruded at a 4:1 extrusion ratio. The extruded specimens are then cut and prepared for the characterization process. The produced extruded rods were 10mm in diameter and 89 mm long excluding the end top section.

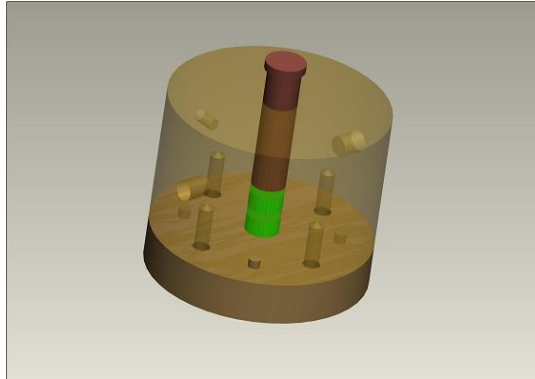


Figure 4-2A model represent the compaction and extrusion die

### 4.3. As-Extruded Consolidated Rods

#### 4.3.1. Physical Properties: Density

The specimens for the density tests were prepared by cutting the 90mm extruded rods into 2-sections of 30 and 60mm long suitable for density measurement and tensile testing, respectively. A Mettler Toledo Digital Densimeter was employed for the density measurements using Archimedes' principles [60]. The 30mm cut sections were weighted in air and then immersed in an auxiliary fluid, Xylene, with a density of  $0.86 \text{ gm/cm}^3$ , where the displaced fluid equals the density of the density of the tested specimen. This process was conducted to at least three extruded plain and mixed composite milled powders.

#### 4.3.2. Mechanical Properties:

For the characterization of the influence of G additions to AA2124 and the extrusion temperature on the mechanical behavior of the processed extrudates, hardness testing was conducted on the macro, micron and nanoscales using macro-VH, micro-VH and Nanohardness testing. Moreover, the tensile behavior of the extrudates was characterized using tensile testing.

#### 4.3.3. Hardness:

##### 4.3.3.1 Macro and Micro Hardness

Macro-hardness for the specimens was measured using a Digital Metallic Vickers Hardness tester at 19.62 N load. For the micro-hardness measurements, a Mettler Toledo VHN was used at 1 kg and 15 seconds dwell time. The average of the five readings is then taken for each specimen.

##### 4.3.3.2 Nanohardness Test

The nanohardness test was conducted using the MTS nanoindenter machine, continuous stiffness method CSM and Berkovich tip. In order to calibrate the tip method a fuse silica specimen was polished and then measured using Oliver and Pharr standard method. The indentations depth is fixed 2000 nm at a loading rate of 10 nm/sec to produce an array of 9X9. The distance between each indentation was 100  $\mu\text{m}$ .

#### 4.3.4. Tensile Testing

The remaining two thirds of the extruded specimens were machined and prepared to be used for the tensile tests. The dimensions of the specimens were produced in accordance to the ASTM E8 specimen standards as follows:

GL (Gauge length) = 20 mm

Gd (Gauge Diameter) = 4mm

Sl = So (Shoulder Length) = 22mm

Sd (Shoulder Diameter) = 8 mm



Figure 4-3 Tensile Specimen

An Instron screw driver universal testing machine, with a maximum capacity of 100 kN, was used to test out the tensile specimen. The following were the required tension test parameters:

- Strain rate:  $0.1 \text{ S}^{-1}$
- Test stop when load dropped by 90%
- Preload : 5N

#### 4.3.5. Tribological Behavior

##### Pin on Disc Testing

In order to test for the tribological properties, a tribotech pin-on-disc wear test machine (Figure4.4) was used. The machine can apply uniaxial load from 1 to 100 N and variable speed from 50 to 350 rpm. The parameters were tested in accordance with the ASTM G 99 standards where the test was conducted under room temperature and under dry conditions. The test used a standard pin on disk tribometer. Before the wear test, the specimens were carefully prepared and formed into cylindrical pins with diameters of 7 mm and length of 12 mm. The flat surface of the pin was ground using 400-1200 grid silicon carbide papers and then polished using  $0.5 \mu\text{m}$  alumina powder. On the other side, the stainless-steel disc was designed to have hardness of 63HRC, which acted as a counterface. While the disc's surface was designed to have an approximate roughness (Ra) of 0.3 microns. Prior to testing, both the pin and the disk were thoroughly cleaned with Isopropane.



Figure 4-4 Wear test machine

It must be noted that the track radius was set to be equal to 30 mm using a scaled arm that was connected to the load unit. The disk rotational speed was fixed at 300 rpms.

In order to identify the weight loss associated with wear, the specimen's weight was measured both before and after the test on a sensitive balance with an accuracy of 0.01 mg.

#### 4.3.6 Nanoscratch Test

The scratch test was also used to characterize the resistance of the composites surfaces on the nanoscale level using an XP nano-scratch method. A Berkovich diamond tip was used to scratch the film under a single pass wear test at a constant load of 50mN over a scratch distance of 700 $\mu$ m. The scratch test was conducted on surfaces cut perpendicular to the extrusion direction (transverse sections) which were ground and polished following the same procedure used for OM imaging (see section 4.3.8).

#### 4.3.7. Structural Characterization

In order to explain the physical, Mechanical and Tribological behavior of the extruded plain and composite powders before and after extrusion, structural evolution was investigated using,

Raman spectroscopy, X-Ray Diffractometry (XRD), Optical and scanning electron microscopy, as well as bulk texture analysis.

#### 4.3.8 Raman Spectroscopy

A high-performance laboratory Raman spectroscopy was used to study the influence of milling time on G structure. A 532-nm laser shutter control source was exposed to the milled powders. The laser excited the specimens with a continuously integrated beam at 35 watt.

#### 4.3.9. X-ray Diffractometry

The X-ray Diffractometry (XRD) is an analytical technique used for the determination composition and structural evolution of the as received powder before and after milling and in the hot extruded conditions. XRD was employed for the detection of carbide and oxides formation as a function of milling as well as influence of increasing graphene content on the crystallite size and lattice strain variation before and after milling. The powder specimens were taken in batches of 2 grams each prepared in the glove box under Argon Gas. Bruker powder XRD machine at the following scan parameters copper source  $\lambda$  01.540, step size  $0.05^\circ$  and angle range  $25-100^\circ$  was used. The Full Profile software was used to aid in applying the Retveld data refinement method. In addition to the Retveld method, Williamson-Hall (Eq.1) and the d spacing using brag's Law (Eq.2) were used to calculate the crystallite size and the lattice strain as follows:

$$\beta \cos \theta = \left( \frac{K\lambda}{D} \right) + 2A \sqrt{\epsilon} 2 \sin \theta \quad \text{Eq. 1}$$

$$n\lambda = 2d \sin \theta \quad \text{Eq. 2}$$

Where:  $\beta$ , is the full width half maximum and K is the Sherer constant which equals to 0.91. The D is the crystallite size and  $\epsilon$  is lattice strain and d is the interplaner spacing.

#### 4.3.10. Bulk Texture Analysis

Bulk Texture analysis of the as-extruded consolidate composite powders producing the highest mechanical and tribological properties at the as a function of the two extrusion temperatures (300 and 450°C). A Panalytical MRD X-ray diffraction system at the Wollongong University was used for bulk texture characterization. (110) Pole Figures (OF) were characterized. Subsequently, Orientation distribution function (ODF) was estimated using an academic software Matlab and J.texture. The test was performed at the following scan parameters 40 KV and 30m Amp and the source used was Cu with  $\lambda$  equals to 1.540, step size 0.05°,  $\omega$ , is the angle between the incident beam and the sample surface. In this machine both source and detector are movable.

Therefore, it should be aligned before each test to add ( $\theta + \omega$ ) and to be subtracted from the  $\theta$  in the diffracted beam calculation. Gonio Alignment is usually the rotation axis of the sample and detector with respect to x-ray beam, and Z axis, which represents the alignment required to ensure that incident beam will touch the surface height.



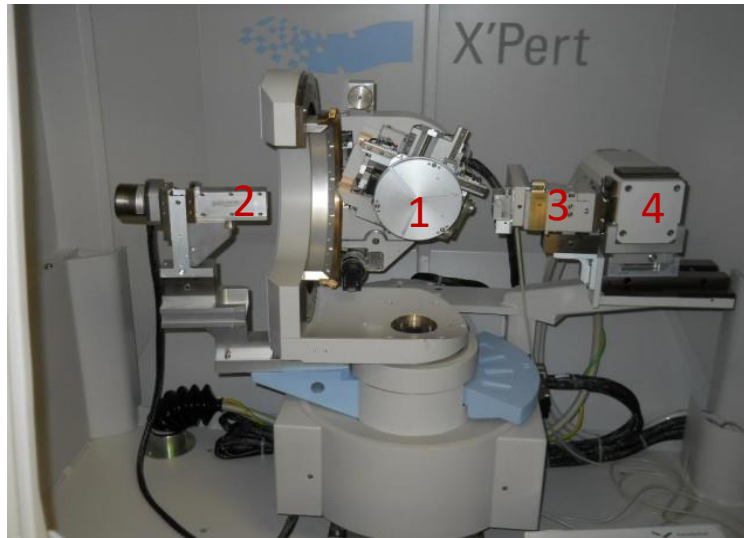


Figure 4-5 Panalytical MRD XRD machine components 1. Goniometer stage -2. Linear detector 3- solar slits, Cu-Ni filter and optics 4- Cu-Alpha

#### 4.3.11. Optical Microscopy (OM)

High and low magnifications of the microstructures of the hot extruded specimens were examined using the Leica inverted optical microscope. The obtained images were primarily used to examine the effect of the dispersion of the graphene on the specimens and to what extent they were consolidated. Before examination, the specimens were ground using several grit sizes: 180, 240, 320, 400, 600, 800, 1000, and 1200 particles per square inch. After grinding, the specimens were polished and then etched. The polishing was done using a 0.5  $\mu\text{m}$  alumina solution. The etching process was then done using a solution consisting of: 93 ml of distilled water, 3 ml of nitric acid, 2 ml of hydrofluoric acid, and 2 ml of hydrochloric acid.

#### 4.3.12. Scanning Electron Microscope (SEM)

The SEM was used for several purposes, as will be discussed. Firstly, it was used on the as received powders, the mixed powders, and the milled powders, all before the consolidation

process. Images were taken to determine the powders refinement at each stage and the dispersion of the graphene in the powder matrix. Secondly, it was used to examine the fracture surfaces of the tensile specimens, where voids, oxide particles, cracks, micro-cracks, and the new position of the graphene were all analyzed after the tensile test. Finally, images were also taken to analyze the worn surfaces after the wear and nanoscratch tests, where the width of the scratches were measured. All of the SEM images were taken using the Zeiss FESEM with the aid of an SE2 and In-lens detectors.

## Chapter 5. RESULTS AND DISCUSSION\*

### 5.1 Mixed and Milled Powders

The low energy associated with the mixing process led to a uniform distribution of graphene clusters (GCs) among the polycrystalline aluminum particles as shown in Figure 5-1a. The milled powders show the disappearance of the G-particles and the encapsulation of the aluminum particles by a graphene layer as shown in Figure 5-1b. Figure 5-1c shows the graphene layers stacked on the surface of an aluminum particle. It is suggested that 2-hrs of milling was enough for the cold welding of the soft Al-particles while entrapping the G-layers in between and around them. Cold welding between the individual AA2124 particles and the AA2124 with G-particles was the dominant mechanism [59]. It is also suggested that during the cold welding G could be entrapped between the flaked Al-particles forming layered microstructure [60, 46, 38] .

BM for 2-hrs resulted in the cold welding of the Al-particles both with and without reinforcement as shown for the 0, 3, and 5wt.% images displayed in Figure 5-2(a, b), (c, d) and (e, f), respectively at low and high magnifications. BM for 2 hours of the AA2124 powders shows evidence for cold welding of the milled soft as received (AR) powders as shown in Figure 5-2(b, d, f). The milled composite powders show the disappearance of the G-particles and the encapsulation of the aluminum particles by a graphene layer (Figure 5-2 d, f) for the AA2124 containing 3- and 5-wt.%G, respectively. It is suggested that 2-hours of milling was enough for the cold welding of the soft Al-particles, while entrapping the G-layers in between and around them. Cold welding between the individual AA2124 particles and the AA2124 with G-particles was the dominant mechanism [61, 62]. It is also suggested that during the cold welding graphene could be entrapped between the flaked Al-particles forming layered structure [60, 11]. This agrees with the findings of Khorshid et. al. [46], who investigated the influence of adding 0.1 and 1.0-

wt.% G to AA2024. The dominating cold welding mechanism for such short durations of milling resulted in the entrapment of the G layers within the flaked and cold welded particles [46].

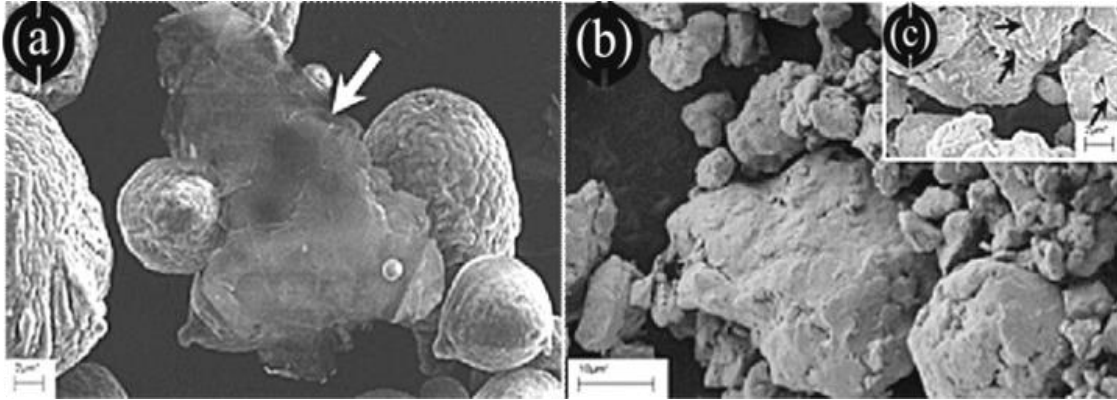


Figure 5-1 FESEM micrographs for (a) mixed Al/G powders, arrow points at G particle (b) milled AL/G powders and (c) graphene layers stacked on and in between Al-particles pointed at by black arrows [63].

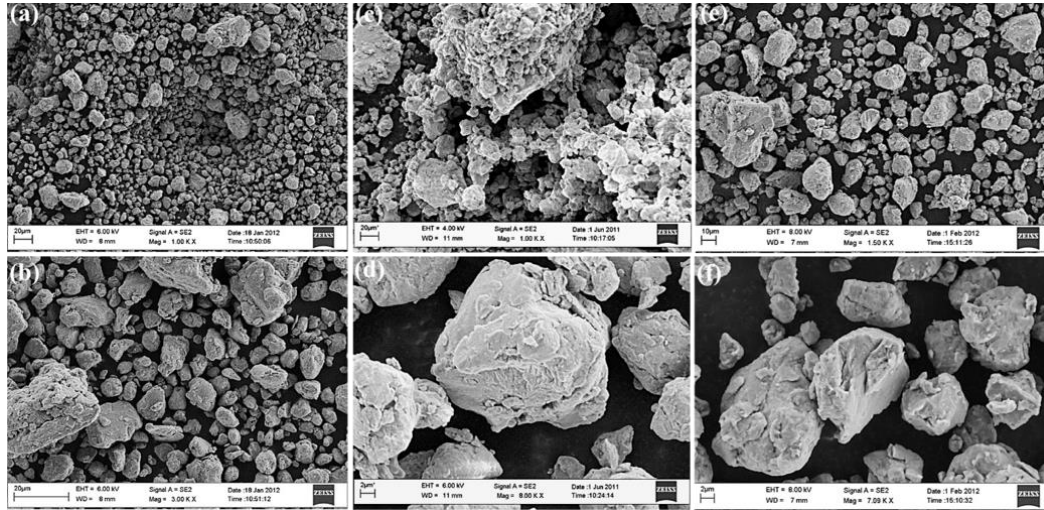


Figure 5-2 FESEM micrographs for the AA2124 milled powders (a, b) 0 wt.% G, (c, d) 3wt% G and (e, f) 5 wt.% G at low and high magnifications, respectively [64].

\* Parts of this chapter were published in papers entitled:

- (1) Ghazaly, A., Seif, B., & Salem, H. G. (2013). Mechanical and Tribological Properties of AA2124-Graphene Self Lubricating Nanocomposite. *Light Metals* 2013, 411-415.
- (2) El-Ghazaly, A., Anis, G., & Salem, H. G. (2017). Effect of graphene addition on the mechanical and tribological behavior of nanostructured AA2124 self-lubricating metal matrix composite. *Composites Part A: Applied Science and Manufacturing*, 95, 325-336.

## 5.2 Hot Extruded Bulk AA2124-G Nanocomposites at 300 °C

Mixed and milled powders of AA2124-G nanocomposites 0,3and 5wt.%G were consolidated via cold compaction then followed by hot extrusion at 300°C. This section characterizes the physical and mechanical properties of the produced rods.

### 5.2.1 Relative density

Relative density measurements were plotted for the hot extruded rods as shown in Figure 5-3. For the as received AA2124 it was observed that the average relative density value for the cold pressed was about 99.4% of the theoretical density. It can be seen that the monolithic AA2124 achieved the highest densification; however, the density decreased significantly with G additions. The reported average relative density of the plain milled AA2124 has not been fully densified due to the relatively low deforming temperature ( $0.45T_m$ ). Moreover, the  $Al_2O_3$  film formed around the individual aluminum particles, which was fragmented with milling and segregated along the boundaries of the hot extruded powders, hindered the particle-to-particle diffusion [24]. It was observed by Salem et.al [65]work that poor consolidation is a result of high cold compaction pressure, which leads to the fragmentation of  $Al_2O_3$  particles.

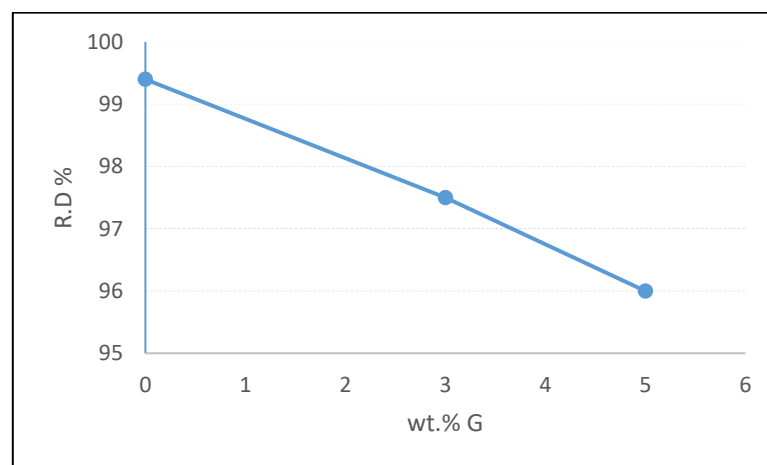


Figure 5-3 Relative density (RD%) variation as a function of increasing G-content [63]

AA2124 reinforced with G-particles displayed deteriorated consolidation of the composite powders by 20 and 34% for the 3 and 5 wt.% G content compared to the plain alloy. This could be attributed to the coating of the G-particles around the AA2124 individual particles, which retarded diffusion along the Aluminum interfaces. This agrees with the observations made by Xin Gao who successfully coated aluminum powder with graphene oxide sheets [66].

## 5.2.2 Mechanical Properties

### 5.3.2.2. Hardness

Figure 5-4 Vickers micro- and macro-hardness variation as a function of G-content for the hot extruded BM powders at 300C shows the variation of macro-Hv of the extrudates sections cut parallel to the extrusion direction (longitudinal) and perpendicular to extrusion direction (transverse) compared to the micro-Hv measured on the transverse directions as a function of increasing G-content. It is clear that the highest Hv-values were displayed by the 3wt% G containing composites, while increasing G-content up to 5 wt.% resulted in a decrease in hardness. In case of 5 wt. % G, the excessive G form their agglomerates and also conglomerate with the matrix and hence cause defects in the material. These defects, which are mainly composed of G agglomerates, are weak regions and as the indenter comes in contact with the material, these defects do not only cause indents of greater size but also relatively non-uniform indent. This results in reduced hardness of the composite. These results agree with the work conducted in reference [67] which studied the influence of adding various amount of nanographite till 5wt.% on the mechanical properties of aluminum. Adding 1,2 and 3 wt.% of nanographite has improved the mechanical properties due to stopping the grain growth through grain boundaries pinning mechanism which resulted into formation of finer grains. However, the 5wt.% specimens had the

lower hardness due to the inhomogeneous dispersion of the nanographite in the aluminum matrix. Ji Li et al. [68] has introduced the difficulty of dispersing high amount of G in aluminum matrix especially the G layers with high aspect ratio which increases the probability of agglomerations

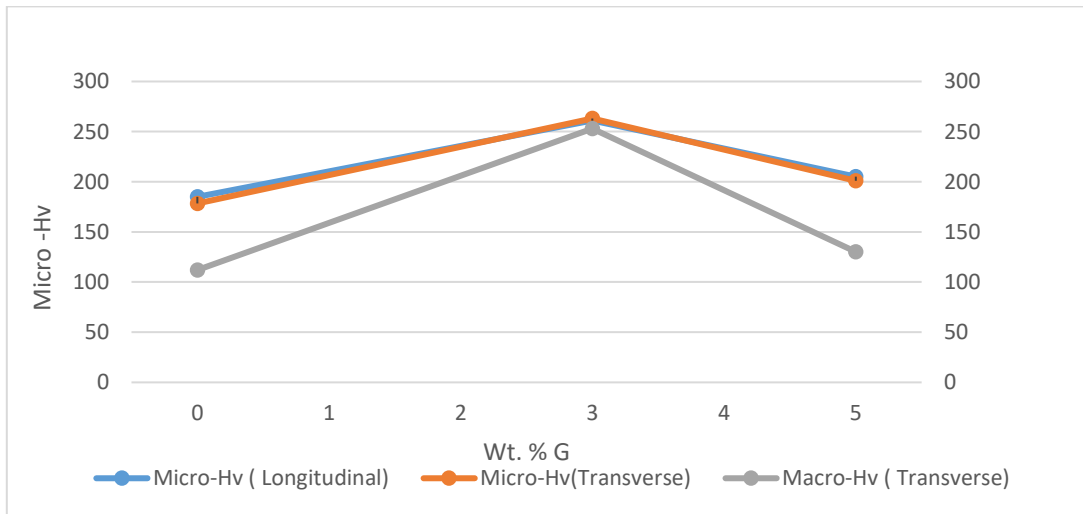


Figure 5-4 Vickers micro- and macro-hardness variation as a function of G-content for the hot extruded BM powders at 300°C [63].

### 5.3.2.3. Tensile properties

The tensile properties of the AA2124 extruded milled powders at 300°C are listed in Table 5-1. The 5 wt.% G composites, fractured at the fillet section for all 3-tested specimens. For the Plain AA2124 milled and extruded powders displayed the highest strength compared to the 3 wt.% G composite, but with relatively lower ductility, which can be explained by the relatively low consolidation temperature employed which was not high enough to allow for the diffusion along the boundaries of the AA2124 particles (pointed at by blue arrows, Figure 5.5(b)). This was evident in Figure 5.5 (a, b), where the blue arrows point at the inter-particle decohesion. However, the surfaces of the individual AA2124 particles revealed the formation of fine dimpled fracture

features, which supports the observed limited ductility (Table 5.1). Figure 5.5 (c, d) show evidence for the matrix micro-cracking at low magnification SEM images (circled in Figure 5.5 c), while evidence for crack initiation occurring at the G-layer that encased the Al-matrices (pointed at by black arrows, Figure. 5.5d) were be observed. Evidence for the G-clusters delamination at the matrix boundaries as well as ultrafine nano-dimples about 50nm in size revealed at very high magnifications (Figure. 5.5d). This explains the relatively lower strength and ductility exhibited by the AA2124-3 wt.%G composite rods. Accordingly, increasing G-content up to 5wt.% at such low extrusion temperature, resulted in the additional deterioration of tensile properties of the composite.

Table 5-1 Tensile Properties of the AA2124 rods with and without G-Additions

<b>G</b>	<b>wt. %</b>		
	$\sigma_Y$ (MPa)	$\sigma_{UTS}$ (MPa)	% Elongation
<b>0</b>	325±28	590 ±15	6.8 ±1
<b>3</b>	183±12	450 ±10	4.9 ±0.5
<b>5</b>	Failed	Failed	Failed



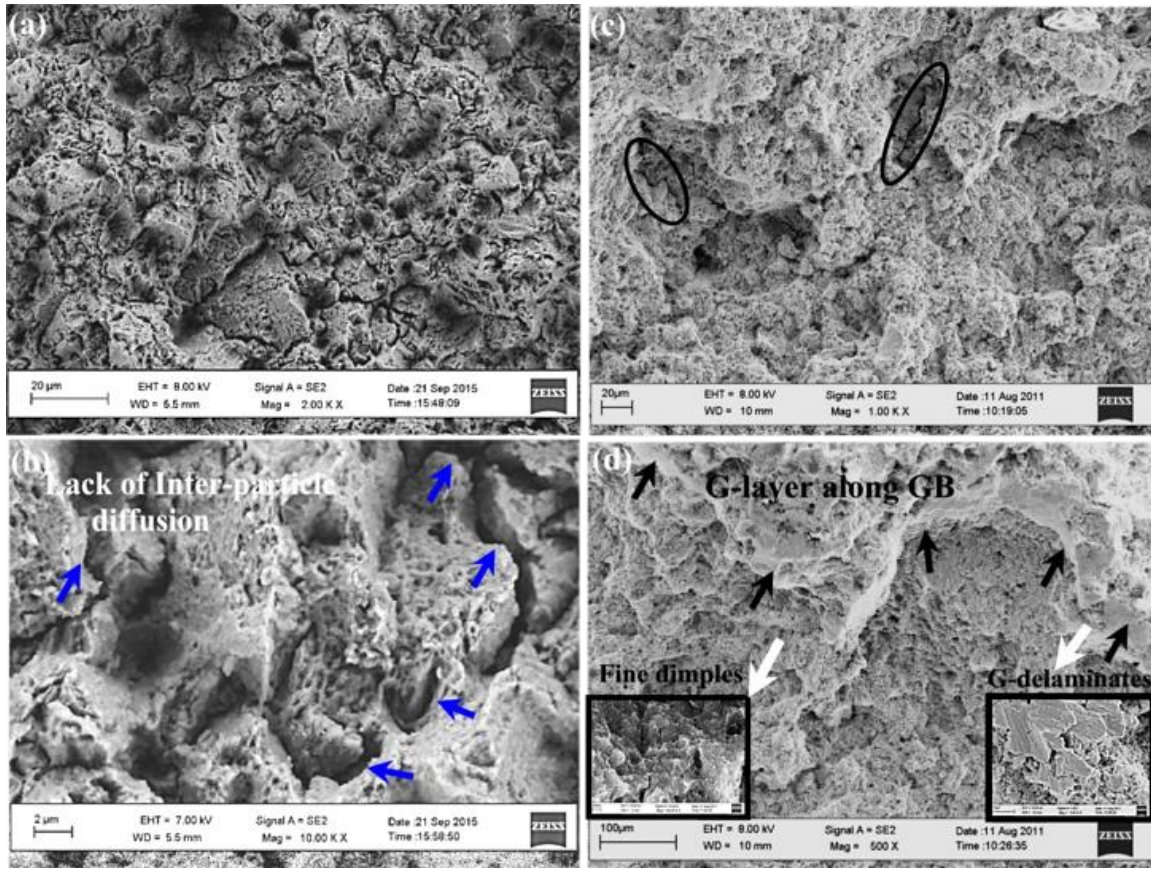


Figure 5-5 FESEM images showing Fractography of the tensile tested AA2124 extruded rods at 300°C (a, b) 0 wt.%G, (c, d) 3 wt.%G and (e) 5 wt.%G.

### 5.2.3 Structural Evolution

Microstructural investigation was conducted using optical microscope to explain the physical and mechanical behavior for AA2124 consolidated milled powders with and without G-additions. Figure 5.6 shows OM images for the AA2124 with and without graphene addition post hot extrusion for sections cut on the longitudinal and transverse directions. It clear that the elongated grains in plain AA2124 are decorated with fine dark particles aligned along their boundaries in the extrusion direction. Those particles are suggested to be the fragmented  $\text{Al}_2\text{O}_3$  films formed on the surfaces of the Al-particles during the milling operation (Figure 5.6 b). On the other hand, thicker continuous dark black films are observed encasing the elongated Al-grain representing graphene

(Figure 5.6 d) [63] Macrocrackes cutting through the transverse and longitudinal sections were evident on the surfaces of the 5-wt.%G composites as shown in Figure 5.6(d, f) respectively. On the longitudinal direction, it is clear that, the microcracks propagate along the grain boundaries of the Al-matrices along the G-layers which agrees with the observations made in Figure 5.5. This explains the brittle fracture and premature failure of the 5wt.% G containing composites caused by shear localization associated with relatively low consolidation temperatures (300°C).

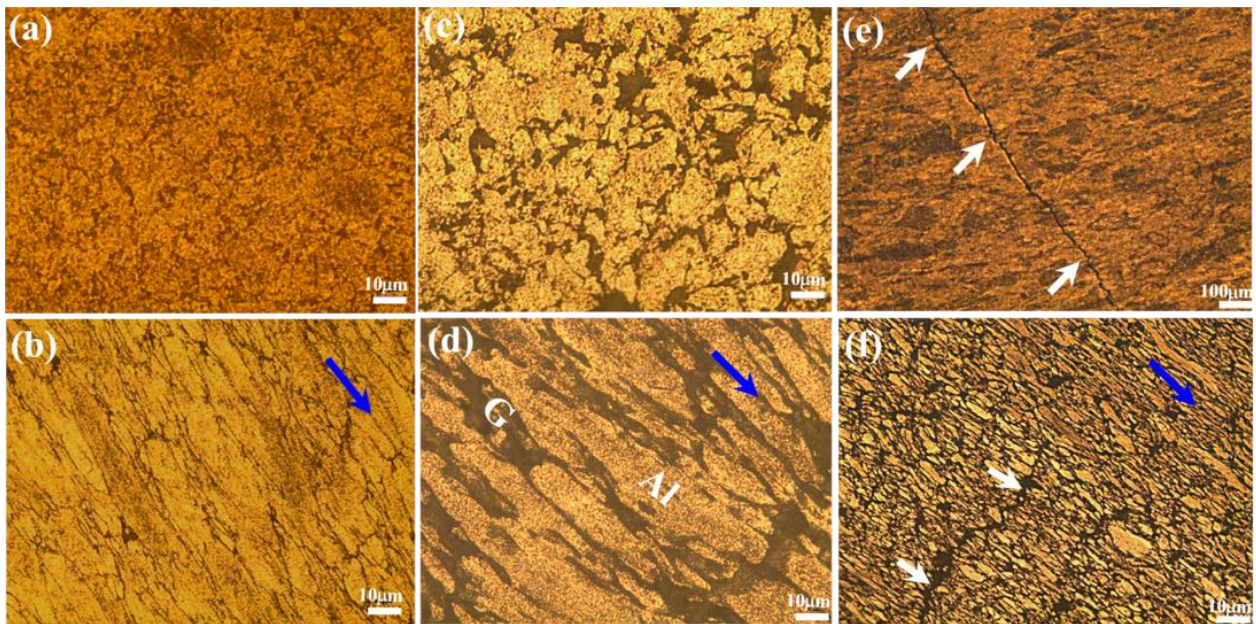


Figure 5-6 Optical Microscope images for AA2124 Composites (a, b) 0wt.%G, (c, d) [63]. 3Wt.%G and (e, f) 5Wt.%G on the sections cut longitudinal and transverse to the extrusion direction, respectively. Blue arrows point at extrusion direction, while arrows pint at microcracks.

#### 5.2.4 Tribological Properties

The tests were employed under 50,100 and 150 N applied loads for a fixed sliding distance of 1000 meters. The weight of specimens was measured before and after the test for determination of the wear rate Figure 5-7 .Severe wear rates and was measured at 150N load, while lower wear rates

were measured under 100N of loading and insignificant wear took place under 50N loads. The 3wt. % G again produced relatively the lowest wear rates and weight loss compared to the 0 wt% G and the 5 wt,%G composites, which suffered from the highest wear rates. This agrees with the Hv-Values displayed for the plain and composite hot extruded powders. The highest displayed hardness-values by the 3 wt.%G composite resulted in the enhanced wear resistance compared to the two other conditions. Dry wear testing of the hot extruded AA2124/graphene sample under 50 and 100N loads showed relatively much lower wear rates compared to similar alloys reinforced with CNT or ceramic particles [38].

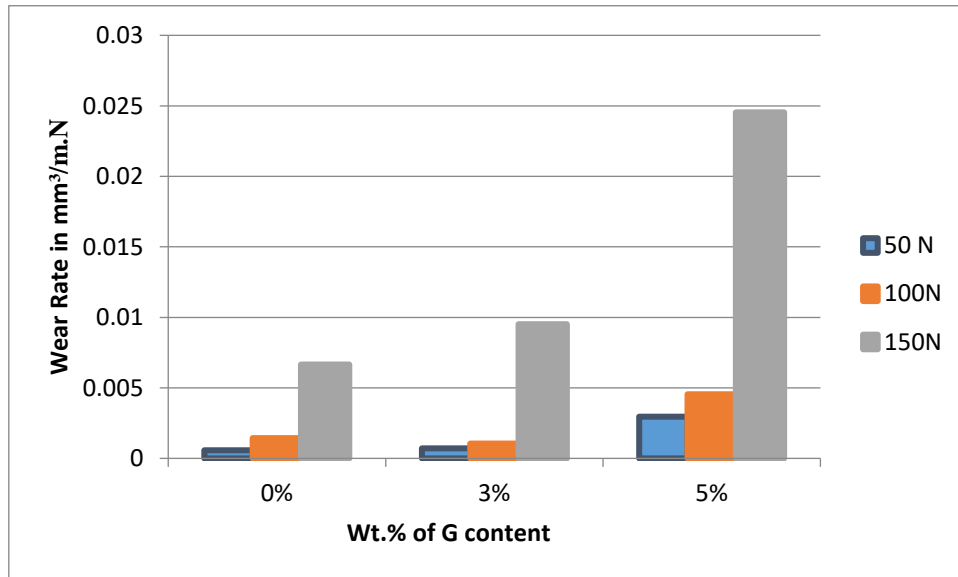


Figure 5-7Wear rate for monolithic AA2124 and the composite as function of load and graphene contents.

For understanding the wear behavior of the AA2124 hot extruded and milled powders with and without G addition, the worn surfaces by SEM for 100N loaded surfaces under 100N load were investigated as shown in Figure 5-8 . For the plain AA2124 worn surfaces, longitudinal grooves about 25microns wide can be (Figure 5-8 a ) suffered clearly from the formation of debris entrapped in between delaminated surfaces which was absent in the worn surfaces of the

composites Figure 5-8b .Such debris could be alumina fragmented films or strain hardened particles from the heavily milled consolidated powders which were detached under the load during the wear test [69]. The observed microvoides and loose particles (Figure 5.8(b)) are indicative of sever plastic deformation caused by impingement of the 1.3  $\mu\text{m}$  loose particles on the aluminum matrix.

On the other hand, Mild scratches can be observed on the surface of the 3wt% Graphene-composite worn surface relatively with shallow parallel grooves about 23 microns and ridges (Figure 5.8 c), which revealed graphene particles shown subsurface (dark spots). These parallel groves are an indication for a change of the wear mechanisms from delamination to be abrasive wear. Higher magnification images show the release of the graphene forming a lubricating film on the surface, which explains the decreased wear rate (Figure 5.7).

The worn composite surfaces with the high graphene content of 5wt% (Figure 5.8 e) show sever delamination in the direction of sliding as well as wide grooves and cracks with severely damaged surfaces. This explains the significant increase in wear rates observed in Figure 5-7, respectively. Narrower grooves about 16 $\mu\text{m}$  wide were observed on the worn surfaces of the 5% G composite surfaces compared to the 3%wt.G ones; however, this was associated with ploughing, sever plastic deformation and delamination (Figure 5.8 f). In addition, debris in the form of G-layers were detached from the worn surfaces as shown in Figure 5.8g with the features manifesting a pealed G-layer. Conversely, it is clear that the 3 wt.% G composite worn surfaces produced debris containing both the G-layers entrapped between Al-matrices, indicative of strong bond of the matrix and filler. For the plain AA2124 alloy worn surfaces, bulk hard abrasive debris impinged on the rubbing surfaces resulting in the formation of the cavities observed in Figure 5.8b.



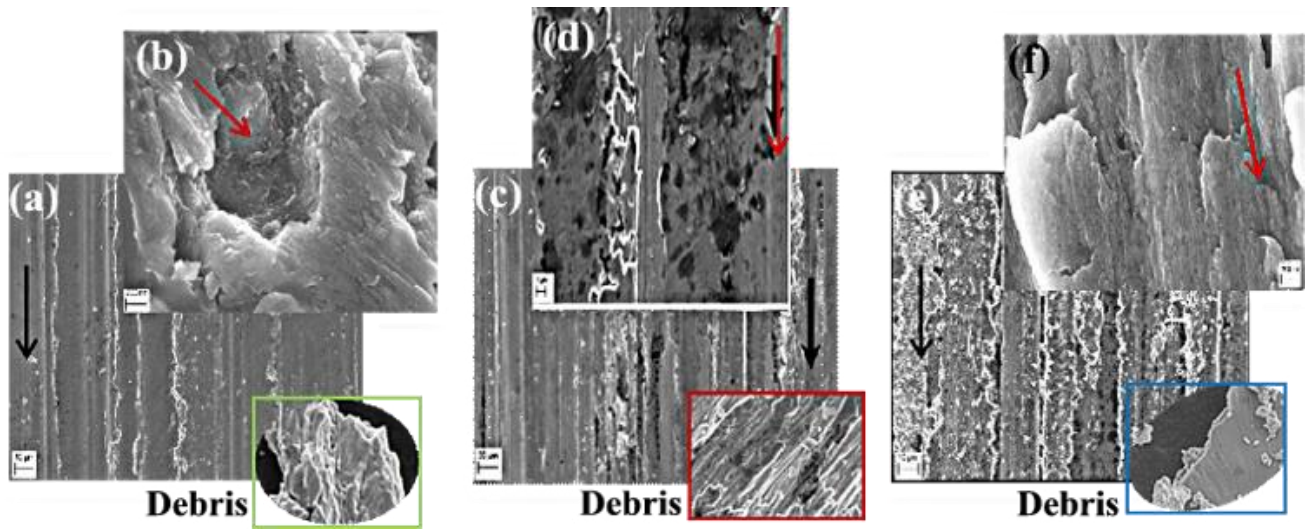


Figure 5-8 SEM images for the worn surfaces of the AA2124 matrices containing (a, b) 0 wt.%G, (c, d) 3wt.%G and (e, f) 5wt% G under 100N load. Representative debris are shown at the bottom right corner of each condition [63]..

### 5.2.5 Nanohardness and Nano scratch Behavior

The load-displacement diagram, and hardness and Young's Modulus variation as a function of increasing G-content are displayed in Figure 5-9 (a, b). In the current work, Oliver and Pharr method [70] was employed in measuring hardness and Young's Modulus. It is clear that 3 wt.% G containing composites displayed the highest load bearing capacity on the nanoscale testing (Figure 5-9 a), compared followed by the plain alloy, while the 5 wt.%G composites displayed the lowest of all. This was also reflected on the nanohardness results shown in Figure 5.9b, which agrees with results displayed for the macro and micro-Hv Figure 5-4Vickers micro-and macro-hardness variation as a function of G-content for the hot extruded BM powders at 300C .G addition up to 3 wt.% resulted in a consistent increase in

the hardness with graphene addition by 72% for 3-wt.% G. which agrees with the findings of Aniruddha Ram et. al., [51].

Similarly, Young’s modulus was highest for the 3-wt.% G composite with a 14% increase over that of the plain AA2124. Addition of 5-wt.% G to AA2124 resulted in the decrease in Young’s Modulus compared to that of the plain alloy and the 3 wt%G ones. It is suggested that the uniform distribution of the 3-wt.% G particles within the Aluminum matrices (Optical microscope (Figure 5-6 (c, d)) resulted in good interfacial shear bonding between the G-and matrix, which facilitated the load transfer and hence higher stiffness [71]. It is also suggested that the localized nature of the nanoindentation test in which the values are influenced by the local graphene content and distribution resulted in an increase in stiffness [51]. Conversely, the observed G-particles micro-segregation and clustering within the Al-matrices for the 5wt.% G composite resulted in interfacial de-bonding and hence overall decrease in stiffness, which was clearly evident in Figure5-6 F(Optical microscope).

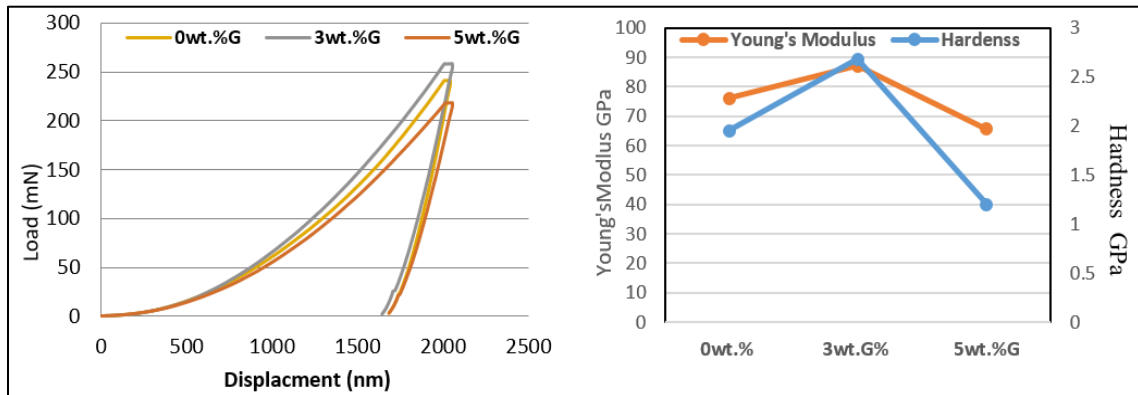


Figure 5-9 (a) Load vs displacement AA2124 alloy as a function of graphene content  
(b) Hardness and Young’s modulus

Figure 5-10 shows the on-load scratch distance and scratch depth variation over a distance of 700µm as a function of the plain AA2124 as a function of increasing G-content. The arrow

represents the sliding direction of the tip during the nanoscratch test. It is observed that the AA2124-5wt.%G displayed the highest most nonuniform depth of penetration (av. depth of -1000nm ( $\pm 400$ )) as shown in Figure 5-10 (a) of the indenter tip along the scratch length. This was associated with fluctuations ranging between -800-to -1500nm. The plain specimen produced the lowest depth of penetration with Av. Depth -650nm, Figure5-10a. Addition of 3wt.% G resulted in the most uniform penetration depth has an average of -500nm (Figure5-10 b). For the G-containing samples the tip is pushed upward during scratch test, which indicates higher resistances to scratching due to enhanced hardness [72]. When the indenter tip confronts graphene layer or particle along the scratch direction this requires more force to move straight forward. It is suggested that the evident nonuniform distribution and clustering of G-particles within the Al-matrices in the AA2124-5wt.% G composite resulted in the observed wide range of penetration depth along the scratch distance. On the other hand, the uniform distribution of G-particles in the AA2124-3-wt.% G composite resulted in an overall uniform penetration along the scratch direction.

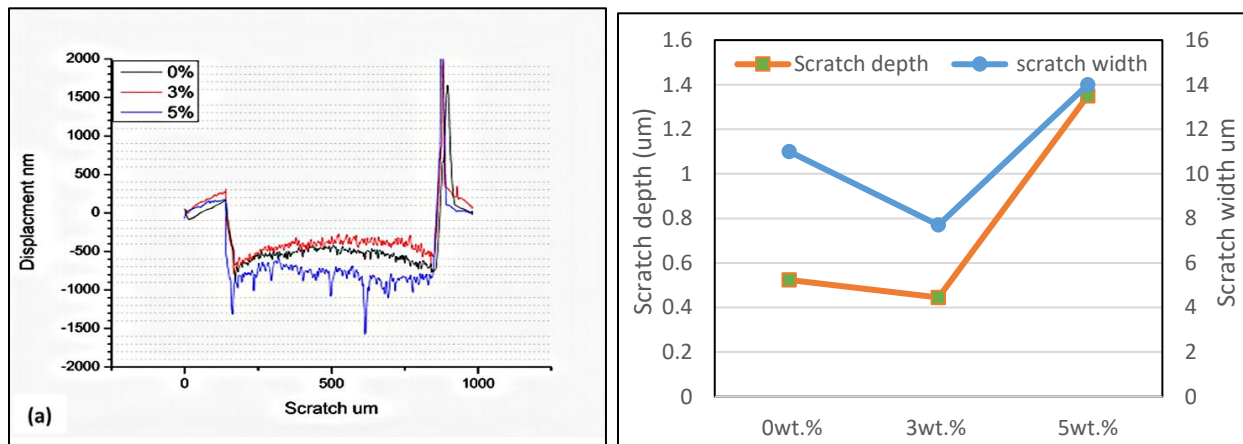


Figure 5-10 Diagrams for representative behavior for the AA2124 hot extruded BM powders (a) scratch depth profile Vs. scratch distance and the (b) variation of scratch depth and width as a function of increasing G-content

Investigation of the nanoscratch surfaces using FESEM, revealed narrowest and least depth scratches for the 3wt.%G (Figure 5-11b) composites surfaces compared to the 0 and 5 wt.% G ones (Figure 5-11(a and c) respectively. Knowing that all displayed images are taken at the same magnification. SEM images (Figure 5-11a,b) shows symmetrical scratch surfaces for the composite AA2124 reinforced with 0 and 3 wt. % G specimens with a limited appearance of debris on the edges. Scratches produced for the plain alloy (Figure 5-11a, a') show large volume fraction of debris on the edges of the scratch as well as evidence for peeling of the material (a') on the edges, which explains the relatively higher wear rates reported in Figure 5-7. The 3wt.%G composite showed a smeared appearance due to the uniform distribution of the G particles within the Al-matrices as shown in Figure 5-6 (c,d). This observation agrees with the derived explanation reported for the minimum local fluctuations in the pin penetration (Figure 5-10 a). Figure 5-11b' shows the fine distribution of G-cluster smeared on the internal surface of the scratch. Conversely, the 5 wt.%G scratched surfaces (Figure 5-11 c) showed evidence for the segregated graphene particles along the scratch central line (pointed at by arrows). This explains the excessive penetration reported for the AA2124-5 wt.%G composite curves shown in Figure 5-10 (a) at some points along the scratch sliding distance associated with the low resistance to pin penetration to the coarse segregated g-particles [46]. Figure 5-11c' shows evidence severe plastic deformation along the side of AA212-5wt.%G scratched surface.



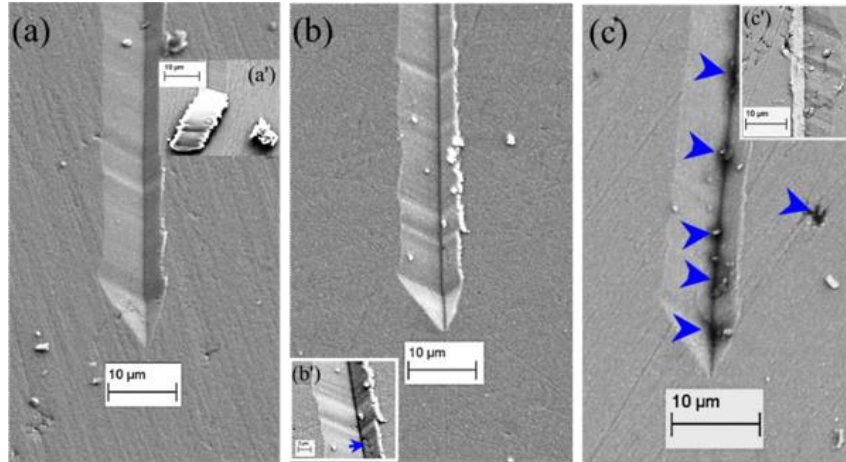


Figure 5-11 SEM images for scratch surfaces of (a, d) plain AA2124, (b, e) 3wt.%G and (b,e) 5wt.%G

### 5.2.6 Conclusion

AA212-graphene composite mixed and milled powders were successfully consolidated in to discs via combination of high energy ball milling and hot extrusion at 300oC.

1. Density of the consolidated discs decreased with increasing content of graphene-content, while the VHN reported highest for the AA 2124-3 wt.% G composites.
2. AA 2124-3 wt.% G composites The lowest weight loss and wear rate compared to the 5 wt.%G and the plain alloy.
3. AA 2124-3 wt.% G composites displayed very smooth surfaces covered with graphene lubricating layer. The formed layer reduced friction and wear.
4. Plain AA2124 matrices suffered from the formation of debris entrapped in between delaminated surfaces
5. AA21124-5%G composite microplouging and sever plastic deformation wear mechanism.
6. AA21124-5%G composite also suffered from severe delamination was also observed on the worn surfaces of the 5 wt.% G composites.

7. Embrittlement and premature failure by formation of micro-cracking of the AA2124-5wt%G was induced with the relatively low HE temperature.
8. The uniform distribution of the G-within the Al-matrices increases the wear resistance on the nanoscale level revealed the produced lowest scratch depth.

### 5.3 Hot Extruded Bulk AA2124-G Nanocomposites at 450 °C

#### 5.3.1 Relative density

The relative densities measured for the extrudates compared to the theoretical densities, was calculated using the rule of mixtures. Figure 5-12 shows the variation of the relative density as a function of increasing G-content. It is clear that the density decreased with increasing G-content, which agrees with the findings of Moghadam et. al., [34] . The sintering temperature at 450°C represents  $0.67T_m$ , which was high enough to facilitate good consolidation via atomic diffusion along the Aluminum particles interfaces during extrusion. This is only applicable for the plain AA2124 hot extruded BM powders, which explains the displayed high degree of consolidation. Conversely, relatively high sintering temperatures will also be associated with high shrinkage effect during the cooling of the hot extrudates, which could have been magnified with increasing G-content. The difference in the coefficient of thermal expansion (CTE) of aluminum and graphene, resulted in high internal stress at the graphene-Al-interfaces, which negatively affected the produced densities [54]. As shown in Figure 5-12, increasing the content of G from 3-5 wt.% resulted in reducing the relative density from 98.3 ( $\pm 0.21$ )-to-97% ( $\pm 0.28$ ), respectively.

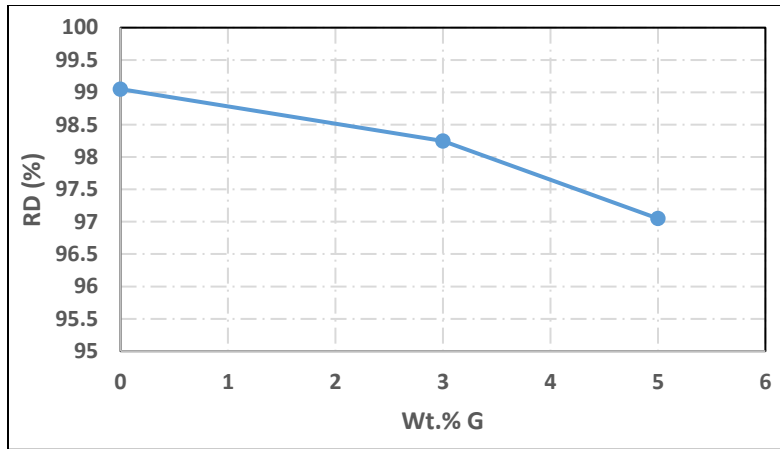


Figure 5-12 Relative density (RD%) variation as a function of increasing G-content

[64]

### 5.3.2 Hardness

Figure 5-13 shows the variation in macro- and micro-hardness (Hv) measured for the BM plain AA2124 and the composite hot extrudates as a function of increasing G-content. The micro-Hv was evaluated on sections cut perpendicular (transverse) and parallel (longitudinal) to the extrusion direction, while the macro-Hv was evaluated on the transverse sections. Macro-Hv measurements on the transverse direction of the composite extrudates increased by 133 and 102%, for the 3- and 5-wt.% G containing composites, respectively compared to the plain alloy extrudates. Although, the displayed micro-Hv values for the hot extruded rods revealed increased hardness with increasing G-content compared to the plain alloy milled under similar conditions, this disagrees with the measured relative density % (RD%) decrease with increasing G-content (Figure 5-12). This could be explained by the nature of microhardness testing, which evaluates the hardness while excluding regions with porosity or cavitation. The displayed micro-Hv values also disagree with the findings of Ghazaly et. al., who reported an increase in micro-Hv values for the 3-wt.% G (Hv-260) and a decrease in Hv for the 5-wt.% G (Hv-215) composite compared to the

plain alloy [60]. This could be attributed to the extrusion temperature, which was 300°C vs. 450°C for the reported values and the currently employed temperature, respectively. However, the current behavior of increasing Hv-values with increasing G-content agrees with that induced by increasing graphite nanoparticle content in Aluminum alloys compacted in the temperature range of 400-600°C [12]. On the other hand, the reduced macro-Hv-values measured for the 5-wt.% G composite could be attributed to the macroscale testing which was influenced by the increasing porosity with increasing G-content. This agrees with the findings made by Ghazaly, et. al., [60]

Moreover, the micro-Hv-values measured for the G-containing composite extrudates were consistently higher on the transverse direction compared to the longitudinal one, while for the plain AA2124 extrudates, micro-Hv-values were almost equal for both directions. This indicates an obvious influence of the graphene on the flow behavior of the aluminum matrices along the extrusion direction. Generally, the results show a 17.1% and 31.8% increase in hardness for the 3- and 5-wt.% G composite extrudates, respectively, compared to the plain AA2124 alloy. The increase in micro-Hv values with increasing G-content can be explained by the induced localized strain hardening associated with micro-indentation [73]. Table 5-2. lists the average micro- and macro- hardness values as a function of G-content. It is clear that the variation is significantly high for the microhardness testing compared to the macrohardness results. This is because the indenter of the microhardness testing is small enough to penetrate either the Al-matrices or the graphene particles, which influenced the displayed variation,

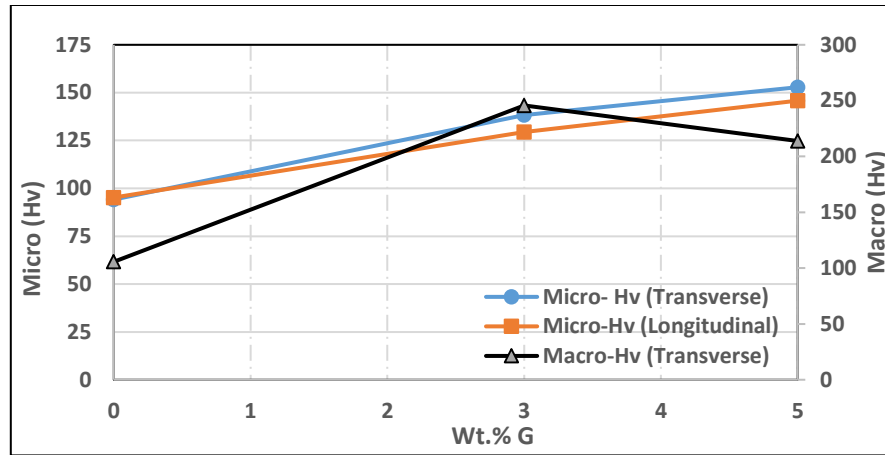


Figure 5-13 Vickers micro- and macro-hardness variation as a function of G-content for the hot extruded BM powders [64]

Table 5-2 represents the Micro -Macro hardness as function of G content [64].

Hardness (HV)	0 wt. %	3 wt. %	5 wt. %
Micro Transverse	94.14±9.7	138.2±23.7	152.8±23
Micro Long	95.2±12.1	129.4±11.4	145.82±15.5

### 5.3.3 Tensile Properties

The tensile properties of the composites were also investigated, where averaged tensile behavior over three-tested samples per condition is shown in Figure 5-14. The plain AA2124-extrudates exhibited the lowest yield and ultimate tensile strength associated with the highest ductility. Composite extrudates with the 3 and 5-wt.% G displayed higher yield and tensile strengths and lower ductility compared to the plain ones. Table 5-3 lists the average values

(measured from 3-samples) for the ultimate and yield strength as well as % elongation for the tested extrudates as a function of increasing G-content. It is clear that 3 and 5 wt.% G additions to AA2124 matrices resulted in 104 and 127% increase in yield strength, respectively, and 20.4 and 21.6% increase in ultimate tensile strength, respectively. Conversely, G-addition resulted in about 56 and 62% decrease in ductility for the 3 and 5 wt% G, respectively. This behavior agrees with the measured increase in hardness of the composites due to graphene addition. Similar results were reported by Wang et al. [74]. On the other hand, work of other researchers reported an increase in ductility as a function of G-addition [75]. This could be explained by the fact that the reported increase in ductility was for G-content ranging between 0.1 and 1.0wt.% [76, 77] which much lower than the investigated G-content in the current work. Therefore, despite the decrease in ductility observed in our results, the enhanced strength and hardness of the fabricated composites was an indication of the effectiveness of processing via hot extrusion on the mechanical behavior of composites containing up to 5wt% G in Al-matrices.

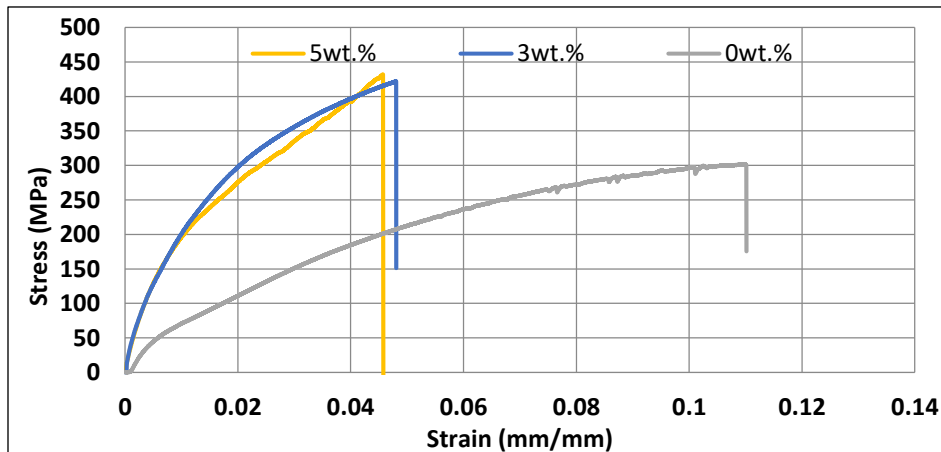


Figure5-14. Representative behavior of composites as a function of wt.% G [64].

**Table 5-3.** Average values for tensile properties of extrudates as a function of increasing G content [64]

wt.% <b>G</b>	content [64]		
	$\sigma_Y$ (MPa)	$\sigma_{UTS}$ (MPa)	% Elongation
<b>0</b>	88±10	350 ±35	11.5±0.1
<b>3</b>	180±5	421.7±14	4.8 ±2
<b>5</b>	200±12	425.6±8	4.4±1

Investigation of the hot extruded BM composite and plain powders using OM revealed high degree of consolidation with almost no cavitation or porosity as shown in Figure 5. For the plain AA2124 extrudates, boundaries of the grains were decorated with second phase particles and oxides as revealed by XPS analysis (Figure5-15 a). G-containing extrudates showed evidence for elongated structure parallel to the extrusion direction (Figure 5-15(d, f)), while the plain alloy showed insignificant structural elongation (Figure5-15b) This indicates the influence of the G- which facilitated the plastic deformation and structure flow in the extrusion direction. This agrees with the reported hardness results displayed for the composite extrudates compared to the plain one (Figure5-15) for the transverse and longitudinal sections. Sections cut transverse to the extrusion direction 3-wt.% G addition to AA2124 revealed the formation of uniform distribution of the G-particles along the boundaries of the consolidated individual Al-particles. On the other hand, for the 5-wt.% G composite, G formed thin film around the Al-particles and mainly formed coarse G-lumps segregated non-uniformly within the Al-matrices. The coarse G-lumps were about

15 $\mu$ m in average size as revealed both on the transverse and longitudinal sections (Figure 5-15 e, f), respectively. [78]

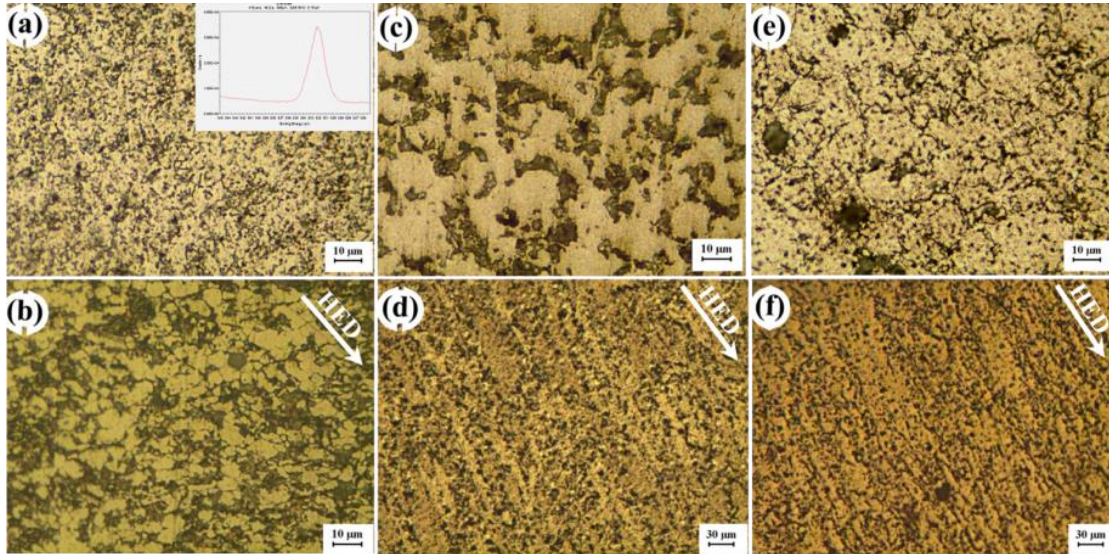


Figure 5-15 OM micrographs for the transverse and longitudinal sections of hot extruded AA2124 reinforced with (a,b) 0 wt.%, (c,d) 3wt.% and (e,f) 5wt.% graphene, respectively.

Arrows represent the hot extrusion direction [64].

FESEM images of the tensile fracture surfaces of the fabricated composites at different compositions at low and high magnifications are shown in Figure . The 0-wt.% G composite in Figure 5-16 (a-c) show deep dimples indicating high ductility prior to failure, which agrees with the displayed tensile behavior shown in Figure 5-16. Oxide particles scattered within the fractured surface (pointed at with red arrows in Figure 5-16 (b and c)) can also be observed in the form of segregated fragmented oxide particles as well as second phase particles acted as nucleation sites for void sheet mechanism Figure 5-15 b . Figure C shows cracked oxide film surrounded by dimpled fracture features representing the typical behavior of AA2124 soft matrix. AA2124 reinforced with 3 and 5-wt.% G revealed the G-monolayer clusters in the same Figures 5-15 (d-f) and (g-i), respectively. Both composites show finer and relatively shallower dimples compared to the plain AA2124 fracture surfaces (Figure 5-16 (a-c)), which reflects the higher strength and lower ductility



duplicated in Figure 5-14. Comparing the 3 and 5-wt.% G composite fracture surfaces at relatively intermediate magnification, for the 3-wt.% G composite the G-particles were aligned along tripple junction (Figure 5-16 e, between white lines) of dimpled Al matrices.

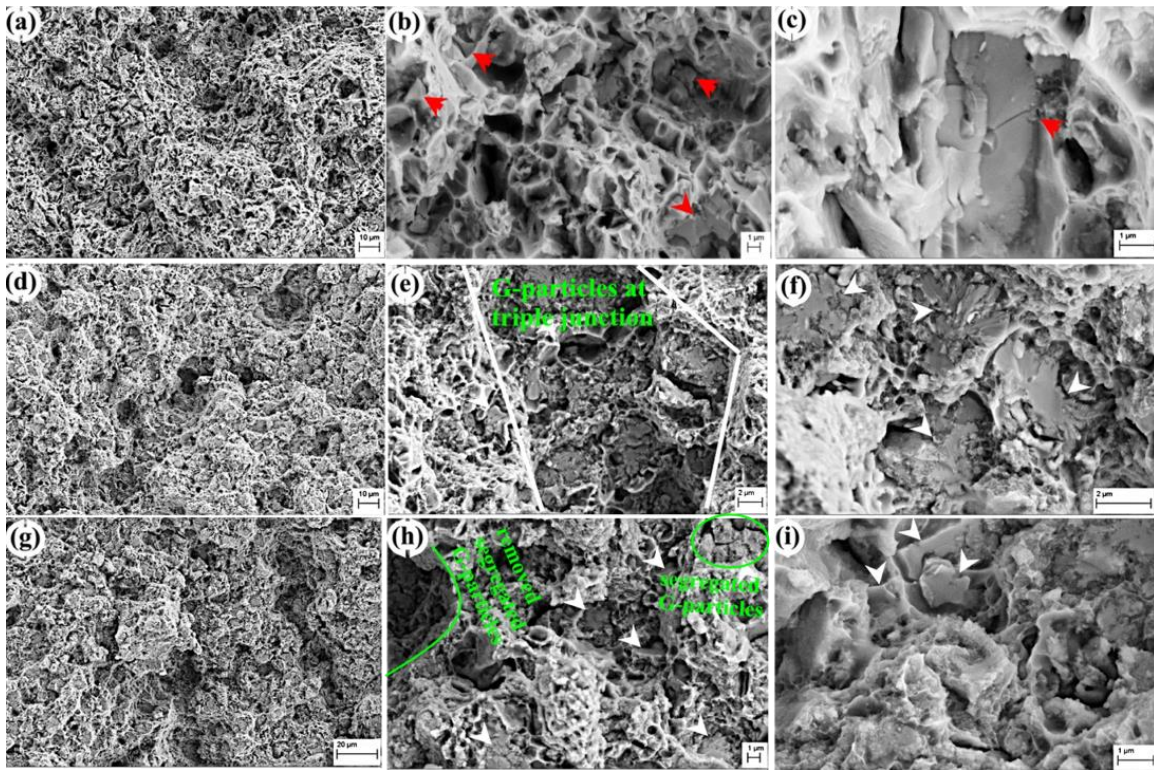


Figure 5-16 FESEM images for the fractured surfaces of the tensile testes AA2124 processed composites (a-c) 0 wt.% G, (d-f) 3 wt.% G (g-i) 5 wt.% G, at increasing magnifications, respectively. Red arrows point at  $\text{Al}_2\text{O}_3$  particles and films, white arrows point at G-particles and green circles point at removed or segregated G-particles [64].

On the other hand, small fraction of the 5-wt.% G was distributed within the Al-matrices on the fractured surfaces (Figure 5-16 h). Regions with segregated and agglomerated G-particles were also evident as shown in the circled regions in Figure h, which agrees with the observation made in Figure 5-16 c. Higher magnification images, showed evidence for the G-cohesion with the Al-matrices for the 3-wt.% G composite Figure 5-16f, (pointed at by arrows), which indicates

interfacial shear stress transfer from the matrix to the reinforcement. This was evident by the delaminated the G-layers along the shear direction (pointed at by arrows in Figure 5-16 f).

Conversely, intact G-particles' pullout and interfacial decohesion with the surrounding matrix was evident for the 5wt.% G composite (pointed at by arrows in Figure 5-16 i). Unlike the findings made by Yan et. al., [14] , dimple tear ridges observed when nanographene clusters were used, using grapene clusters didn't allow for the expected good metallurgical bond with Al-matrices. This reflects the relatively measured lower tensile properties for the micronscale compared to the nanoscale graphene particles. It is also suggested that the decrease in ductility of the G-containing AA2124 comapred to the plain one was attributed to the formation of aluminum carbides, which form during sintering due to the relatively high temperature.

#### 5.3.4 XRD analysis

To further explain the physical and mechanical behavior of AA2124 as a function of increasing G-content in the hot extruded condition, XRD patterns of the BM powders before and after extrusion were investigated. The XRD results displayed in Figure5-17 b, c and d show the influence of hot extrusion as a function of increasing G-content (0,3,5wt.%, respectively) compared to that of the as-milled AA2124-5wt.% G powders .XRD results for the hot extruded composites revealed the formation of aluminum carbide phase at  $31.1^\circ$ ,  $55^\circ$  and  $72^\circ$ . The  $Al_4C_3$  compound formed by the chemical reaction between G and aluminum was evident in the G-containing AA2124 composites as shown in Figure 5-17. Under high temperatures aluminum and their alloys have high affinity to carbon based materials forming carbides. Carbide formation has been reported by Bartolucci et. al., [55] and Rashad et al., [79]

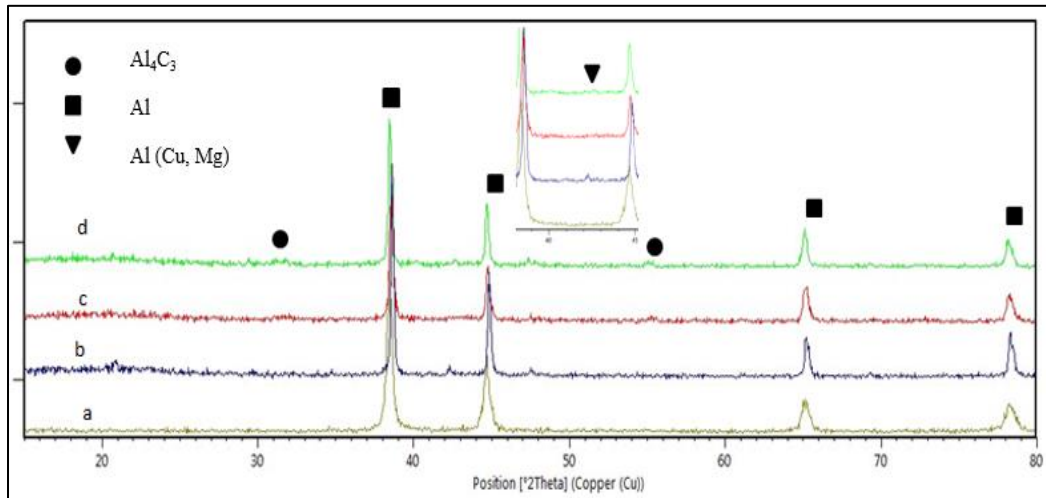


Figure 5-17 XRD patterns for (a) AA2124–5-wt.% G as-BM powders compared to hot extruded conditions for (b) 0-wt.% G, (c) 3-wt.% G and (d) 5-wt.% G [64]

From the displayed chart the width of the BM powders' peaks increased and their intensity became weaker. This was attributed to the decrease in the crystallite size and increase the lattice strain [80] as a function of milling time and G-content. Moreover, a slight shift in the peaks angles was also observed indicative of lattice parameters' change induced by increased solubility of the alloying elements or due to the suspension of impurities such as iron into aluminum lattice during milling [80].

Figure 5-18 shows the influence graphene additions on the crystallite size (a) and lattice strain percent (b) variation for the AA2124 alloy powders in the as-BM condition and post hot extrusion compared to the as-received (AR) Al-powders. From the displayed results it is clear that the crystallite size of the AR-Al-powders decreased from 46-to-20.5nm after 2-hrs of milling. G-additions up to 5-wt.% had an insignificant influence on the crystallite size (Figure5-18a), while an

increase in percent lattice strain Figure 5-18(b) of 12% was measured with increasing G-content for the BM powders.

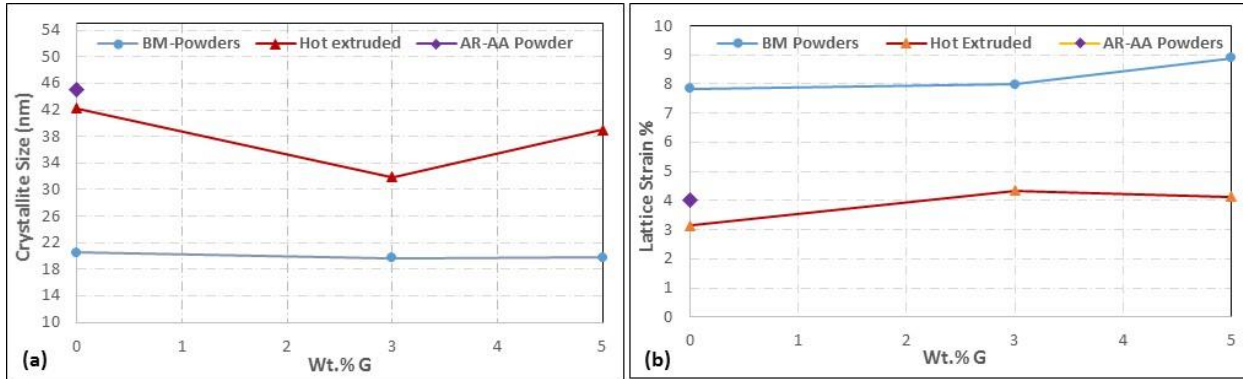


Figure 5-18 Diagrams showing the variation of the (a) Crystallite size and (b) lattice strain % as a function of increasing G-content for the ball milled and Hot extruded powders compared to the as-received AA2124 [64].

Hot extrusion of the milled powders at 450°C resulted in coarsening of the nanoscale structure from 20-to-42nm for the plain alloy, which represents 200% increase. On the other hand, G additions resulted in 160% and 196% coarsening for the 3 and 5-wt.% G hot extruded composites, respectively. Similar behavior was measured for the percent lattice strain variation with increasing G-content, where the highest lattice strain was reported for the 3-wt.% G hot extruded composite. From the displayed results; although, increasing G-content didn't have significant influence on the structural refinement of the ball milled AA2124 composites compared to the plain condition, 3-wt.% G addition caused the partial impedance of crystallites growth during sintering at 450°C. This could be attributed to the uniform distribution of G-particles within the Al-matrices compared to the AA2124-5 wt.% G composite and the plain alloy.

### 5.3.5 Tribological Properties

#### 5.3.5.2. Pin-on-Disc Test

The volumetric wear rates of AA2124 as a function of graphene content at constant speed and under 100N axial load pin-on-disc test are shown in Figure 5-19a (a). The 3-wt.% G composite showed the lowest wear rates compared to the plain and 5-wt.% G composite. The highest wear rates were displayed for the plain AA2124 hot extruded powders. According to Rajkumar et.al., [49] increasing G-content decreases wear rates, especially when higher hardness and lower porosity associated with finer microstructure occurs. Accordingly, it is suggested that the deteriorated density (Figure 5-12) and macro-(Hv) (Figure 5-13) and the relatively lower tensile properties for the 5-wt.% G containing Al-matrices resulted in the increased wear rates compared to the 3-wt.% G composite.

Figure 5-19 (b) shows the variation of Coefficient of Friction (COF) as a function of increasing G-content. From the displayed results, consistently 3-wt.% G-addition to AA2124 produced the lowest average COF of 0.31 compared to 0.35 and 0.4 for the 5wt.% G and the plain Al-alloy, respectively. The high value of COF for the 0wt.% plain is due to the low mechanical properties.

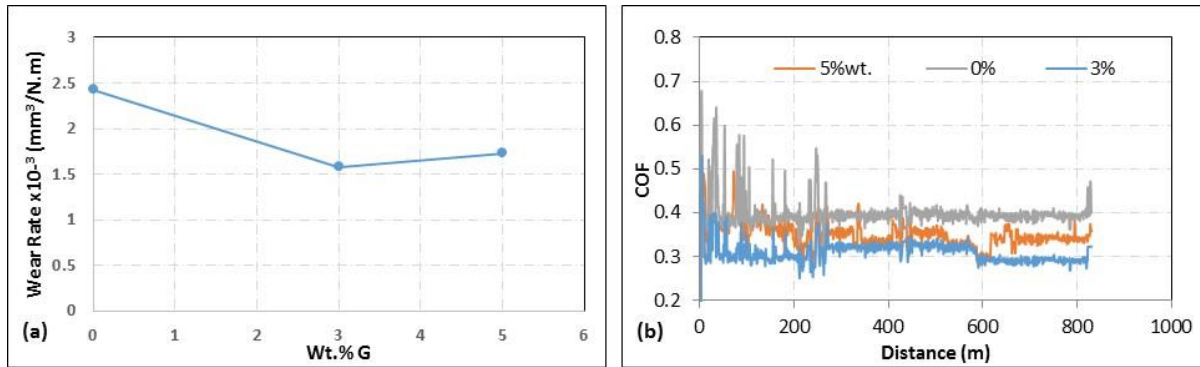


Figure 5-19 shows pin-on-disc results displayed for the hot extruded milled powders of AA2124 (a) wear rate, (b) Coefficient of friction (COF) as a function of G-content at 100 N load dry sliding tests [64]

Self-lubrication is primarily influenced by the content of graphene or graphite spatial distribution within the matrices and their particle size [49]. In the case of plain AA2124 hot extrudates, metal-to-metal contact is increased under the applied normal load, which creates asperities separated from the surfaces of the AA2124 tend to plow in the surfaces of the pin. On the other hand, 3-wt. % G addition resulted in increased wear resistance (lowest wear rates and COF) due to the preferential allocation of the G-particles along the Al-grain boundaries, which easily smeared out uniformly on the sliding surfaces. This provided a continuous graphene layer between the rubbing surfaces and hence increased wear resistance [81]. The observed segregation of the G-particles within the Al-matrices encountered with increasing G-content up to 5wt.%, which was revealed by OM (Figure5-15) and SEM (Figure 5-16) images attributed to the increased wear rates and increased COF.

The FESEM characterization of the worn surface revealed an abrasive wear mechanism for both the plain AA2124 matrices Figure 5-20. Deep longitudinal grooves (craters) were observed in the direction of sliding accompanied by severe abrasive wear manifested by the high-volume



fraction of debris observed on the worn surfaces [82] [76]. This indicates the progressive transfer of material in between the sliding plastically deformed surfaces [83].

Conversely, 3-wt.% G-addition to AA2124, developed much smoother surfaces compared to the 5-wt.% G composite Figure 5-20 (c-f). This was attributed to the formation of continuous G-film covering the Al-matrices, with the formation of very small volume fraction of debris on the surface (Figure 5-20 b). Evidence for G-particles uniform smearing on the surface of the pin resulted in preventing further plastic deformation as pointed out by arrows in Figure 5-20 d. Mild delamination can be observed at high magnifications (Figure 5-20 d) for the 3-wt.% G composite compared to sever delamination for the 5-wt.% G one (Figure 5-20 c and e) respectively. Segregation of G-particles associated with increasing the G-content up to 5-wt.% was also evident on the worn surfaces (see circles in Figure5-20 ). From Figure 5-20 f there was no clear smearing of G-surrounding the segregated particles, which attributed to the deteriorated tribological properties as depicted by the exhibited wear rates and COF.

In general, the G composites showed superior wear behavior compared to the plain AA 2124. This was reflected by the wear rate and COF measurements as well as the FESEM images of the worn surfaces. This was also supported by the exhibited enhanced mechanical properties of the composites compared to the plain AA2124 alloy. Generally, adding graphene to metal matrices is expected to improve their wear behavior due to its self-lubricating mechanism associated with the squeezing out of G in between the sliding surfaces. Moreover, the G present in the composites contributes to the material's load-bearing ability and hence is capable of decreasing wear rates [59].

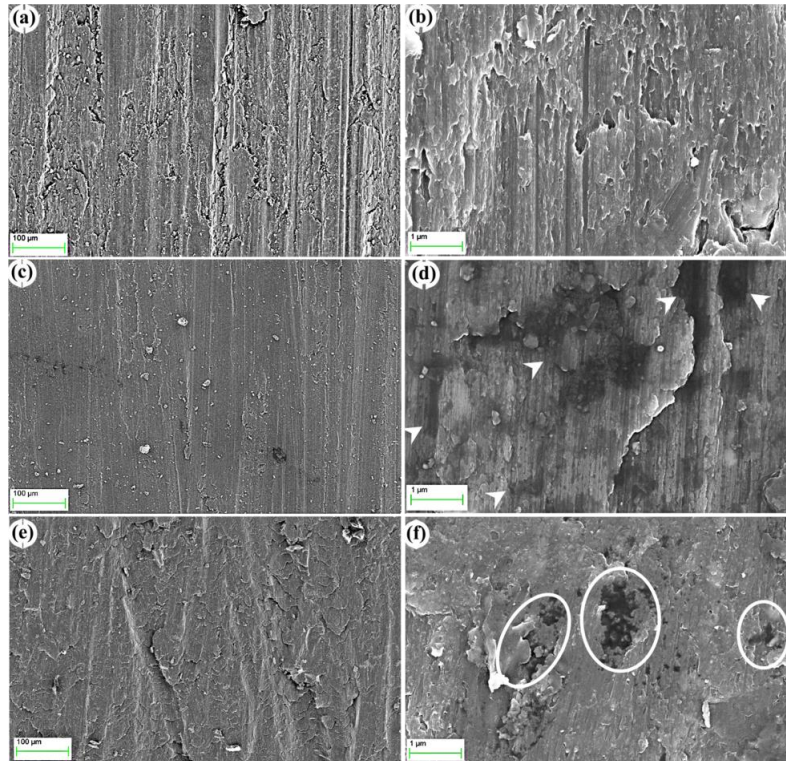


Figure 5-20 FESEM of worn surfaces after pin-on-disc test (a-c) 0wt.% (d-f) 3wt.% (e-f) 5wt.% at low and high magnifications, respectively [64]

Raman investigation of the worn surfaces of the composites for the 3-wt.% containing graphene composite was selected for the inspection of the tribofilms formed on the worn surfaces. Figure. 5-21 (a) shows the worn 3-wt.% G composite pin at low magnification and a higher magnification SEM image with the G tribofilms smearing on the surface of the Al-matrix (Figure. 5-21(b)).

Investigation of the worn surfaces of the AA2124-3 wt.%-G revealed the formation of a G-tribofilms, which was evident by the Raman spectrum. G, D and 2D peaks were observed on the worn composite surfaces compared to the plain multilayered graphene as-received powders as shown in Figure. 5-21c [84]. The observed slight shift in the G and 2D peaks of the composite tribofilm, could be attributed to the strain induced by the infiltration of the Al atoms into G during



the wear test, which resulted into strain in the G the alteration of their sp<sup>2</sup> bonding structure. Similar shifts were reported by Mohiuddin et al. [84]. and Iqbal et al. [85]

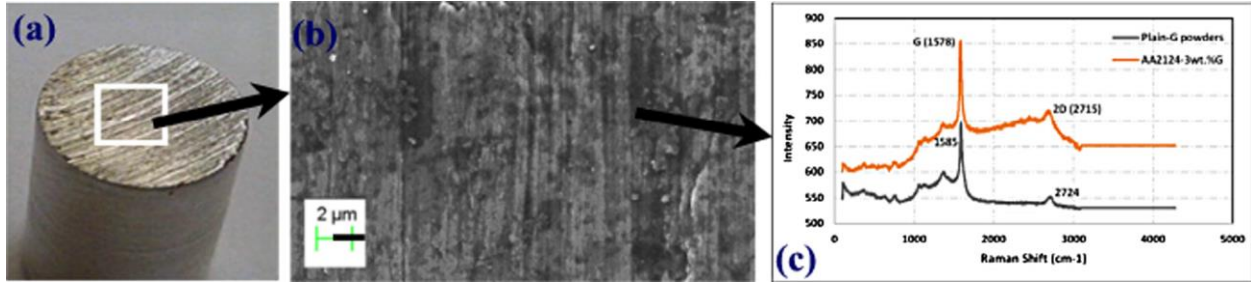


Figure 5-21 Tribofilms formed on the worn surfaces of the AA2124-3 wt.% G composite pins (a) Macrograph, (b) FESEM micrograph and (c) Raman spectrums for the composite compared to the G as-received powders. [64]

### 5.3.6. Nanohardness and Nanoscratch Behavior

The load-displacement diagram, and hardness and Young's Modulus variation as a function of increasing G-content are displayed in Figure 5-21(a, b), respectively. In the current work, Oliver and Pharr method [70] was employed in measuring hardness and Young's Modulus. Increasing G-content resulted in increasing the load bearing capacity on the nanoscale testing which agrees with results displayed for the micro-Hv resulting from the localized average strain hardening induced locally. This was also reflected on the nanohardness results shown in Figure 5-21 b. There is a consistent increase in the hardness with graphene addition by 63% and 114% for 3-wt.% G and 5-wt.% G respectively, which agrees with the findings of Aniruddha Ram et. al., [51].

On the other hand, Young's modulus was highest for the 3-wt.% G composite with an 22% increase over that of the plain AA2124. Addition of 5-wt.% G to AA2124 resulted in insignificant increase in Young's Modulus of the plain alloy. It is suggested that the uniform distribution of the 3-wt.% G particles within the Aluminum matrices (Figure 5-15 c, d) resulted in good interfacial

shear bonding between the G-and matrix (Figure 5-16 f), which facilitated the load transfer and hence higher stiffness [71]. It is also suggested that the localized nature of the nanoindentation test in which the values are influenced by the local graphene content and distribution resulted in an increase in stiffness [51]. Conversely, the observed G-particles micro-segregation and clustering within the Al-matrices for the 5wt.% G composite resulted in interfacial de-bonding and hence overall decrease in stiffness.

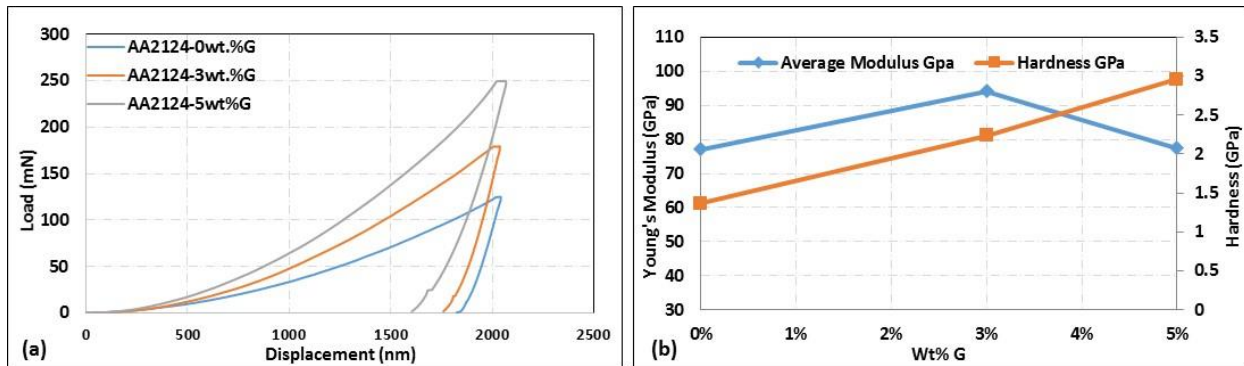


Figure 5-22 Nano-hardness test results: (a) Load-displacement and (b) Young's Modulus for AA2124 hot extrudates as a function of increasing G-content [64]

Figure 5-22 a, shows the on-load scratch distance and scratch depth variation over a distance of  $700\mu\text{m}$  as a function of the plain AA2124 as a function of increasing G-content. The arrow represents the sliding direction of the tip during the nanoscratch test. It is observed that the plain AA2124 displayed the highest most uniform depth of penetration (av. depth of  $-1005\text{nm}$  ( $\pm 2.12$ ), Figure 5-22 of the indenter tip along the scratch length. Increasing the G-content up to 3 wt.% produced the lowest depth of penetration (Av. Depth  $-877\text{nm}$  ( $\pm 3.53$ ), Figure 5-22 b), which was associated with fluctuations ranging between  $-760$  to  $-977\text{nm}$  ( $\pm 34.64$ ). Addition of 5wt.% G resulted in the most uniform depth of penetration ranging between  $-875$  to  $-1081\text{nm}$  with an average of  $-946\text{nm}$ . For the G-containing samples the tip is pushed upward during scratch test, which

indicates higher resistances to scratching due to enhanced hardness [72]. When the indenter tip confronts graphene layer or particle along the scratch direction this requires more force to move straight forward. It is suggested that the evident nonuniform distribution and clustering of G-particles within the Al-matrices(Figure 5-15c)(Figure 5-16h) and (Figure5-20 f) in the AA2124-5wt.% G composite resulted in the observed wide range of penetration depth along the scratch distance. On the other hand, the uniform distribution of G-particles in the AA2124-3-wt.% G composite resulted in an overall uniform penetration along the scratch direction.

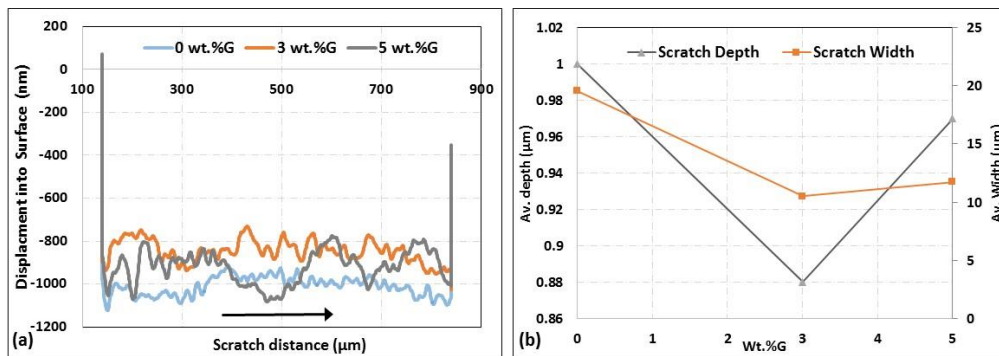


Figure 5-23 Diagrams for representative behavior for the AA2124 hot extruded BM powders (a) scratch depth profile Vs. scratch distance and the (b) variation of scratch depth and width as a function of increasing G-content [64].

As discussed earlier, the enhanced young's modulus of these parameters gives higher elastic recovery and less deformation under constant load. Accordingly, the displayed Nanoscratch and nanoindentation results influenced the scratch groove depth and width as shown in Figure 5-22(b). The average scratch width was measured using FESEM images as shown in Figure 5-23. It is clear from the displayed results in Figure 5-22(b) that the average scratch width follows similar behavior to that of the scratch depth as expected, where the average scratch width decreased from 19.5μm

( $\pm 1.10$ ) for the plain AA2124 to 10.5 ( $\pm 0.43$ ) and 11.7 ( $\pm 0.66$ )  $\mu\text{m}$  for 3 and 5 wt.% G composites, respectively. Knowing that the displayed results were average over 3 scratches per specimen.

The SEM images in Figure 5-23 show representative scratches for the AA2124 hot extrudates as a function of increasing G-content at low and high magnifications, respectively. The 3 wt.% G (Figure 5-23 b) composite displayed scratches with the narrowest width and least debris and flash along the scratch edges compared to the 5wt.% G composite and the plain alloy. This agrees with the results displayed in Figure 5-21(b) and supports the enhanced tribological properties displayed in section before 3wt.% G addition to the AA2124 resulted in a smooth scratch surfaces free from debris. However, sever damage occurred by the formation of long flash segments sheared on the edges of the scratch over the length of the scratch (Figure 5-23c). The sheared segments are an indication of the formation of nonuniform thick layer of smeared graphene, which was easily piled up and peeled out under shear stresses induced by the indenter. Hodge and Nieh suggested that the higher the material pile up during scratching, the higher the COF [86]. This is due to the higher the contact area between the indenter and the test specimen, which increases the lateral force associated with sliding. This agrees with the reported behavior of AA2124-5wt.% G and the relatively higher average COF and wear rates displayed in (Figure 5-19) compared to that of the AA2124-3-wt.% G composites. This was not in agreement with the behavior of the 3wt.% G-composite, which didn't suffer from the delamination or the peeling of the formed smeared thin layer of graphene, which increased the overall resistance to scratching. The scratched surfaces of the plain AA2124 extrudates showed the typical behavior of complicated alloy containing multiple phases, which result in relatively higher indenter penetration associated with high degree of debris formation, which agrees with the displayed results in Figure 5-20a

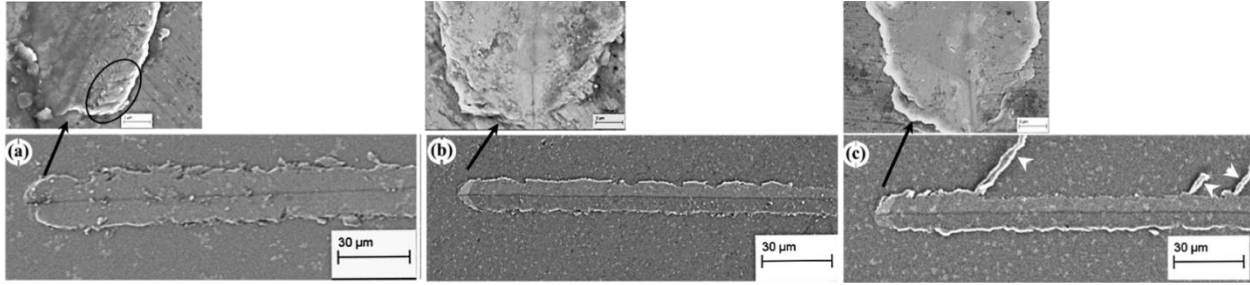


Figure 5-24 SEM images for representative scratches formed on the surfaces of the hot extruded AA2124 with a) 0wt.% G b) 3-wt.% G and c) 5wt.% G [64]

The scratch morphology for the plain AA2124 hot extrudates (Figure 5-23) showed relatively high volume of debris on the scratch surfaces, which was associated with irregular scratch edges indicative of the most damaged condition compared to the composites containing 3 and 5wt.%. In addition, investigation of the plain alloy scratches at high magnification (circled in Figure 5-23(a)) reveals evidence for shear bands, which were not observed in the G-containing scratches at high magnification (Figure 5-23 (b) and (c)), respectively.

#### 5.3.6.2. Conclusions:

In the current study, AA2124 self-lubricating composites were successfully produced via a combination of ball milling and hot extrusion at 450°C. Addition of 3-wt.%G to AA2124 matrices produces composite rods with the highest mechanical and tribological properties due to the uniform distribution of G within the Al-matrices, while increasing G-content up to 5 wt.% results in the clustering of graphene into coarse lumps. This is achieved due to the

- Hindering structural growth associated with effective lattice strain during consolidation via hot extrusion compared to the 5-wt.% G composite and the plain alloy.

- Developing good interfacial shear bonding of the G-particles within the Al-matrices, which results in successful shear stress transfer from the matrix to the reinforcement. While G-particles pullout and interfacial decohesion from surrounding Al-matrices occurs with increasing G-content up to 5-wt.%G.
- Producing the lowest wear rates and COF due to the preferential allocation of the G-particles along the Al-grain boundaries, which easily and uniformly smear out on the sliding surfaces. While the non-uniform distribution of G-particles within the Al-matrices of the 5-wt.% containing G composites results in formation of thick layers of G-film which is easily delaminated and peeled-off on rubbing.
- Producing highest stiffness and highest resistance to scratching using Nanoscratch test compared to the 5-wt.% G composite and the plain alloy

#### 5.4. Influence of Extrusion Temperature on the Behavior of AA2124-3wt.G Composite: A comparative Study:

Defects and imperfections, such as porosity and non-uniformity in the distribution of the reinforcing fillers, may be encountered in the composite as a result of inadequate control of the processing parameters. For instance, particle-porosity may be formed due to the difference in the thermal coefficient of expansion of reinforcements and the matrix which results in the detachment along the interfaces separating between both. This in turn results in the formation of porosities associated with high stress concentrations leading to premature failures in service. In that respect, improving the particle-matrix interfacial bonding becomes a vital step for the successful deployment of such composites [11]. Quintessentially, thermomechanical

techniques such as extrusion, rolling, etc., are applied as enhancing techniques to reduce the resultant imperfections and to produce a rather homogenous particle dissemination within the composite. However, incidental to the use of such consolidation techniques, a number of prevailing issues are encountered. The occurrence of reinforcing particles increase the need for higher applied forces, which in effect leads to particle cracking and fracture and hence formation of microporosity [87]. To that end, processing temperatures are increased to enable the decrease in the applied forces [88]. It is argued that the application of elevated temperatures within limits, allow for a sufficient flow of the alloy through the particle-cluster voids and collectively cease particle cracking. Hong et al. [89] provided empirical evidence reporting an increase in the tensile strength of SiCw-2124 composite after the extrusion temperature was raised. Limited increase in extrusion temperature is recommended as deploying very high temperatures may result in a reversed scenario where surface cracking occurs and the properties degrade instead [90] or in similar cases, ceramic particles accumulate at grain boundaries creating a defect [91]. One major problem with raising the consolidation temperatures, is the excessive grain growth associated with heating, which results in the loss of the refined structure gained by prior milling. This also adds to the cumulative effect of decreasing mechanical and tribological properties of the composite.

In the current section the AA2124-3wt.% G hot extrusion composite at 300 and 450oC were selected for summarizing the influence of the G-addition to AA2124 on the structural, textural behavior as well as the mechanical, tribological properties for its superior properties compared to the 5wt.%G and the plain alloy.

## 5.4.1. Physical and Structural Behavior

### 5.4.1.1. Microstructure

From the displayed results in Figures (5-3 and 5-12) HE at 300 and 450 °C produced averaged relative densities about 97.5 and 98.25%, respectively, which is indicative of an enhanced densification with increasing the processing temperature as anticipated. Figure 5-25 shows optical micrographs for the AA2124-3Wt.%G composite extrudates at processed at both temperatures. For the composite rods extruded at 300°C (Figure 5-25 a), continuous dark bands are encapsulating the Al-matrix particles which are elongated along the extrusion direction. These band areas are structurally made of graphene. On the other hand, an interrupted non continuous graphene bands were formed for the rods extruded at 450°C (Figure 5-25b). Many studies investigated the effect of both temperatures and extrusion ratio on the homogeneity of composites and the flow of matrix during extrusion. It was found that increasing the extrusion temperature up to certain temperature facilitates the flow of matrix (Plastic flow). In addition, increasing the extrusion temperature to certain degrees resulted in grain coarsening and suspension of reinforcement particles near grain boundaries [92]. It is suggested that the relatively low extrusion temperatures of 300°C (0.45 T<sub>m</sub>) resulted in lower matrix flow which was low enough to maintain equal flow of both the matrix and the graphene encapsulating bands/layers. It is worth noting, the uniform distribution combined with the internal lubricating effect of the Graphene filler was responsible for facilitating the plastic flow of the Al-matrices (AA2124 is a complicated alloy) without encountering shear localization under such low extrusion temperatures. Conversely, extrusion at 450°C (0.68 T<sub>m</sub>) was high enough to allow for higher rates of plastic flow (softening) of the Al- matrices, compared to that of the encapsulating graphene band/layers. This in turn resulted in the breakage of the Graphene



layers creating the observed discontinuous fragmentation of the reinforcement around the Al-matrices as shown in Figure 5-25 b.

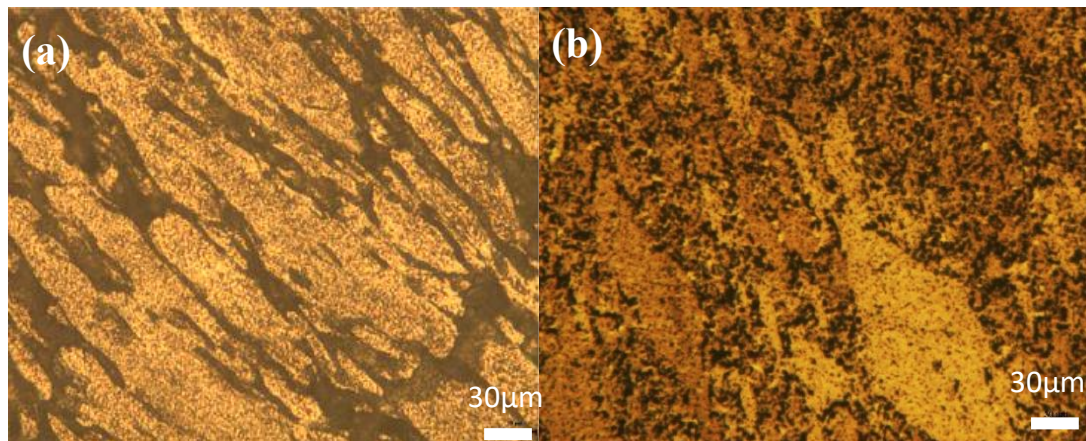


Figure 5-25 shows optical microscope images for as extruded AA2124/G nanocomposite.

#### 5.4.2. Mechanical and Tribological Behavior:

##### 5.4.2.1. Mechanical Properties

Table 5-4 lists the tensile and hardness data produced for the AA2124-3wt%G rods extruded at 300°C and 450°C, and for comparative purposes, results reported by researchers for the same 2024/2124 reinforced with ceramics such as SiC, Al<sub>2</sub>O<sub>3</sub> as well as carbon based fillers such as graphene, graphite, CNT and MWCNT are also listed in the table.

It is clear from the displayed results that increasing the extrusion temperature didn't have a significant influence on the tensile properties of the AA2124-3wt.%G composites. In addition, only 3% increase in Hv-values was exhibited for the low temperature extrudates compared to the high temperature ones. It is anticipated that; low temperature extrusion didn't allow for a significant strengthening due to the dominating lubrication effect of the G-layer surrounding the Al-matrices. This was evident by the measured much higher tensile yield and ultimate tensile

strength of the plain alloy (325 and 590 MPa, respectively) extruded at the same temperatures compared to that of the 3 wt.% G containing composite. On the other hand, it is suggested that extrusion of the composite at 450°C was dominated by the strengthening effect of the G-fragmented layer, which was opposed by the strain softening associated with higher extrusion temperature. This was evident by the significantly lower yield and ultimate tensile strength displayed by the plain alloy extrudates (88 and 350 MPa, respectively), which sustains the suggestion made for the excessive softening of the Al-matrices at 450°C and the strengthening effect of 3 wt % G addition to the alloy.

Comparing the results displayed by the AA2124-3wt.%G composites processed in the current research with those reported by other researchers for the AA2024/2124 reinforced with ceramics such as SiC and Al<sub>2</sub>O<sub>3</sub>, are listed in Table 5-4[86,87,88,89]. From the listed properties, reinforcement of AA2124 with ceramic dispersions up to 25 wt.% results in relatively higher yield and ultimate tensile strength with and without heat treatment compared to the AA2124-3wt.%G composites. On the other hand, the hot extruded AA2124-3wt%G composite rods at 300°C produced higher modulus of elasticity values compared with the values reported for the same alloy reinforced with 25 wt.% SiC [93] or 15wt.% Al<sub>2</sub>O<sub>3</sub>, , [94] and comparable values for the composites processed at 450°C. However, the displayed hardness values for the processed AA2124-3 wt%G is almost 3x higher than that displayed by the ceramic reinforcements. It is suggested that the uniform distribution of the 3-wt.% G particles within the Aluminum matrices (Figure 5-15c and d) resulted in good interfacial shear bonding between the G-and matrix (Figure 5-15), which facilitated the load transfer and hence higher stiffness of the composite [95]. In addition, the well-known significant difference in thermal coefficient of expansion between the ceramic fillers and

the Al-matrices results in decohesion along the dispersion-Al interfaces, which reduces the lattice strain and hence results in relatively lower hardness [38].

The nature of the metal-Graphene bond type is not really clear however, limited attempts were made for providing an explanation. According to Woo et. al., the formation of  $Al_4C_3$  at the Al-G interfaces results in improving the bond strength between the reinforcement and the metallic matrices [33]. In addition, a simulation using density function theory (DFT), which was conducted by Wang et. al., predicted that the formation of covalent bonds between the metal atoms and the dangling Carbon atoms located preferentially in the valleys of the G zigzag edges forms self-assembled atomic chains of metal atoms on the zigzag edge. Moreover, Wang et. al., classified the Al-Graphene interface interaction strengths as a weak adsorption (physisorption) which does not significantly affect the  $\pi$ -band dispersion of graphene but can affect its doping due to the charge transferred from/to these metals [96]

Nanographite, Nano diamond, carbon foams, CNTs, and graphene showed good capabilities in industry due to their low thermal coefficient of expansion, good thermal conductivity, high strength and self-lubrication behavior. As reported earlier, the enhancement in mechanical properties may be related directly to the nanofiller dispersion, type, size, amount and/or the processing parameters such as temperature and pressure. Variable degrees of strengthening were reported [67, 38, 7] . Table 5-4 lists the mechanical properties variation, as reported by other researchers for AA2024/2124 reinforced with carbon based fillers compared to the produced AA2124-3 wt.%G composite rods hot extruded at 300 and 450°C.

In general, the displayed results in table 5-4 that the mechanical properties of the fabricated AA2124-3wt.%G composites are higher than those reported similar alloys reinforced with 0-5wt% CNTs or 0-0.5 wt% G, especially when 300°C extrusion temperature was employed [ [75], [94],

[97]]. The high tendency of agglomeration for carbon nano-tubes and high surface energy resulted into a great difficulty in dispersion of CNTs within the metal matrices. The most common technique used was ball milling with variable milling conditions. Bustamante et. al., dispersed 0.5,1,2,3,4,5 wt.% CNTs inside AA2024 matrix via ball mill for 30 h. The dispersion quality was homogenous and hardens for the bulk specimens has improved by 280% for the 5wt.% CNTs. However, the damage in CNTs structure was reported. This explains the observed significant increase in hardness for the alloy reinforced with 3 wt.% G (current research work, 245-Hv) compared with 3 wt% CNTs in AA2024(14-Hv) [98] Knowing that both composites were processed via combination of BM and hot extrusion.

The formation of Van der Waal forces between G sheets is known to be a dominant feature [38] . This nature facilitates the folding and clustering of G sheets, which reduces the ability to disperse easily in matrices and minimize the G surface area. Wet mixing followed by hot isostatic pressing (HIP) of 0.5 wt% G single sheets in Al-Cu alloy [51] showed the highest tensile strength (463 MPa) and elongation (11%) compared to the plain alloy. Wet mixing followed by HIP resulted in slightly higher tensile properties compared to that produced by BM and HE AA2124-3wt.% G processed in the current research. It is well known that HIP processing is capable of closing all porosity associated with sintering, which directly enhances the tensile strength and ductility compared to hot compaction and extrusion [75]

Table 5-4 Effects of reinforcement type and processing technique on the Mechanical properties of Aluminum alloys

Process	Al Alloy 2xxx	Reinforce ment	Fraction Wt. %	YS (MPa)	UTS (MPa)	E (GPa)	%Elongation	Hardness
<b>Cold Compaction -hot Extrusion 300°C</b>	<b>2124</b>	<b>G</b>	<b>0</b>	<b>350</b>	<b>590</b>	<b>73</b>	<b>6.8</b>	<b>173</b>
			<b>3</b>	<b>183</b>	<b>450</b>	<b>122.4</b>	<b>4.9</b>	<b>253</b>
<b>Cold Compaction -hot Extrusion 450°C</b>	<b>2124</b>	<b>G</b>	<b>0</b>	<b>88</b>	<b>350</b>	<b>70.53</b>	<b>11.5</b>	<b>105</b>
			<b>3</b>	<b>180</b>	<b>421</b>	<b>117.82</b>	<b>4.8</b>	<b>245</b>
Cast [93]	2124	SiC	20	490	630	116	3	-
			T4	25	405	560	105	7
Hot Extruded 500°C [94]	2124	Al <sub>2</sub> O <sub>3</sub>	0	262	416	76	-	80
			5	227	392	72	-	89
			10	246	406	79	-	91
			15	260	425	84	-	98
Milling, compaction 1500 Mpa, sintering 500°C and Extrusion 500°C [98]	2024	CNTs						HV
			0	-	-	-	-	90
			1	-	-	-	-	100
			3	-	-	-	-	140
			5	-	-	-	-	219
Mixing-Hot compaction 475 MPa, 500°C -hot extrusion [97]	2124	CNTs	0	150	-	-	25	-
			0.5	178	-	-	22	-
			1	200	-	-	18	-
Wet mixing – HIP 480° C [ [75] ]	Al+(3.9 wt.%Cu, Mg)	G	0	214	373	73	11	-
			0.15	262	400	72	12	-
			0.5	319	464	71	11.5	-

#### 5.4.2.2. Tribological Properties

It is well known that the research in automotive and aircraft industrial sectors focus on the development of lightweight materials with mechanical components with ultrahigh specific strength and wear resistance, aiming for improved performance with higher durability in service [99]. Mechanical components such as gears, bearings, ball bearing cages, motor bodies, connecting rods, aircraft pistons and generators' housing requires high wear resistance composite materials. Therefore, using a suitable lubricant between the interfaces, which are based on increased hardness, especially for the dry mechanism based wear ceramic reinforced metallic materials [22]. Adding carbon-based fillers such as micron or nanographite, CNTs, or nanographene forms tribofilm on the interfaces between the rubbing surfaces, which minimizes wear and hence decreases wear rates and COF in service [69]. Accordingly in this section, the tribological behavior of the AA2124-3wt.%G hot extruded rods at 300 and 450°C fabricated are compared with those produced by other researchers.

Table 5-5 lists the tribological properties of AA2024/2124 reinforced with 3wt.%G (current research), CNTs, and graphite. It is worth noting that the displayed wear rates for the 3 wt.%G composites under 50N load has been included in table 5-5 for the sake of comparison with the reported results of other researchers. From the displayed results, AA2124-3wt.G composites extruded at 300°C and tested under 100N load exhibited about 35% lower wear rates compared to the rods extruded at 450°C. Higher processing temperatures has a direct influence on the strain hardening and strain softening behavior of the processed composites. It is suggested that hot extrusion at 450°C resulted in lower strain hardening and relatively higher strain softening, which was evident by the Hv-values displayed in Table 5-5 for both conditions. Accordingly, the reported

higher wear rates for the higher temperature extruded rods can be explained by the lower hardness values, which reduced the resistance of the rubbing surfaces to wear.

In this research work, 3-wt.% G-addition to AA2124 for specimens extruded at 300 and 450° C , developed much smoother surfaces compared to the 0-wt.% G (plain AA2124) . This was attributed to the formation of continuous G-tribofilm covering the Al-matrices, with the formation of very small volume fraction of debris on the surface. The uniform G-tribofilm formation and smearing on the surface of the worn pins resulted in preventing further plastic deformation. Mild delamination can be observed at high magnifications for the 3-wt.% G composite compared to sever delamination for the 5-wt.% G reinforced AA2124 matrices.

Comparing the wear rates and COF produced for the AA2024 T6 reinforced with 0-20wt.% Graphite and sintered at 600°C [35] with the fabricated AA2124 composites containing 0 and 3 wt.% G as-extruded and dry tested under 50N loads, show a significant decrease in wear rates. Moreover, the pin on disc testing of the 450°C fabricated AA2124-3 wt.%G under 100N, produced slightly higher COF (0.32 $\mu$ ) values compared to (0.24 $\mu$ ) that produced for the AA2024-5wt.%G composites worn under 50N. Accordingly, the currently processed A2124 reinforced with 3 wt.% G extruded at 300 and 450°C, has proven enhancement in the tribological behavior compared to the same alloys reinforced with graphite or CNTs.

Recently, solid self-lubricating materials such as CNTs and G developed to maintain weak shear strength layers between surfaces and improve the strength of the matrices at the same time [Ref]. Bastwors et al., added 5 wt.% CNTs to pure aluminum and measured the dry wear under 20N load, the results showed a change in the wear mechanisms from adhesion and abrasion pure aluminum dominant wear mechanisms to be an abrasion wear [37]. Bustamante who worked on AA2024- 5wt.% CNTs under abrasive wear test at 1 N, reported a reduction in wear loss by 37 %

compared to plain alloy, which was evident by the formation of fine scratches and notable reduction in craters on the worn surfaces [100]

Lin et al. investigated the proper amount of CNTs to avoid agglomeration and to work as an effective solid lubricating reinforcement material [100]. The results confirmed adding more than 15 vol. % resulted in reduction in hardness and increases in wear rates. Accordingly, the tubular shape of CNTs reduced the shear forces between the material and the pulled-out debris when they act as rollers on the worn surface which resulted in decreasing the wear rates. It was obviously proven by several research as shown in [101] that CNTs, G and graphite works as sufficient solid lubricants, which spread out carbon tribofilms on the material surface. However, the soft nature of graphite is a reason for not maintaining the lubricant film on the surface under the continuous contact stresses. Consequently, it is easily removed, causing delamination and high wear rate. On the other contrary, G and CNTs protective mechanisms is different. They spread out during the test filling the micro cracks and voids developed, which diminish the delamination problem. Xu. et al., has confirmed the superior anti wear properties of graphene and CNTs compared to graphite [102].

Table 5-5 Tribological properties of Aluminum alloys-carbon composite

Process	Matrix	Reinforcement	Fraction Wt. %	Test condition	Wear rate (mm <sup>3</sup> /m) Mass loss(mg)	COF
<b>Cold Compaction - hot Extrusion 300C</b>	AA2124	G	0	Dry ,Pin on disc,50N,300 rpm	0.00057	-
			3		0.0007	
<b>Cold Compaction -</b>	AA2124	G	0	Dry ,Pin on disc,100N,300 rpm	0.00143	
			3		0.00106	



<b>hot Extrusion 300C</b>						
<b>Cold Compaction - hot Extrusion 450C</b>	AA2124	G	0	Dry ,Pin on disc,100N,300 rpm	0.0025	0.4
			3		0.00163	0.32
<b>Milling, Compaction and sintering [98]</b>	AA2024	CNTs	0	Abrasive (220grit) 1N, 300m, wet	Mass loss 71	-
			1		69	-
			3		65	-
			5		58	-
<b>Insitu PM processeing  Sintered 600°C, 30min [35]</b>	2024-T6	Graphite	0	Pin on disc 50N, 1000m dry	0.16	0.35
			5		0.0017	0.24
			10		0.0035	0.16
			15		0.004	0.12
			20		0.0058	0.12

#### 5.4.2.3. Texture analysis

The development of Cu and Shear components in the aluminum alloys produced during the extrusion process mainly belongs to the formation of subgrains due to high stacking fault energy [67]. In addition, it was reported that the Shear component can be formed due to friction along the die-rod interface during the extrusion process [68]. In the current work the results produced by the bulk texture analysis has proven that both the Cu-and Shear are the dominating texture components for the AA2124-G composites extruded at 300 and 450°C.

Figure 9-3 shows the Orientation Distribution Function (ODF) for the AA2124-3wt.%G longitudinal cross sections hot extruded at (a) 300° C and (b) 400 °C taken at 0, 45 and 90° Euler angles. The produced texture is influenced by the material flow in the direction of deformation, which is a function of the operating temperature and the material crystal structure, pure, alloy, monolithic or composite [103].Grains of monolithic (plain) FCC structural materials elongate

along the extrusion direction, which produces texture different from that produced when ceramic or other reinforcement such as carbides, oxides or carbon based fillers are used [103].

In this work the change in texture intensities has changed from 1.2-to-1.78 for the composites extruded at 300 (Figure 5-26 a) and 450°C (Figure 5-26 b), respectively. This was evident by the exhibited low radial symmetry for the 300°C extrudates compared to that of the 450°C ones.

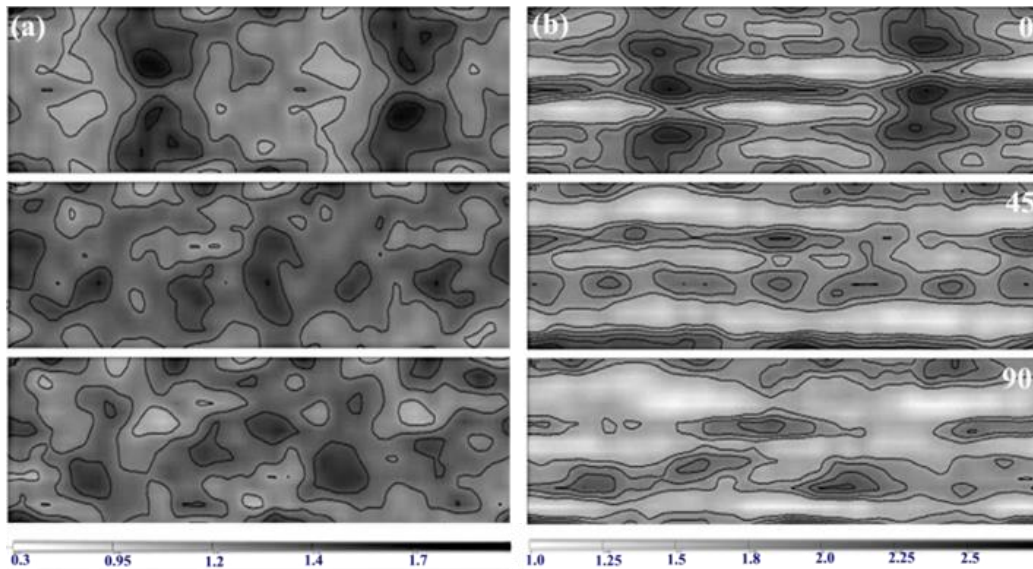


Figure 5-26 images for the Orientation Distribution Function (ODF) for AA2124-3wt.%G longitudinal cross sections hot extruded at (a) 300° C and (b) 450 °C for the 0, 45 and 85° Euler angles

Figure 5-27 shows the variation in micro-hardness measured along longitudinal sections sliced at the center of the rod (0 mm), 2mm and 4 mm from the center. The 4mm measurements represents 1 mm from the rod edges at which the texture analysis were carried out. It is clear that the hardness on the edge for the hot extruded specimen at 300 °C has the highest value (250 Hv) compared to the 450°C specimen (140.9). Moreover, extrusion at 450°C resulted in an insignificant variation in hardness across the rod thickness from the edge-to-the center, while significant variation occurred for the 300°C extrudates. Higher extrusion temperatures decreased the friction at the die-rod

interface which explains the reported results. It is therefore concluding that the change in the texture symmetry was influenced by the operating temperature, which in turn affected the hardness of the composite. The texture components volume fraction, shows that the specimens HE at 300° C has the highest shear components of 6.2 % compared to 3.1% for the 450 °C extrudates (Figure 5-26 a and b, respectively). There was no evidence for dynamic recrystallization for both temperatures, since the cube texture component {001} [100] in FCC metallic unit cells did not form [69].

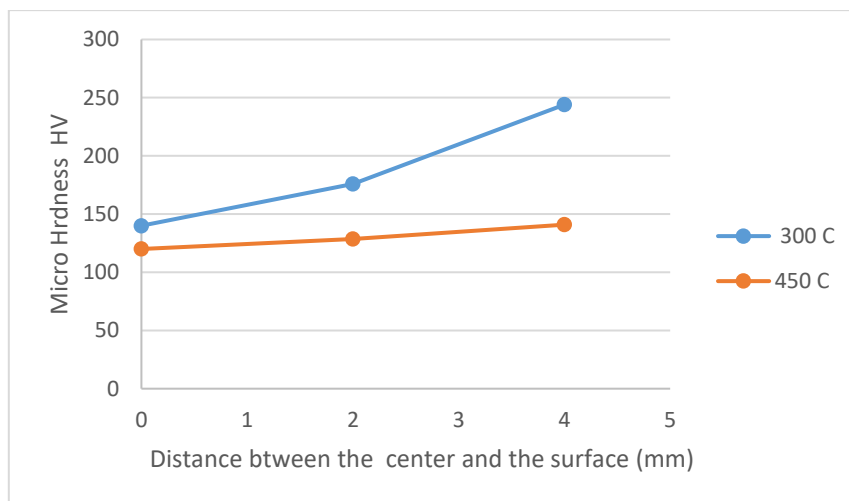


Figure 5-27 represents hardness profile for the AA2124-3wt.% from center to edge hot extruded at 300 and 450o C

## Chapter 6. Conclusions

In the current study, higher wt.% of G-containing AA2124 self-lubricating composites were successfully produced via combination of BM and hot extrusion compared to recently conducted researchers. The processed solids show that AA2124-3-wt.%G composite

1. AA212-graphene nanocomposite mixed and milled powders were successfully extruded at 300°C and 450°C.
2. 3wt.% G has the highest mechanical properties due to the G-uniform distribution within the Al-matrices, while increasing G-content up to 5 wt.% results in clustering of graphene into coarse lumps.
3. Effectively retards structural growth during consolidation via hot extrusion compared to the 5-wt.% G composite and the plain alloy.
4. Develops good Cohesion of the G-particles with the Al-matrices, which results in the shear stress transfer from the matrix to the reinforcement. While G-particles pullout and interfacial decohesion from surrounding Al-matrices occurs with increasing G-content up to 5-wt.%G.
5. Produces the lowest wear rates and COF due to the preferential allocation of the G-particles along the Al-grain boundaries, which easily smear out uniformly on the

sliding surfaces. While the nonuniform distribution of G-particles within the Al-matrices results in formation of thick layers of G-film which is easily delaminated and peeled-off on rubbing.

Accordingly, the AA2124-3wt.%G composite processed via combination of ball milling and extrusion either as 300 or 450°C exhibit significant enhancement in the tribological properties compared to AA2024/2124 alloys reinforced with same content of cremates or carbon based fillers (CNTs, graphite and graphene). This is due to the relatively strong interfacial bonding between graphene and the Al-matrices coupled with the uniform distribution. Almost doubling the hardness values of the composite coupled with the formation of uniform smeared G-tribofilm in between the rubbing surfaces produces the superior tribological properties reported in the current research.

## Chapter 7. Future work

1. Investigate the effects of dispersing different size of G in AA2124 matrices.
2. TEM investigation for the hot extruded specimens.
3. Study the wear behavior of AA2124- 3wt.%G under various wear parameters
4. Investigate other mechanical properties such as compressive and fatigue strength for the 3wt.%G Composite.
5. Investigate the formation of oxides and carbide within the sintering process by conducting differential scanning calorimeter test for the milled powders.
6. Investigate the effect of adding G on the damping ratio and energy absorption

## References

- [1] R. German, Powder metallurgy and particulate materials processing: the processes, materials, products, properties, and applications., Metal powder industries federation, 2005.
- [2] S. Werner and K.-P. Wieters, Powder metallurgy: processing and materials, European Powder Metallurgy Association, 1997.
- [3] C. Suryanarayana, "The structure and properties of nanocrystalline materials: issues and concerns.," Journal of the Minerals, Metals and Materials Society, vol. 54, no. 9, pp. 24-27, 2002.
- [4] K. CC, "Synthesis of nanostructured materials by mechanical milling: problems and opportunities," Nanostructured Materials, vol. 9, no. 1, pp. 13-22, 1997.
- [5] M. J. Zehetbauer and Y. T. Zhu, Bulk nanostructured materials, John Wiley & Sons, 2009.
- [6] K. Novoselov, G. A and Morozov, "A Electric Field Effect in Atomically Thin Carbon Films," Science, vol. 306, no. 5696, pp. pp. 666-669, 2004.
- [7] A. Terrones and R. Borello-Mendez, "Graphene and Graphite Nanoribbons Morphology, Properties, Synthesis, Defects and Applications," Nanotoday, vol. 5, no. 4, pp. 351-372, 2010.
- [8] W. Lee, S. Jang and M. J. K. a. J.-M. M. young, "Interfacial Interactions and Dispersion Relations in Carbon Aluminium Nanocomposite Systems," Nanotechnology, vol. 28, no. 19, p. 13, 2008.
- [9] J. R, P. Daniel, C. Bielawski and R. S. Ruoff, "Graphene-Based Polymer Nanocomposites," Polymer, vol. 1, pp. 5-25., 2011.
- [10] D. Berman, A. Erdemir and A. Sumant, "Graphene: a new emerging lubricant," Materials Today, vol. 17, no. 1, pp. 31-42, 2014.
- [11] T. Khorshid, E. Meysam Omrani, P. L. Menezes and R. P. K, "Tribological performance of self-lubricating aluminum matrix nanocomposites: Role of graphene nanoplatelets," Engineering Science and Technology, vol. 19, no. 1, pp. 463-469, 2016.
- [12] A. D. Moghadam, E. Omrani, P. L. Menezes and P. K. Rohatgi, "Mechanical and tribological properties of self-lubricating metal matrix nanocomposites reinforced by carbon

nanotubes (CNTs) and graphene – A review," *Composites Part B: Engineering*, vol. 77, pp. 402-420, 2015.

- [13] J. Wang, Z. Li, G. Fan, H. Pan and Z. C. a. D. Zhang, "Reinforcement with Graphene Nanosheets in Aluminum Matrix Composites," *Scripta Materialia*, vol. 66, no. 12, pp. 594-597, 2012.
- [14] S. Yan, S. Dai, X. Zhang, C. Yang, Q. Hong and J. Che, "Investigating aluminum alloy reinforced by graphene nanoflakes," *Material Science and Engineering A*, vol. 612, pp. 440-444, 2014.
- [15] W. Zhang, M. Gu, D. Wang and Z. Yao, "Rolling and annealing textures of a SiCw/Al composite.," *Materials Letter*, vol. 58, no. 27, pp. 3414-3418, 2004.
- [16] Jeon, Chi-Hoon, et al. "Material properties of graphene/aluminum metal matrix composites fabricated by friction stir processing." *International journal of precision engineering and manufacturing* 15.6 (2014): 1235-1239..
- [17] M. Rashad, F. Pan, H. Hu, M. Asif and S. Hussain , "Development of magnesium-graphene nanoplatelets composite," *Journal of Composite Materials*, vol. 3, no. 49, pp. 281-293, 2015.
- [18] R. M. Jones, *Mechanics of composite materials*, Washington, DC: CRC, 1998.
- [19] D. M. Afsaneh, S. B. F, J. B. Ferguson and O. Emad, "Functional metal matrix composites: self-lubricating, self-healing, and nanocomposites-an outlook," *JOM*, vol. 66, no. 6, pp. 872-881, 2014.
- [20] B. Fohahnolo, J. Robert and T. J, "Effect of mechanical alloying on the morphology, microstructure and properties of aluminium matrix composite powders," *Materials Science and Engineering: A*, vol. 342, no. 1, pp. 131-143, 2003.
- [21] A. Sannion and . H. Rack, "Dry sliding wear of discontinuously reinforced aluminum composites.," *Wear*, vol. 189, no. 1, pp. 1-9, 1995.
- [22] M. Ibrahim and F. A. Lavernia, "Particulate reinforced metal matrix composites," *Journal of materials science*, vol. 26, no. 5, pp. 1137-1156., 1991.
- [23] . A. Mortensen and L. Javier , "Metal matrix composites," *Annual review of materials research*, vol. 40, pp. 243-270, 2010.



- [24] H. G. Salem and A. A. Sadek, "Fabrication of High Performance PM Nanocrystalline Bulk AA2124," *Journal of materials engineering and performance*, vol. 19, no. 3, pp. 356-367, 2010.
- [25] M. Rosso, " Ceramic and metal matrix composites: Routes and properties.," *Journal of Materials Processing Technology* , vol. 175, no. 1, pp. 364-375., 2006.
- [26] A. D. Moghadam,, B. F. Schultz and J. B. Ferguson, "Functional metal matrix composites: self-lubricating, self-healing, and nanocomposites-an outlook," *JOM*, vol. 66, no. 6, pp. 872-881, 2014.
- [27] N. T. Aboulkhair and A. M. Esawi , "Bi-modally structured pure aluminum for enhanced strength and ductility," *Materials & Design*, vol. 83, pp. 493-498, 2015.
- [28] C. Suryanarayana, *Mechanical alloying and milling.*, CRC Press, 2004.
- [29] Hutchings, Ian M., and Philip Shipway. "Tribology: friction and wear of engineering materials." (1992): 156.
- [30] Bayer, Raymond G. "Tribological and Wear Testing." *Characterization of Materials PP17*. 2012..
- [31] A. Paknia , A. R. Dixit, and Chattopa, "Effect of Size, Content and Shape of Reinforcements on the Behavior of Metal Matrix Composites (MMCs) Under Tension," *Journal of Materials Engineering and Performance*, vol. 25, no. 10, pp. 4444-4459, 2016.
- [32] "Miracle, D. B.. Metal matrix composites—from science to technological significance. *Composites science and technology*, 65(15), 2526-2540." 2005.
- [33] Woo, D. J., B. Sneed, F. Peerally, F. C. Heer, L. N. Brewer, J. P. Hooper, and S. Osswald. "Synthesis of nanodiamond-reinforced aluminum metal composite powders and coatings using high-energy ball milling and cold spray." *Carbon* 63: 404-415.2013.
- [34] "Moghadam, A. D., Omrani, E., Menezes, P. L., & Rohatgi, P. K. Mechanical and tribological properties of self-lubricating metal matrix nanocomposites reinforced by carbon nanotubes (CNTs) and graphene—a review. *Composites Part B: Engineering*, 77, 4"2015.
- [35] F. AKhlaghi and A. Zare-Bidaki, "Influence of graphite content on the dry sliding and oil impregnated sliding wear behavior of Al 2024—graphite composites produced by in situ powder metallurgy method," *Wear*, vol. 266, no. 1, pp. 37-45., 2009.

- [36] D. Jeyasimman, K. Sivaprasad and S. Sivasankaran, "Fabrication and consolidation behavior of Al 6061 nanocomposite powders reinforced by multi-walled carbon nanotubes.," Powder Technology, vol. 258, pp. 189-197, 2014.
- [37] M. M. Bastwros, A. M. Esawi and A. Wifi, "Friction and wear behavior of Al–CNT composites," wear, vol. 307, no. 1, pp. 164-173, 2013.
- [38] Z. Baig, O. Mamat and . M. Mustapha, "Recent Progress on the Dispersion and the Strengthening Effect of Carbon Nanotubes and Graphene-Reinforced Metal Nanocomposites," Critical Reviews in Solid State and Materials Science, vol. 1, pp. 1-46, 2016.
- [39] Singh, B. P., Nayak, S., Nanda, K. K., Jena, B. K., Bhattacharjee, S., & Besra, L.. The production of a corrosion resistant graphene reinforced composite coating on copper by electrophoretic deposition. Carbon, 61, 47-56. 2013.
- [40] Singh, E., Thomas, A. V., Mukherjee, R., Mi, X., Houshmand, F., Peles, Y., & Koratkar, N. Graphene drape minimizes the pinning and hysteresis of water drops on nanotextured rough surfaces. ACS nano, 7(4), 3512-3521.2013.
- [41] Vidu, Ruxandra, Masoud Rahman, Morteza Mahmoudi, Marius Enachescu, Teodor D. Poteca, and Ioan Opris. "Nanostructures: a platform for brain repair and augmentation." Frontiers in systems neuroscience vol. 8 'pp91.2014.
- [42] Zheng, Q., & Kim, J. K. . Graphene for transparent conductors: synthesis, properties and applications (Vol. 23). Springer.2015.
- [43] Berman, D., Erdemir, A., & Sumant, A. V. Reduced wear and friction enabled by graphene layers on sliding steel surfaces in dry nitrogen. Carbon, vol 59, pp167-175. 2013.
- [44] V. Randle and O. Engler, Introduction to Texture Analysis: Macrotecture, microtexture, CRC, 2000.
- [45] in Senatore, A., D'Agostino, V., Petrone, V., Ciambelli, P., & Sarno, M. (2013). Graphene oxide nanosheets as effective friction modifier for oil lubricant: materials, methods, and tribological results. ISRN Tribology, 2013.
- [46] T. Khorshid, E. Meysam Omrani, P. L. Menezes and R. P. K, "Tribological performance of self-lubricating aluminum matrix nanocomposites: Role of graphene nanoplatelets, Engineering Science and Technology, vol. 19, no. 1, pp. 463-469, 2016.
- [47] Li, X., Cai, W., An, J., Kim, S., Nah, J. Large-area synthesis of high-quality and uniform graphene films on copper foils. Science, vol. 324(5932), pp1312-1314.2009.

- [48] Huang, H. D., Tu, J. P., Gan, L. P., & Li, C. Z. An investigation on tribological properties of graphite nanosheets as oil additive. *Wear*, vol 261(2), pp140-144. 2006.
- [49] R. K. and S. Aravindan, "Tribological behavior of microwave processed copper–nanographite composites, *Tribology International*, vol.57pp282-296. 2013.
- [50] Huang, X., Qi, X., Boey, F., & Zhang, H. Graphene-based composites. *Chemical Society Reviews*, 41(2), pp 666-686.2012.
- [51] S. R. e. a. Bakshi, ""Aluminum composite reinforced with multiwalled carbon nanotubes from plasma spraying of spray dried powders," *Surface and Coatings Technology*, vol. 10, no. 203, pp. 1544-1554, 2009.
- [52] Tjong, S. C. Recent progress in the development and properties of novel metal matrix nanocomposites reinforced with carbon nanotubes and graphene nanosheets. *Materials Science and Engineering: R: Reports*, vol.74(10), pp281-350.2013.
- [53] Sengupta, R., Bhattacharya, M., Bandyopadhyay, S., & Bhowmick, A. K. A review on the mechanical and electrical properties of graphite and modified graphite reinforced polymer composites. *Progress in polymer science*, vol. 36(5), pp638-670.2011.
- [54] F. H. Latief, E.-S. M. Sherif, A. A. Almajid and H. Junaedi, "Fabrication of exfoliated graphite nanoplatelets-reinforced aluminum composites and evaluating their mechanical properties and corrosion behavior," vol. 92, no. 2, 2011.
- [55] S. F. Bartolucci, J. Paras, J. Rafiee, M. A. Rafiee, S. Lee, D. Kapoor and N. Koratkar, "Graphene–aluminum nanocomposites," vol. 528, no. 27, 2011.
- [56] N. Al-Aqeeli and a. et, "Structure of mechanically milled CNT-reinforced Al-alloy nanocomposites.," *Materials and Manufacturing Processes*, vol. 28, no. 9, pp. 984-990, 2013.
- [57] H. T. Bui, B. T. Tran and D. Q. Le, "The effect of sintering temperature on the mechanical properties of a Cu/CNT nanocomposite prepared via a powder metallurgy method.," *Advances in Natural Sciences: Nanoscience and Nanotechnology*, vol. 2, no. 1, p. 015006., 2011.
- [58] SSnano, "www.ssnano.com," Skyspring, [Online]. Available: [http://www.ssnano.com/i/u/10035073/h/Specification/Product\\_Graphene\\_0541DX.pdf](http://www.ssnano.com/i/u/10035073/h/Specification/Product_Graphene_0541DX.pdf).
- [59] W. Zhai, "Effect of graphene nanoplate addition on the tribological performance of Ni3Al matrix composites," vol. 48, 2013.

- [60] A. Ghazaly, B. Seif and H. Salem, "Mechanical and Tribological Properties of AA2124-Graphene Self Lubricating Nanocomposite," TMS Light Metals, pp. 411-415, 2013.
- [61] H. Salem, S. El-Eskandarany, A. Kandil and H. Fattah, Bulk behavior of ball milled AA2124 nanostructured powders reinforced with TiC, Journal of Nanomaterials, vol. 10, pp. 1-12, 2009.
- [62] C. A. Varol T, "Effect of particle size and ratio of B 4 C reinforcement on properties and morphology of nanocrystalline Al2024-B 4 C composite powders," Powder Technology, vol. 246, pp. 462-472, 2013.
- [63] A. Ghazaly, B. Shaeen, Salem, H. G. Mechanical and Tribological Properties of AA2124-Graphene Self Lubricating Nanocomposite, TMS ,2013.
- [64] El-Ghazaly, A., Anis, G., & Salem, H. G. Effect of graphene addition on the mechanical and tribological behavior of nanostructured AA2124 self-lubricating metal matrix composite. Composites Part A: Applied Science and Manufacturing, 95, 325-336. 2017.
- [65] M. El hamid, M. Emar and H. G. Salem, Influence of Mixing Technique on the Mechanical Properties and Structural Evolution of Al-NiAl Composites, Journal of Materials Engineering and Performance, vol. 23, no. 10, pp. 3425-3435, 2014.
- [66] G. Xen, Preparation and tensile properties of homogeneously dispersed graphene reinforced aluminum matrix composites. Msterisl and design, vol. 94, pp. 54-60, 2016.
- [67] N. S. Alam and L. S. Kumar, Mechanical properties of aluminium based metal matrix composites reinforced with graphite nanoplatelets., Materials Science and Engineering: A, vol. 667, pp. 16-32., 2016.
- [68] J. Li, L. Xiong and y. c. wang, Microstructure and tensile properties of bulk nanostructured aluminum/graphene composites prepared via cryomilling., Materials Science and Engineering: A, vol. 626, pp. 400-405, 2015.
- [69] S. Zhu, Q. Bi and J. Yang, Influence of Cr content on tribological properties of Ni 3 Al matrix high temperature self-lubricating composites., Tribology International, vol. 44(10), pp. 1182-1187, 2011.
- [70] O. WC and P. GM, An improved technique for determining hardness and elastic modulus using load and displacement sensing indentation experiments, Journal of materials research, vol. 6, no. 1, pp. 1564-83, 1992.
- [71] Ram, H.A., Koppad, P.G., Nanoindentation studies on MWCNT/aluminum alloy 6061 nanocomposites, Materials Science and Engineering: A, pp. 920-923, 2013.

- [72] M. . Shokrieh, Nanoindentation and nanoscratch investigations on graphene-based nanocomposites, vol. 32, no. 1, 2013.
- [73] M. Rashad, F. Pan, H. Hu, M. Asif, S. Hussain and J. She, "Development of magnesium-graphene nanoplatelets composite," *Journal of Composite Materials*, vol. 49, no. 3, pp. 28-293, 2015.
- [74] J. Wang, Z. Li, G. Fan, H. Pan, Z. Chen and D. Zhang, Reinforcement with graphene nanosheets in aluminum matrix composites, vol. 8, 2012.
- [75] S. Yan, S. Dai, X. Zhang, C. Yang, Q. Hong, J. Chen and Z. Lin, "Investigating aluminum alloy reinforced by graphene nanoflakes," vol. 612, 2014.
- [76] "Meysam Tabandeh-Khorshid, Emad Omrani, Pradeep L. Menezes, Pradeep K. Rohatgi Tribological performance of self-lubricating aluminum matrix nanocomposites: Role of graphene nanoplatelets," vol. 19, no. 1, 2016.
- [77] A. P., Xavier and M. Anthony, "The Effect of Ball Milling & Reinforcement Percentage on Sintered samples of aluminium alloy metal matrix composites," *Procedia Engineering*, vol. 97, p. 1027 – 1032, 2014.
- [78] Gao, Xin, Hongyan Yue, Erjun Guo, Hong Zhang, Xuanyu Lin, Longhui Yao, and Bao Wang. "Preparation and tensile properties of homogeneously dispersed graphene reinforced aluminum matrix composites." *Materials & Design* 94 54-60. 2016.
- [79] M. Rashad, F. Pan, H. Hu, M. Asif, S. Hussain and J. She, "Development of magnesium-graphene nanoplatelets composite," vol. 49, no. 3, 2015.
- [80] C. Suryanarayana, "Characterization of powders," in *Mechanical Milling and Alloying*, Marcel dekkery, p. 110, 2002.
- [81] Liu, Y. B., Lim, S. C., Ray, S., & Rohatgi, P. K. . Friction and wear of aluminium-graphite composites: the smearing process of graphite during sliding. *Wear*, Vol 159(2),pp 201-205.1992.
- [82] J. M, E. MH, A. MH and K. F, Compressive and wear behaviors of bulk nanostructured Al2024 alloy," *Materials & Design* , vol. 31, no. 2, pp. 663-669, 2010.
- [83] Kumar, S., M. Chakraborty, V. Subramanya Sarma, and B. S. Murty. "Tensile and wear behaviour of in situ Al–7Si/TiB 2 particulate composites." *Wear* 265, vol. 1 pp 134-142 2008.

- [84] Mohiuddin, T. M. G., Lombardo, A., Nair, R. R., Bonetti, A., Savini, G. & Novoselov, K. S. Uniaxial strain in graphene by Raman spectroscopy: G peak splitting, Grüneisen parameters, and sample orientation. *Physical Review B*, vol 79(20), 2009.
- [85] Iqbal, M. W., Singh, A. K., Iqbal, M. Z., & Eom, J. Raman fingerprint of doping due to metal adsorbates on graphene. *Journal of Physics: Condensed Matter*, vol. 24(33), 335301.2012 .
- [86] H. AM and N. TG, Evaluating abrasive wear of amorphous alloys using nanoscratch technique, *Intermetallics* , vol. 12, no. 7, pp. 741-748, 2004.
- [87] R. R. Fard and F. Akhlaghi, Effect of extrusion temperature on the microstructure and porosity of A356-SiC p composites., *Journal of materials processing technology*, vol. 187, pp. 433-436, 2007.
- [88] K. Tavighi, M. Emamy and A. R. Emami, Effects of extrusion temperature on the microstructure and tensile properties of Al-16wt% Al<sub>4</sub> Sr metal matrix composite., *Materials & Design*, vol. 46, pp. 598-604., 2013.
- [89] S. H. Hong and K. H. Chung, Effects of vacuum hot pressing parameters on the tensile properties and microstructures of SiC-2124 Al composites., *Materials Science and Engineering: A*, vol. 194, no. 2, pp. 165-170., 1995.
- [90] O. N. Senkov and S. V. Senkova, Compaction of amorphous aluminum alloy powder by direct extrusion and equal channel angular extrusion, *Materials Science and Engineering: A*, vol. 393, no. 1, pp. 12-21, 2005.
- [91] I. M. Low, *Ceramic-matrix composites: Microstructure, properties and applications.*, Woodhead Publishing., 2006.
- [92] R. R. Fard and F. Akhlaghi, Effect of extrusion temperature on the microstructure and porosity of A356-SiC p composites, *journal of materials processing technology*., vol. 187, pp. 433-436., 2007.
- [93] S. V. Prasad and Asthana, Aluminum metal-matrix composites for automotive applications: tribological considerations, *Tribology letters* , vol. 17, no. 3, pp. 445-453., 2004.
- [94] A. D. Leszek and W. Anna , The structure and properties of PM composite materials based on EN AW-2124 aluminum alloy reinforced with the BN or Al<sub>2</sub>O<sub>3</sub> ceramic particles., *Journal of Materials Processing Technology*, vol. 175, no. 1, pp. 186-191, 2006.

- [95] S. Bakshi, V. Singh, S. Seal and A. Agarwal, "Nanoindentation studies on MWCNT/aluminum alloy 6061 nanocomposites," *Materials Science and Engineering: A*, pp. 920-923, 2013.
- [96] Wang, H., Feng, Q., Cheng, Y., Yao, Y., Wang, Q., Li, K., & Yang, W. Atomic bonding between metal and graphene. *The Journal of Physical Chemistry C*, vol.117(9), pp4632-4638. 2013.
- [97] M. M. Emara, Consolidation of 2124 aluminum alloy–carbon nanotube reinforced metal matrix composites," " *Advanced Materials Research*. , vol. 748, pp. 28-31, 2013.
- [98] R. B.-E. Perez-Bustamante, wear behavior in Al2024-CNTs composites synthesised by mechanical milling, *wear*, vol. 292 (2012):, pp. 169-175., 2012.
- [99] Rambabu, P., Prasad, N. E., Kutumbarao, V. V., & Wanhill, R. J. H, *Aluminium Alloys for Aerospace Applications*. In *Aerospace Materials and Material Technologies* (pp. 29-52). Springer Singapore.2017
- [100] Lin, C. B., Chang, Z. C., Tung, Y. H., & Ko, Y. Y. Manufacturing and tribological properties of copper matrix/carbon nanotubes composites.2011 *Wear*, vol.270(5), pp.382-394.2017
- [101] Berman, Diana, Ali Erdemir, and Anirudha V. Sumant. Few layer graphene to reduce wear and friction on sliding steel surfaces." *Carbon* 54 , 454-459.2013.
- [102] Xu, Z., Zhang, Q., Shi, X., Zhai, W., & Zhu, Q. Comparison of tribological properties of NiAl matrix composites containing graphite, carbon nanotubes, or graphene. *Journal of Materials Engineering and Performance*,vol. 24(5), 1926-1936.2015.
- [103] Shin, Keesam, Dongsup Chung, and Sunghak Lee., "The effect of consolidation temperature on microstructure and mechanical properties in powder metallurgy-processed 2XXX aluminum alloy composites reinforced with SiC particulates." *Metallurgical and Materials*, vol. 28.12pp 2625-2636. 1997.
- [105] W. Zhai and X. Shi, "Grain refinement: a mechanism for graphene nanoplatelets to reduce friction and wear of Ni 3 Al matrix self-lubricating composites," *Wear*,, vol. 310(1), pp. 33-40, 2014.
- [106] C. Meriç, "Physical and mechanical properties of cast under vacuum aluminum alloy 2024 containing lithium additions.," *Materials research bulletin*, vol. 35, no. 9, pp. 1479-1494., 2000.

- [107] H. C. Anilkumar, H. S. Hebbar and K. S. Ravishan, "Mechanical properties of fly ash reinforced aluminium alloy (Al6061) composites," *International Journal of Mechanical and Materials Engineering*, vol. 6, no. 1, pp. 41-45, 2011.
- [108] H. G. Kumar and Prashantha, Fatigue and wear behavior of Al6061–graphene composites synthesized by powder metallurgy, *Transactions of the Indian Institute of Metals*, vol. 69, no. 2, pp. 415-419, 2016.
- [109] C. Zhao, "Enhanced strength in reduced graphene oxide/nickel composites prepared by molecular-level mixing for structural applications.," *Applied Physics A*, vol. 118, no. 2, pp. 409-416., 2015.
- [110] Al-Qutub, A. M., A. Khalil, N. Saheb, and A. S. Hakeem. "Wear and friction behavior of Al6061 alloy reinforced with carbon nanotubes." *Wear* 297, vol. 1: pp.752-761.2013.
- [112] Kingery, W. D., & Berg, M. Study of the initial stages of sintering solids by viscous flow, evaporation-condensation, and self-diffusion. *Journal of Applied Physics*, vol.26(10),pp 1205-1212,1955.
- [113] Xu, Zengshi, Qiaoxin Zhang, Xiaoliang Shi, Wenzheng Zhai, and Qingshuai Zhu. Comparison of tribological properties of NiAl matrix composites containing graphite, carbon nanotubes, or graphene. *Journal of Materials Engineering and Performance* 24, no. 5 2015.
- [114] Atkinson, H. V., & Davies, S. Fundamental aspects of hot isostatic pressing: an overview. *Metallurgical and Materials Transactions A*, vol.31(12), pp.2981-3000.2000.
- [115] Munir, Z. A., Anselmi-Tamburini, U., & Ohyanagi, The effect of electric field and pressure on the synthesis and consolidation of materials: a review of the spark plasma sintering method. *Journal of Materials Science*, vol. 41(3), pp763-777.2006.
- [116] Rhodes, M. J. (1990). *Principles of powder technology*. pp19-20,1990.



